Doctoral Thesis

Flexibility of Flexible Perovskite Solar Cells Investigated by Nanomechanics

Seung-min Ahn

Department of Materials Science and Engineering

Graduate School of UNIST

2019

Flexibility of Flexible Perovskite Solar Cells Investigated by Nanomechanics

Seung-min Ahn

Department of Materials Science and Engineering

Graduate School of UNIST

Flexibility of Flexible Perovskite Solar Cells Investigated by Nanomechanics

A dissertation
submitted to the Graduate School of UNIST
in partial fulfillment of the
requirements for the degree of
Doctor of Philosophy

Seung-min Ahn

12. 05. 2018
Approved by

_____

Advisor
Prof. Ju-Young Kim

Flexibility of Flexible Perovskite Solar Cells Investigated by Nanomechanics

Seung-min Ahn

This certifies that the dissertation of Seung-min Ahn is approved.

12/05/2018

signature

_____

Advisor: Prof. Ju-Young Kim

signature

_____

Prof. Myoung Hoon Song

signature

_____

Prof. Ki-Suk Lee

signature

_____

Prof. Eun-chae Jeon

signature

_____

Prof. Seung-Kyun Kang

Abstract

Organic-inorganic halide perovskite solar cells hold promise for next-generation photovoltaic devices because of their remarkable optical properties and high light-absorption coefficient. Mechanical flexibility of the perovskite solar cells together with high photovoltaic efficiency has been attracting attentions because processing temperatures are so low that all the constituent materials can be flexible unlike rigid inorganic solar cells. While various flexible materials used for transparent electrodes and hole- and electron-transport layers have been introduced, irreplaceable perovskite materials have organic-inorganic crystalline structures that can be brittle. In most previous researches, flexibility of the perovskite solar cells has been evaluated empirically; for example, decrease in photovoltaic efficiency by cyclic bending deformation for a certain bending radius. Beyond the empirical studies determining flexibility of the perovskite solar cells based on repeatable bending tests, investigations on mechanical properties of perovskite materials which can be the weakest material among the constituent materials have been conducted by nanoindentations and computational simulations. Because nanoindentations are measured only for local volume, mechanical properties measured by nanoindentations may not represent mechanical properties of film-type perovskite materials including various defects. Computational simulations can be restricted to perfect crystalline structures also. The best way to overcome limitations of nanoindentations and computational studies is to measure uni-axial tensile properties of free-standing perovskite materials because (1) gauge section can include all possible defects that tensile properties represent real mechanical properties of the perovskite materials and (2) deformation and fracture behavior of the perovskite materials at any deformed states of the solar cell can be predicted by solid mechanics with their tensile properties. There has been a computational study on tensile behavior of single- and poly-crystalline perovskite materials, but experimental measurement of tensile properties of free-standing perovskite materials has not been reported so far as far as we know. This is possibly because perovskite materials are so sensitive to environments such as humidity and oxygen that sample preparation and testing procedure are challenging.

Therefore, this work contains dedications to explain mechanical flexibility as followings;

1. To fabricate the ultra-flexible perovskite solar cells via ITO-free transparent bottom electrode.
2. To measure the mechanical properties of constituent materials in flexible PSCs
3. To design the innovated mechanical testing method for vulnerable perovskite materials using in-situ nanoindentation system.
4. To measure direct tensile properties of organic-inorganic perovskite materials via in-situ tensile testing.

The major contribution of this dissertation is to expand our insight into what truly happens in flexibility of flexible perovskite solar cells. New systematic approaches will be discussed in detail in the body of this dissertation.

Contents

List of Figures

List of Table

Explanation of Terms and Abbreviations

Terms

a	Patterned hole radius
B	Bulk modulus
δ	Indentation depth
η	Power conversion efficiency, PCE
E	Elastic modulus
ε	Elastic limit
F	Force
FF	Fill factor
G	Shear modulus
J_{sc}	Short-circuit current density
k	Boltzmann's constant
k_1, k_2, k_3	Rate constant associated with band recombination
r_A, r_B, r_X	Ionic radius for A, B, X ions
σ_0	Pretension in the film
σ_f	Maximum stress at the center point
v	Poisson' ratio
V_{oc}	Open-circuit voltage
R	Indenter tip radius
R_c	Critical bending radius
t	Film thickness
q	Dimensionless constant based on Poisson' ratio

Abbreviations

PSC	Perovskite solar cell
$MAPbI_3$	Methylammonium lead triiodide ($CH_3NH_3PbI_3$)
MAI	Methylammonium iodide (CH_3NH_3I)
MABr	Methylammonium bromide (CH_3NH_3Br)
PbI_2	Lead iodide
FAI	Formamidinium iodide ($HC(NH_2)_2I$)
DSSC	Dye-sensitized solar cells
PCE	Power conversion efficiency
Spiro-MeOTAD	$N^2,N^2,N^{2'},N^{2'},N^7,N^7,N^{7'}N^{7'}$-octakis(4-methoxyphenyl)-9,9'-spirobi[9H-fluorene]-2,2'-,7',7-tetramine
ETL	Electron transfer layer
HTL	Hole transfer layer
VB	Valence band
CB	Conduction band
AM	Air Mass
EQE	External quantum efficiency
IQE	Internal quantum efficiency
IPCE	Incident photon to charge carrier efficiency
XRD	X-ray diffraction
XPS	X-ray photoelectron spectroscopy
DFT	Density functional theory
MD simulation	Molecular dynamics simulation
WVTR	Water vapor transmission rate
NOA 88	Norland optical adhesive 88
PEI	Polyethyleneimine

$PC_{61}BM$	Phenyl-C61-butyric acid methyl ester
DMSO	Dimethyl sulfoxide
DMF	N,N-dimethylformamide
GBL	γ-Butyrolactone
IPA	2-propanol
HMDS	Hexamethyldisilazane
CB	Chlorobenzene
SEM	Scanning electron microscopy
FIB	Focus ion beam
PR	Photo-resist process
Deep RIE	Deep reactive-ion etching
PMMA	Polymethyl methacrylate
TA	Thermal annealed sample
SA	Solvent annealed sample

1. Introduction

The serious environmental and political problems are caused by energy crisis and increased emission of CO_2 during the few decades. Owing to exhaustion of resources such as fossil fuels and increased energy consumption, exploring alternative energy sources is one of important assignment in the world. The sun is a sustainable, reliable and almost infinite source of energy that can make significant contributions to the global demand for energy. Therefore, solar energy is regarded as a promising candidate as next-generation renewable energy [1], and organic-inorganic metal halide perovskite solar cells (PSCs) have been studied as attractive candidates for next-generation photovoltaic devices. The photovoltaic efficiency of PSCs has recently soared rapidly from 3.8% to above 20% in less than 10 years [2-8]. Such PSCs have many advantages: remarkable optical properties, longer charge, electron and hole, diffusion lengths [9], high light absorption coefficients [10] and good cost-effectiveness [11], and show promise not only in photovoltaic applications but also in other applications such as luminescent devices and transistors [12-14]. After all these merits, however, perovskite is suffered from stability and reliability issues until now. In particular, perovskite is easily decomposed by moisture or heat, and it is vulnerable to oxygen. Water react strongly to common perovskite materials for photovoltaic devices, such as methylammonium lead triiodide ($MAPbI_3$, $CH_3NH_3PbI_3$). When the film is exposed to humid environment, resulting in decomposition into solid PbI_2 and CH_3NH_3 ion, and HI. This decomposition process is permanent reaction and causing severe breakdown on devices [15-17]. Likewise, heat and oxygen, and light also decompose materials in a similar manner, reducing the performance of the device. To solve these long-term stability issues multiple studies have been developed such as doped halogen element and mixed cations and coated encapsulation or passivation layer and so on [18-22].

Likewise, there has been rapid studied in long-term stability issues, but precious few theoretical and experimental studies have been demonstrated mechanical properties. For commercialize, especially flexible devices, reasonable comprehension of mechanical response is urgent priority due to stress state has affect strongly on the device performance and reliability follow weakest-link model. Research on mechanical properties of PSCs generally divided into the method of measuring flexibility using hundreds or thousands of times of repeatable bending testing [23, 24] and measuring mechanical properties using direct mechanical testing methods. The latter mechanical testing method has limitations in measuring fracture mechanical properties. Indeed, direct measurement of mechanical properties, especially tensile properties, are challenging because of too hard to fabricate specimen and to progress testing. Several studies have recently demonstrated mechanical properties of PSCs vis nanoindentation testing and computational methods [25-28]. Unfortunately, these methods cannot measure quantitative mechanical properties because nanoindentation methods are indirect methods because there are strongly influenced by substrates. Furthermore, nanoindentation tests are performed only local volume areas. It

is because no considered various structured defects such as grain boundary and pin-holes. The best way to overcome limitation of these is to measure tensile properties of the perovskite materials because it is possible to predict fracture behavior directly. However, experimental measurement of tensile properties has not been reported due to sampling and handling are challenging.

As mentioned above, the study of mechanical properties, especially tensile properties, of flexible perovskite solar cells is a very important since it indicated of device reliability and flexibility. However, it is difficult to directly measure the mechanical properties at small-scale due to limitations of experimental methods and fabrication of samples [28]. Perovskite material is easily decomposed in atmosphere condition, where mechanical properties are drastically decreased. Therefore, it would have to be measuring the mechanical properties in fully isolated from external environments. For this reason, in this thesis, I fabricated flexible perovskite solar cells, and then carried out repeatable bending tests. I showed that critical bending radius of flexible device is dominated by the flexibility of the perovskite material using hole-nanoindentation tests, which carried out on free-standing component thin films of entire PSC devices using same process as devices on hole-patterned substrate. And then I have measured tensile properties of perovskite material via direct experimental method such as in-situ tensile testing using push-to-pull apparatus. To evaluate the mechanical flexibility, the tensile strain applied to the device was predicted through the tensile properties as shown predicted critical bending radius, which is well-agreement with actual bending radius through repeatable bending tests. Furthermore, the mechanical properties of the perovskite materials were improved by adding additives to the surface and internal defect points. As a result, it has been improved flexibility of the entire device through the mechanical properties of perovskite material. The mechanical properties of the perovskite were analyzing from the nanomechanical point of view, and through this discussed the flexibility of the flexible devices.

Reference

[1] N. Armaroli *et al.*, "The future of energy supply: challenges and opportunities," *Angewandte Chemie International*, vol. 46, no. 1-2, pp. 52-66, 2007.

[2] A. Kojima *et al.*, "Organometal halide perovskites as visible-light sensitizers for photovoltaic cells," *Journal of the American Chemical Society*, vol. 131, no. 17, pp. 6050-6051, 2009.

[3] J. Burschka *et al.*, "Sequential deposition as a route to high-performance perovskite-sensitized solar cells," *Nature*, vol. 499, no. 7458, p. 316, 2013.

[4] M. Liu *et al.*, "Efficient planar heterojunction perovskite solar cells by vapour deposition," *Nature*, vol. 501, no. 7467, p. 395, 2013.

[5] N. J. Jeon *et al.*, "Solvent engineering for high-performance inorganic–organic hybrid perovskite solar cells," *Nature Materials*, vol. 13, no. 9, p. 897, 2014.

[6] N. J. Jeon *et al.*, "Compositional engineering of perovskite materials for high-performance solar cells," *Nature*, vol. 517, no. 7535, p. 476, 2015.

[7] S. S. Shin *et al.*, "Colloidally prepared La-doped BaSnO3 electrodes for efficient, photostable perovskite solar cells," *Science*, vol. 356, no. 6334, pp. 167-171, 2017.

[8] W. S. Yang *et al.*, "Iodide management in formamidinium-lead-halide–based perovskite layers for efficient solar cells," *Science*, vol. 356, no. 6345, pp. 1376-1379, 2017.

[9] Q. Dong *et al.*, "Electron-hole diffusion lengths> 175 μm in solution grown CH3NH3PbI3 single crystals," *Science*, p. aaa5760, 2015.

[10] S. De Wolf *et al.*, "Organometallic halide perovskites: sharp optical absorption edge and its relation to photovoltaic performance," *The Journal of Physical Chemistry Letters*, vol. 5, no. 6, pp. 1035-1039, 2014.

[11] D. Vak *et al.*, "3D printer based slot-die coater as a lab-to-fab translation tool for solution-processed solar cells," *Advanced Energy Materials*, vol. 5, no. 4, p. 1401539, 2015.

[12] H. Cho *et al.*, "Overcoming the electroluminescence efficiency limitations of perovskite light-emitting diodes," *Science*, vol. 350, no. 6265, pp. 1222-1225, 2015.

[13] H. Wei *et al.*, "Sensitive X-ray detectors made of methylammonium lead tribromide perovskite single crystals," *Nature Photonics*, vol. 10, no. 5, p. 333, 2016.

[14] G. Xing *et al.*, "Low-temperature solution-processed wavelength-tunable perovskites for lasing," *Nature Materials*, vol. 13, no. 5, p. 476, 2014.

[15] J. H. Noh *et al.*, "Chemical management for colorful, efficient, and stable inorganic-organic hybrid nanostructured solar cells," *Nano Letters,* vol. 13, no. 4, pp. 1764-9, Apr 10 2013.

[16] J. You *et al.*, "Moisture assisted perovskite film growth for high performance solar cells," *Applied Physics Letters*, vol. 105, no. 18, p. 183902, 2014.

[17] G. E. Eperon *et al.*, "Morphological control for high performance, solution-processed planar heterojunction perovskite solar cells," *Advanced Functional Materials*, vol. 24, no. 1, pp. 151-157, 2014.

[18] A. Dualeh *et al.*, "Thermal behavior of methylammonium lead-trihalide perovskite photovoltaic light harvesters," *Chemistry of Materials*, vol. 26, no. 21, pp. 6160-6164, 2014.

[19] A. Seemann *et al.*, "Influence of oxygen on semi-transparent organic solar cells with gas permeable electrodes," *Organic Electronics*, vol. 10, no. 8, pp. 1424-1428, 2009.

[20] A. Dualeh *et al.*, "Effect of annealing temperature on film morphology of organic–inorganic hybrid pervoskite solid-state solar cells," *Advanced Functional Materials*, vol. 24, no. 21, pp. 3250-3258, 2014.

[21] M. O. Reese *et al.*, "Photoinduced degradation of polymer and polymer–fullerene active layers: experiment and theory," *Advanced Functional Materials*, vol. 20, no. 20, pp. 3476-3483, 2010.

[22] M. Manceau *et al.*, "Effects of long-term UV–visible light irradiation in the absence of oxygen on P3HT and P3HT: PCBM blend," *Solar Energy Materials and Solar Cells*, vol. 94, no. 10, pp. 1572-1577, 2010.

[23] B. J. Kim *et al.*, "Highly efficient and bending durable perovskite solar cells: toward a wearable power source," *Energy & Environmental Science,* vol. 8, no. 3, pp. 916-921, 2015.

[24] K. Poorkazem *et al.*, "Fatigue resistance of a flexible, efficient, and metal oxide-free perovskite solar cell," *Journal of Materials Chemistry A,* vol. 3, no. 17, pp. 9241-9248, 2015.

[25] Y. Rakita *et al.*, "Mechanical properties of APbX 3 (A = Cs or CH3NH3; X = I or Br) perovskite single crystals," *MRS Communications,* vol. 5, no. 04, pp. 623-629, 2015.

[26] S. Sun *et al.*, "Mechanical properties of organic–inorganic halide perovskites, CH3NH3PbX3 (X = I, Br and Cl), by nanoindentation," *Journal of Materials Chemistry A,* vol. 3, no. 36, pp. 18450-18455, 2015.

[27] J. Feng, "Mechanical properties of hybrid organic-inorganic CH3NH3BX3 (B = Sn, Pb; X = Br, I) perovskites for solar cell absorbers," *APL Materials,* vol. 2, no. 8, 2014.

[28] J. Yu *et al.*, "Probing the Soft and Nanoductile Mechanical Nature of Single and Polycrystalline Organic-Inorganic Hybrid Perovskites for Flexible Functional Devices," *ACS Nano,* vol. 10, no. 12, pp. 11044-11057, Dec 27 2016.

2. Research Backgrounds and Literature Reviews

2.1. Brief History of Perovskite Solar Cells

The basic structural component of the perovskite is the ABX_3 structure, which was first discovered in the Ural Mountains Gustav Rose in 19th century and is named after Lev Perovski who is Russian mineralogist. A general formula of perovskite with ABO_3 was first defined by Victor Goldschmidt in 1926, in his work on tolerance factors. When the tolerance factor, *t*, is about 0.75 ~ 1.0 range, almost inorganic elements are keeping the steady state in the perovskite structure. It has attracted widespread attention due to enormous size of the chemical classifications and the unique physical properties and physical ambilaterality they exhibit [1]. One of the widely known and early understanding was $BaTiO_3$, it because of its unique ferro-electric properties and higher dielectric constant in the relative field [2].

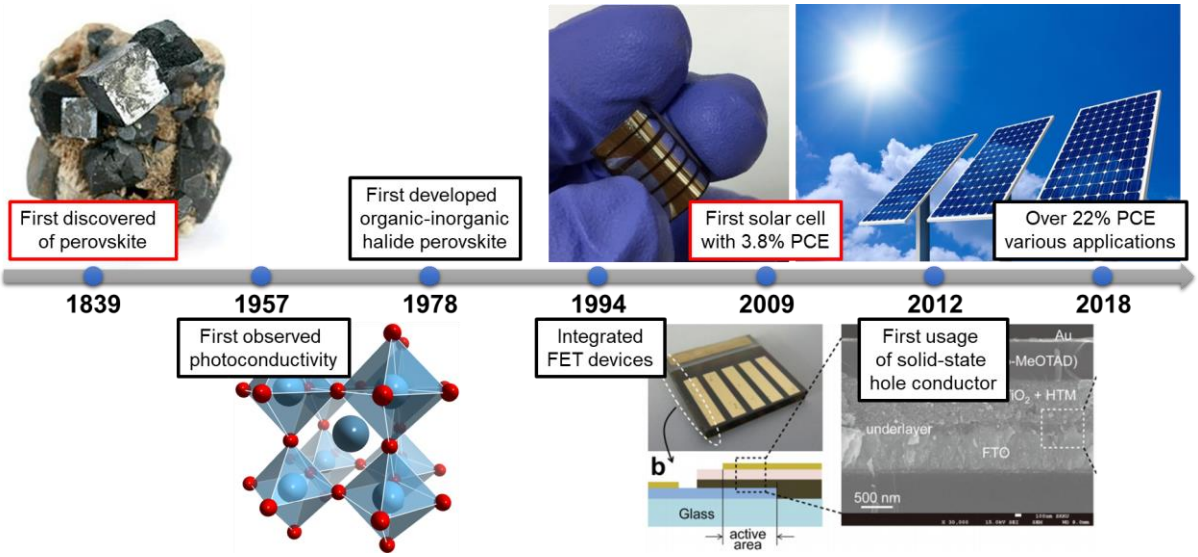

Figure 2.1. Origin of perovskite optoelectronic devices.

The perovskite structure exists perovskite oxides and halides perovskite. The halogen-based perovskite is ABX_3 in which A is a cation such as $CH_3NH_3^+$ (MA), $HC(NH_2)_2$ (FA) or Cs^+, etc., B is Pb^{2+} or Sn^{2+}, and the X is a halogen-atoms (typically I^-, Br^-, or Cl^-). Typically, perovskite structure reveals cubic structure and composed with corner-sharing BX_6 octahedral cage with cations in interstices. The primary study of semiconductor halide perovskite was made by Möller in late 1950's by observing photoconductivity in all-inorganic $CsPbX_3$ systems [3]. Afterward, Weber discovered that mergence of organic cation can gain same perovskite structure by forming an organic-inorganic halide perovskite $CH_3NH_3PbX_3$, which exhibits interesting physical properties [4]. Having first demonstrated the promising properties of perovskite in electronics in the mid-1990's, Mitzi successfully integrated this exciting material into a filed effect transistors (FETs) [5].

In 2009, Miyasaka developed the first perovskite solar cell with 3.8% efficiency [6]. They first used perovskite materials as visible-light sensitizers for DSSCs. However, the device performance and stability were significantly reduced by the liquid electrolyte contained in the DSSC to dissolve the perovskite materials. To solve the perovskite decomposition problem, in 2012, Park and Grätzel obtained 9.7% efficiency by replacing the liquid electrolyte with a solid-state hole conductor (Spiro-MeOTAD). It has been improved compared to the liquid electrolyte of perovskite solar cells. After using solid-state hole conductors, research on perovskite solar cells drawn keen attention, and several device architectures and high-quality perovskite material manufacturing methods have been proposed [7]. As results, the certified power conversion efficiency (PCE) of PSCs skyrocketed from 3% to more than 22% in just 7 years of academic research. The excellent efficiency of such perovskite solar cells can ultimately lead to the challenge of crystalline silicon solar cells.

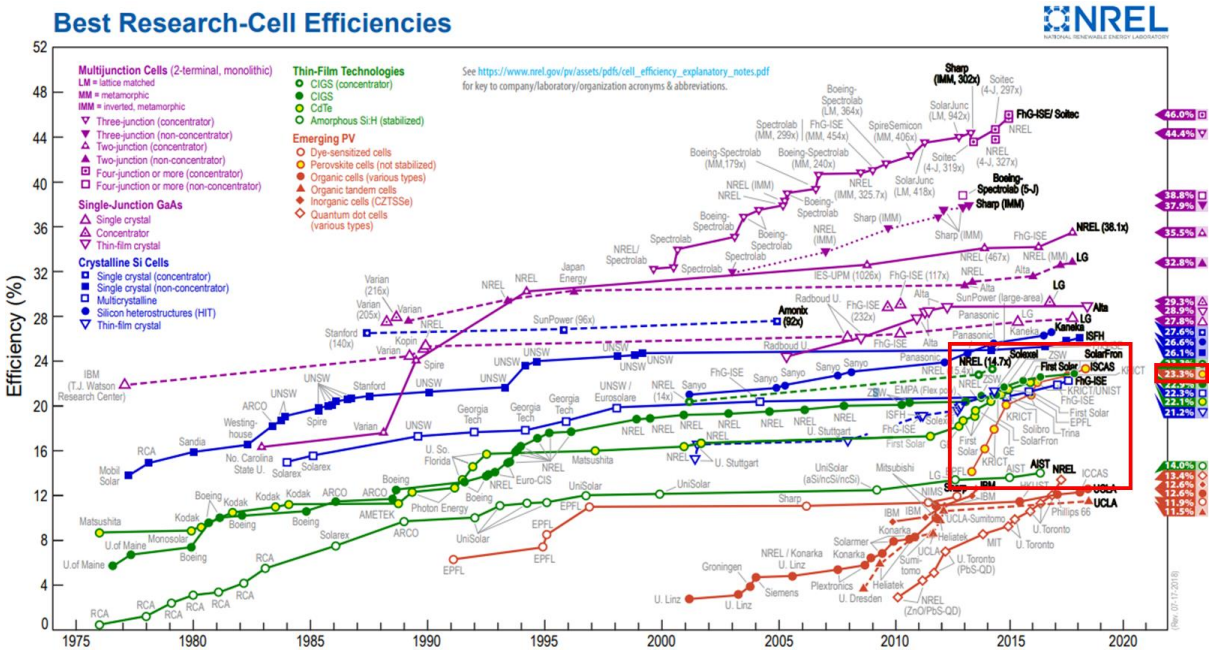

Figure 2.2. Best research-cell efficiencies of various solar cells. Reprinted with permission from [8]. Copyright 2018 NREL.

2.2. Fundamentals of Perovskite Solar Cells

2.2.1. Introduction of Perovskite Solar Cell Devices

The general material architecture of perovskite is shown in **figure 2.3**. A, B and X are three different types of ions. Typical perovskite material used in solar cells is $CH_3NH_3PbI_3$ (hereafter referred to the $MAPbI_3$). The perovskite structure formation is assessed by Goldschmidt's tolerance factor, *t*, is defined by [1]:

$$t = \frac{r_A + r_X}{\sqrt{2}(r_B + r_X)}$$

where r_A, r_B, and r_X are ionic radius for A, B, and X ions, respectively. A modification in the combination of anions and cations is lead to different crystal sizes, band gaps, and performance of the solar cells. The structure of perovskite is strongly affected by the organic cation size. The three-dimensional perovskite crystal structure maintains the same as the smaller sized organic cations. However, in the case of larger cations, the layer structure is formed with an inorganic layer, instead of organic layer, and associated with van der Waals forces. The three-dimensional perovskite crystal (Multi-layered) has three solid phases (α, β, and γ). In addition, one non-perovskite phase (δ) exists but is still unclear and will not be mentioned. In the case of $MAPbI_3$, the solid α-phase is found in a pseudo-cubic structure at high temperature (T > 54°C) and is occurring the phase transformation to tetragonal phase (β) at below 54°C. The organic cations (MA) are disordered in both α and β phases and ferroelectric reactions are required for rearrangement. The orthorhombic phase (γ) is found at lower temperature (T < -112°C) [9], where organic cations (MA) are ordered, as shown **figure 2.3**. The degree of distortion of MA ions were investigated at different phases and no distortion was observed at high temperature, rapid rotation and low temperature. This molecular motion of the cations induces a highly ordered arrangement along the C-N axis. This is the reason for phase transformation from cubic-tetragonal-orthorhombic phase as the temperature decreases.

A device structure of PSCs is composed of five function layers with anode, n-type electron transfer layer (ETL), active perovskite layer, p-type hole transfer layer (HTL), and the cathode, which is shown in **figure 2.3**. the perovskite layer is a core layer in which light is absorbed, and excitons are generated, occurred charge separation and transferred. The ETL is used for transferring electrons and blocking holes. The electrons are extracted in interface between ETL and perovskites. On the contrary, the HTL is conducting holes and blocking electrons. In general, photons and excitons are absorbed in perovskite layer, while electrons and holes are separated at the interfaces. There are three typical structures in PSCs. The most common structure is shown at **figure 2.3** in which photons collide through ETL [10, 11]. Another structure is inverted structure in which light incidents on HTL-side [13, 14].

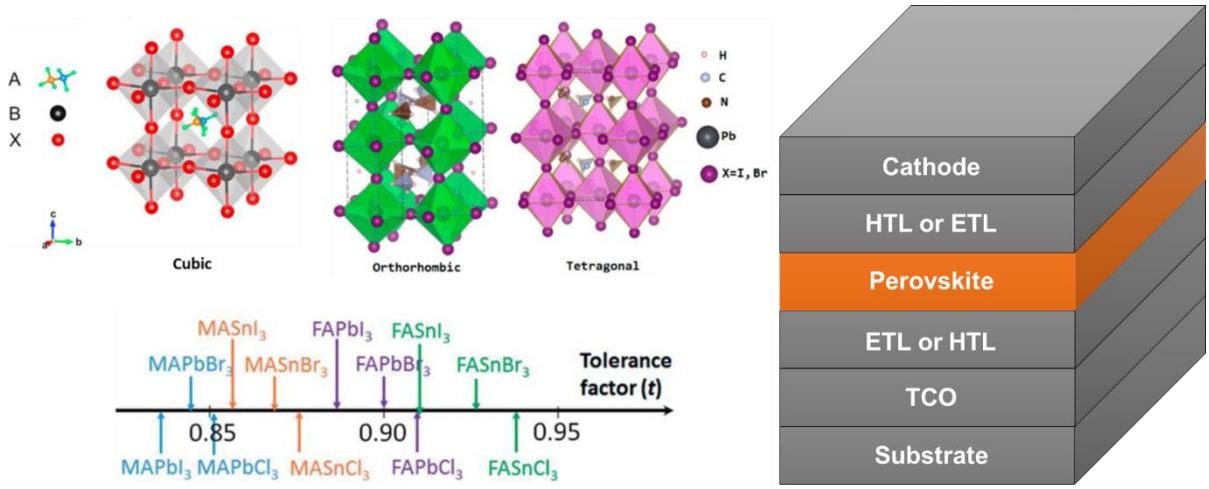

Figure 2.3. The structure of perovskite materials and device architecture of solar cells. Reproduced with permission from [12]. Copyright 2016 MDPI.

Inverted solar cells are developed more intensively because they are more stable and shows less hysteresis. The other structure is HTL-free solar cells [15], which are lack of hole-transporter due to HTL materials are very expensive.

2.2.2. General Properties of Perovskite Solar Cells

2.2.2.1. Characteristics of Perovskite Solar Cells

■ Operational Mechanism of Perovskite Solar Cells

Generally, PSCs are consisting of three-type core layers (electrode, electron- or hole- charge transport layer, active layer). A simplified operational mechanism of PSCs involves the absorption of photons by active perovskite layer. The perovskite layer has low exciton binding energy, which means that free charge carrier generation occurs during the photon absorption within a few picoseconds. This working mechanism of PSCs occurs desirable process in three-steps (as shown **figure 2.4**):

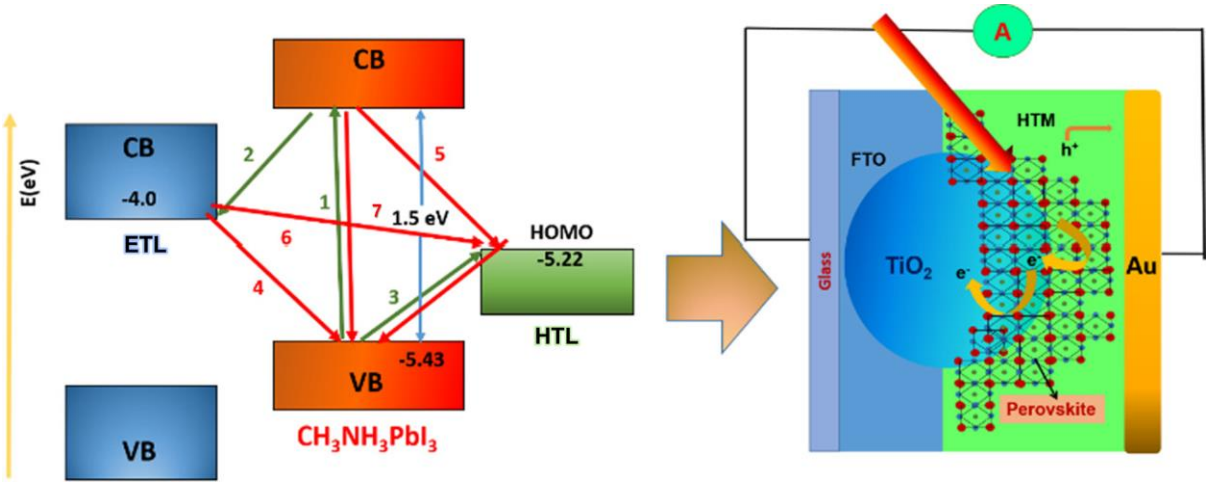

Figure 2.4. The schematic illustration of charge transfer and recombination process in PSCs. The green arrows show desirable process and red arrows show undesirable process. Reproduced with permission from [16]. Copyright 2017 Elsevier.

photo-exciton occurs in perovskite absorber (1), transfer of electrons to ETL and hole to HTL (2, 3). Several undesirable processes occur that is made up back charge transfer at interface of ETL and HTL (4, 5), direct contact between ETL and HTL (6), and recombination of generated species (7). Finally, once the extraction barrier has been overcome at the interface, the remaining charge carriers can be transfer through extracted by cathode and anode [17].

(a) Charge generation

An important question with regard to charge generation is whether the photo-excited species is excited or non-excited. In the perovskite, low exciton binding energy (~2 meV) determines that charge generation is non-exciton. Therefore, efficient creation of free holes and electrons at one-step is on of the main advantages of PSCs [18].

(b) Charge transport and recombination

The movement of charge carriers in semiconductors is related to the electronic band structure, and most importantly, the effective mass and mobility of holes and electrons. In perovskite, this effective mass is much closer to inorganic semiconductors, which benefit greatly from the heavily spin-orbit coupling effect in band structures due to the existence of weighty atoms. This strong spin-orbit coupling induces a decrease in bandgap and greatly changes the electron-hole effective mass [19-21]. Key parameter in the solar cell is charge carrier lifetime for defining a time window in order to efficiently extract the charge from each electrode before recombination. The deterioration of the free charge carrier density is defined by following equation:

$$\mathrm{dn/dt} = -k_3^{n3} - k_2^{n2} - k_1^{n}$$

where, k_1 is rate constant associated with trap-assisted recombination, k_2 is rate constant associated with radiative or direct or band to band recombination, and k_3 is rate constant associated with augur recombination which is highly dependent on the carrier charge density [22]. According to previous studies, the dominant recombination is non-radiative trap-assisted recombination, which mainly reduces V_{oc} [23]. **Figure 2.5** shows the schematic of recombination in PSCs.

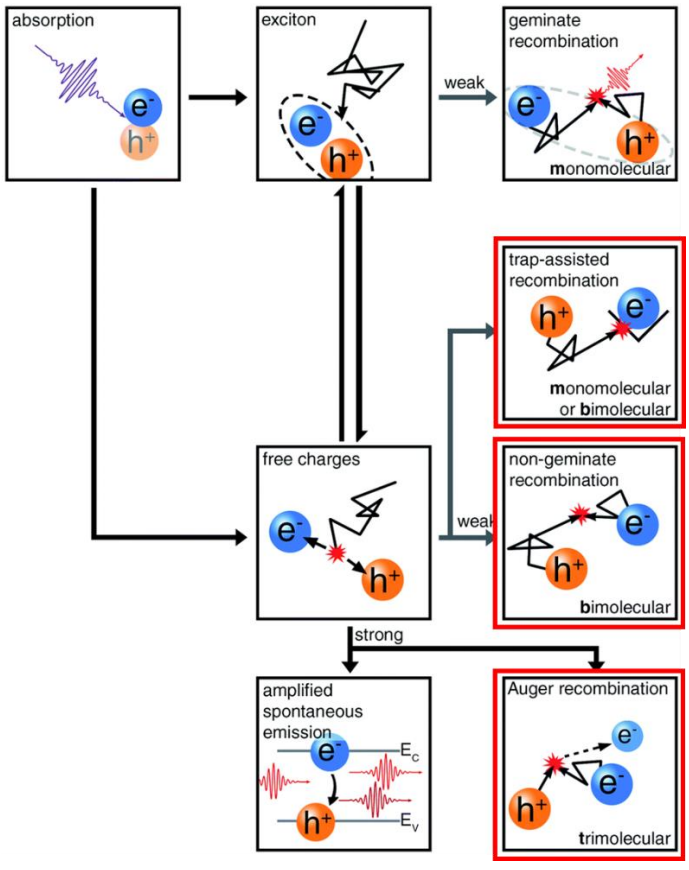

Figure 2.5. The schematic of charge transfer and recombination process in PSCs. Reproduced with permission from [24]. Copyright 2014 The Royal Society of Chemistry.

(c) Charge extraction

To efficiently extract charge from PSCs, it is necessary to select the ETL and HTL with the preferred band alignments (VB and CB) with the perovskite layer. Balanced charge transfer at the interface is further important for improving photovoltaic performance [25].

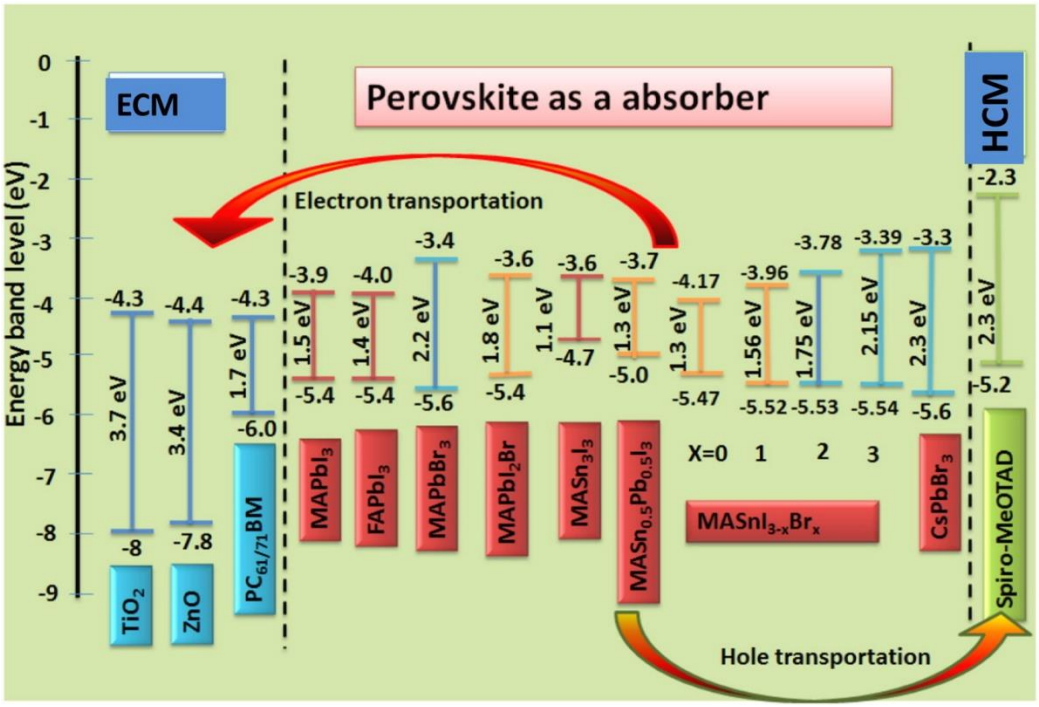

Figure 2.6. The band alignment diagram of different perovskite materials with some ETLs and HTLs. Reprinted with permission from [16]. Copyright 2017 Elsevier.

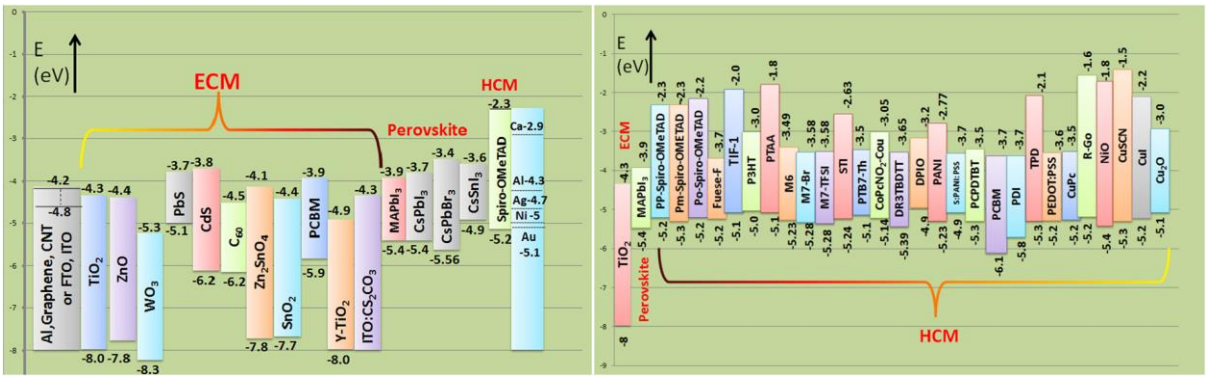

Figure 2.7. The band alignment diagram of ETLs and HTLs used for PSCs. Reprinted with permission from [16]. Copyright 2017 Elsevier.

■ **Standard Solar Spectral Irradiance**

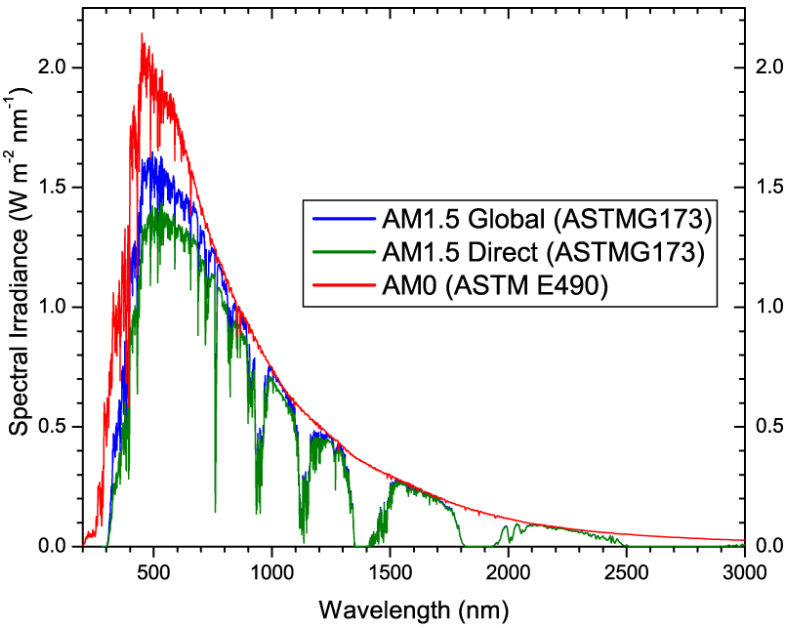

Figure 2.8. Standard Solar spectra for space (AM 0, ASTM E490) and terrestrial (AM 1.5G, ASTM G173)

One of the most important factors in the photovoltaic properties is the solar spectrum used to determine the performance of solar cells. Typically, performance of solar cells is measured by AM 1.5 based by ASTM standard, as shown in **figure 2.8**. The 'Air Mass (AM)' is the path length through the Earth's atmosphere normalized to the shortest possible path length of light, when the sun is directly overhead as shown in **figure 2.9**. The Air Mass defined as:

$$AM = \frac{1}{\cos\theta}$$

where, θ is the angle from the vertical (zenith angle). When the sun is directly overhead, the AM is 1. The AM 0 refers to the extraterrestrial irradiance due to no air mass in space. The efficiency of solar cells is sensitive to changes in the power and spectrum of incident light. Standard spectral and power densities have been defined for radiation in the Earth's atmosphere and surface to assist in accurate comparisons between different times and locations. The standard spectrum of the Earth's surface is called AM 1.5G (G includes both direct and diffuse radiation) or AM 1.5D (including direct radiation only) [26]. The intensity of AM 1.5D radiation can be approximated by reducing the AM 0 spectrum by 28% (18% due to absorption and 10% due to scattering, as shown in **figure 2.10**) 55. The global spectrum (AM 1.5G) is 10% higher than the direct spectrum (AM 1.5D). This calculation provides approximately 970 W/m^2 for AM 1.5G. However, the standard AM 1.5G spectrum has been standardized to provide 1,000 W/m^2 due to the convenience of round number and essentially a change in solar radiation [27].

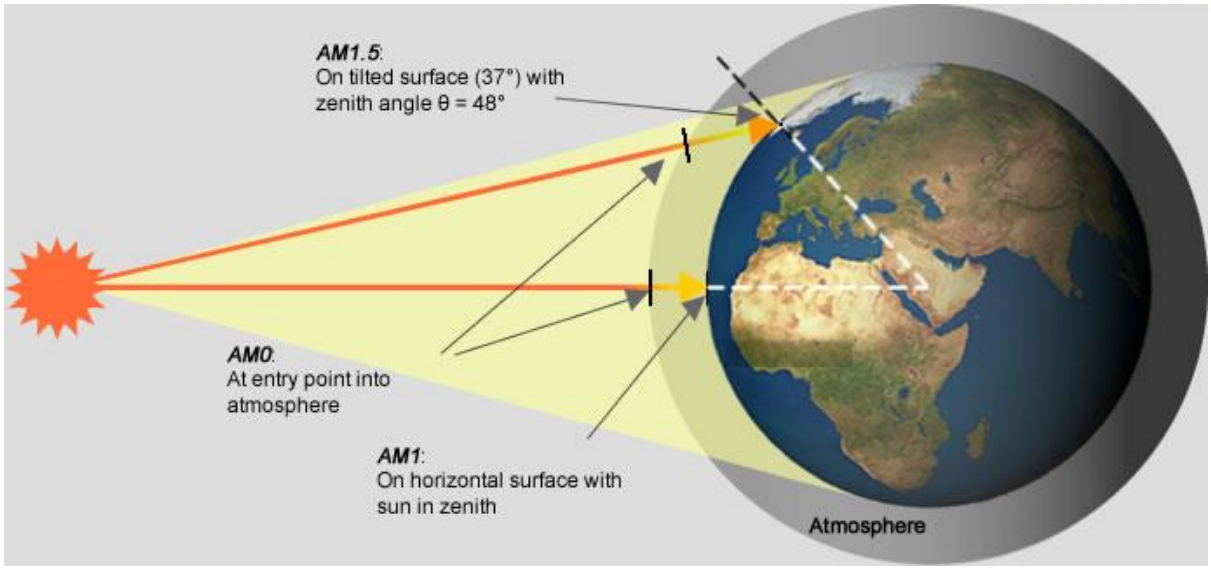

Figure 2.9. The path length change along the zenith angle in the different Air Mass condition.

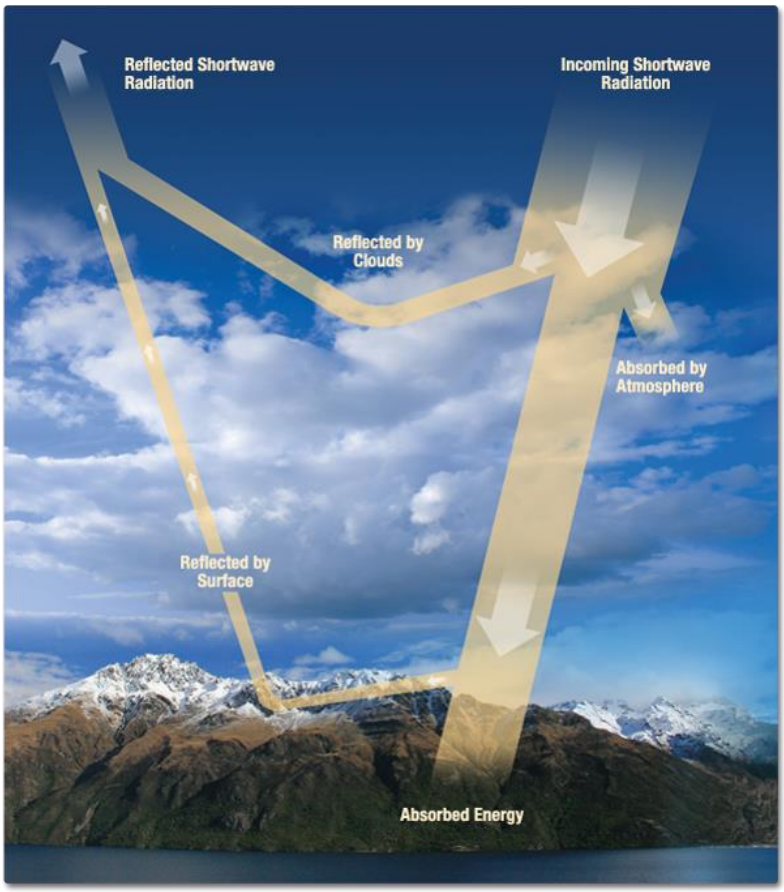

Figure 2.10. The global radiation on the atmosphere and ground.

■ **Characterization of Perovskite Solar Cells**

The device performance of the PSCs is decided by the current density-voltage measurement. The J-V curve of the PSCs is the superimposition of the J-V curve photovoltaic diode in the dark with the light-generated current. The typical J-V curve is calculated under dark and illumination (1.000 kW/m^2) conditions, as shown **figure 2.11**.

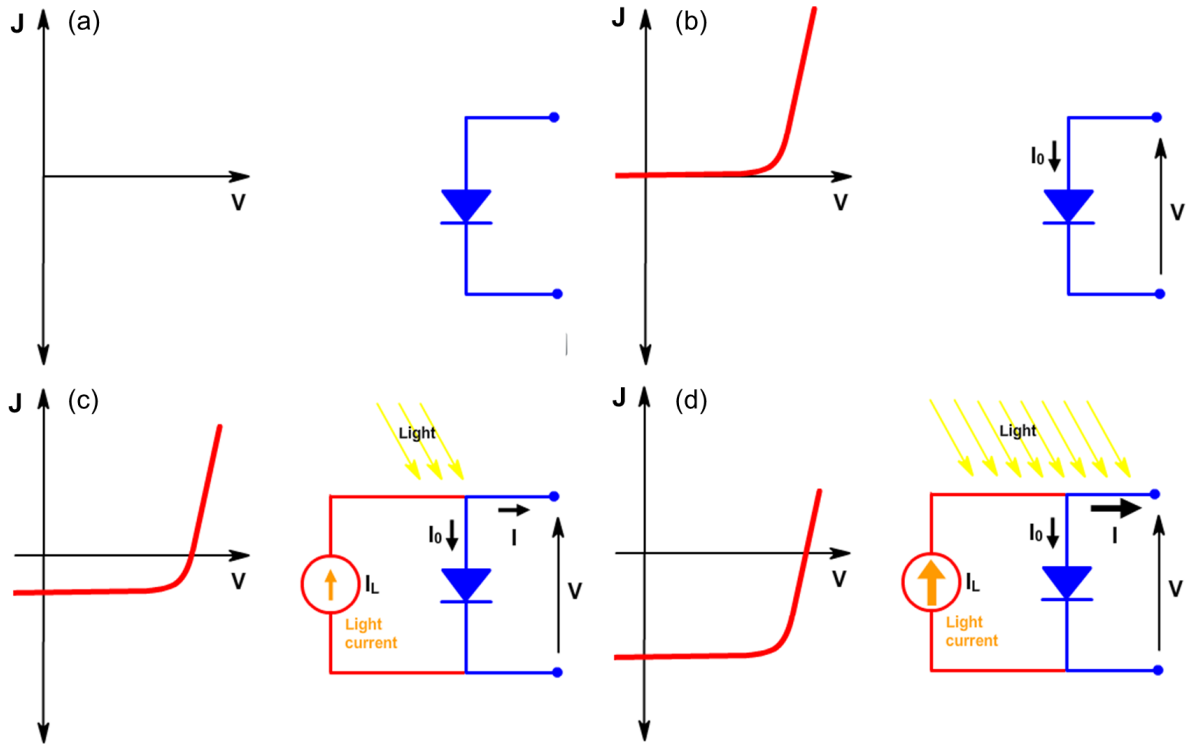

Figure 2.11. J-V curves of PSCs evaluated under dark and illumination conditions.

The light has the effect of moving the J-V curve to the fourth quadrant where power can be extracted from the diode. It goes through the following three steps ((b)-(d)): (a) electrical non connected solar cells, (b) without illumination, a solar cell has the same electrical characteristics as a large diode, (c) when light incident on the cell, the J-V curve shifts as the cell begins to generate power, and (d) the greater the light intensity, the greater the amount of shift until photo-stable state. From J-V curves of PSCs measured under full illumination, the following four factors can be obtained, as shown in **figure 2.12**.

(a) Short-Circuit Current Density, J_{sc}

The short-circuit current is, when the voltage across the solar cell is zero, the current through the solar cell. To remove the dependence of the solar cells area, it is typically used to short-circuit current density rather than the short-circuit current, which is because the generated and collected photo-generated carriers in unit area. For most moderate resistance loss mechanisms, ideal solar cells have the

same short circuit current and photo-generated current. Therefore, the short circuit current is the maximum current that can be drawn from the solar cell.

(b) Open-Circuit Voltage, V_{oc}

The open-circuit voltage is the maximum voltage that can be used in a solar cell, which occurs at zero current. The open-circuit voltage represents to the amount of the forward bias of the solar cell due to the photo-generated current and bias of the solar cell junction. The open-circuit voltage depends on the saturation current of the solar cell and the photo-generated current. The short-circuit current usually has a small deviation, but the important thing is saturation current. This is because the magnitude of the saturation current can be different. The saturation current, I_0, depends on the recombination in the solar cell. Therefore, the open-circuit voltage is an index of the amount of recombination in the device.

(c) Fill Factor, *FF*

The short-circuit current density and the open-circuit voltage are respectively the maximum current density and voltage from the solar cell. however, in both operating points, the power from the solar cell is zero. The fill factor is a parameter that determines the maximum power of a solar cell in conjunction with the open-circuit voltage and the short-circuit current density. Graphically, the fill factor is an index of the squareness of solar cell and is largest area of the rectangle that can fit into the J-V curve. A solar cell having a higher voltage has a larger possible fill factor because the round portion of the J-V curve to take up less area. The maximum theoretical fill factor from the solar cells can differentiate power from the solar cell to the voltage determined by this is to find out where is zero.

(d) Solar Cell Efficiency, PCE, η

The efficiency is a parameter that is most commonly used to compare the performance of solar cells and the other. It is defined as the ratio of output energy from solar cell to input energy from the sun. Besides the reflecting the performance, it depends on the incident angle of the sunlight, intensity of spectrum, and temperature of the solar cell. Therefore, in order to compare the performance between solar cells, it must carefully control the external conditions which the efficiency is measured. Terrestrial solar cells are measured at 25℃ and under AM 1.5 conditions. The PCE of PSCs is defined by the following equation:

$$FF = \frac{J_{MAX} \cdot V_{MAX}}{J_{SC} \cdot V_{OC}}$$

$$PCE, \mu = \frac{P_{max}}{P_{in}} \times 100 = \frac{J_{MAX} \cdot V_{MAX}}{P_{in}} \times 100 = \frac{J_{SC} \cdot V_{OC} \cdot FF}{P_{in}} \times 100\ (\%)$$

2.2.2.2. Consideration of Characterization of Perovskite Solar Cells

Furthermore, a series resistance, R_s, and a shunt resistance, R_{sh}, can be added to the equivalent circuit of solar cell to explain the resistance losses. An equivalent circuit of the solar cells with the parasitic resistance is shown in **figure 2.13**. In the the presence of both series and shunt resistances, the J-V curve of solar cell is described by the following equation [28]:

$$J = J_{ph} - J_0\left[exp\left(\frac{q(V + JR_s)}{nkT}\right) - 1\right] - \frac{V + JR_s}{R_{sh}}$$

where, J_{ph} is photo-generated current density, J_0 is reverse saturation current density, n is ideality factor of a diode, k is Boltzmann's constant, q is elementary charge. Likewise, PCE of the PSCs is mainly depending on the saturation current density, J_0, and parasitic resistance, R_s and R_{sh}. The resistance effect of the solar cell reduces the PCE of PSCs by dissipating power in the resistance. In most cases, the main effect of parasitic resistance, on the typical values of shunt and series resistance, is to reduce the fill factor. The size and impact of series and shunt resistors depends on the geometry of the solar cell at the operating point of the solar cell.

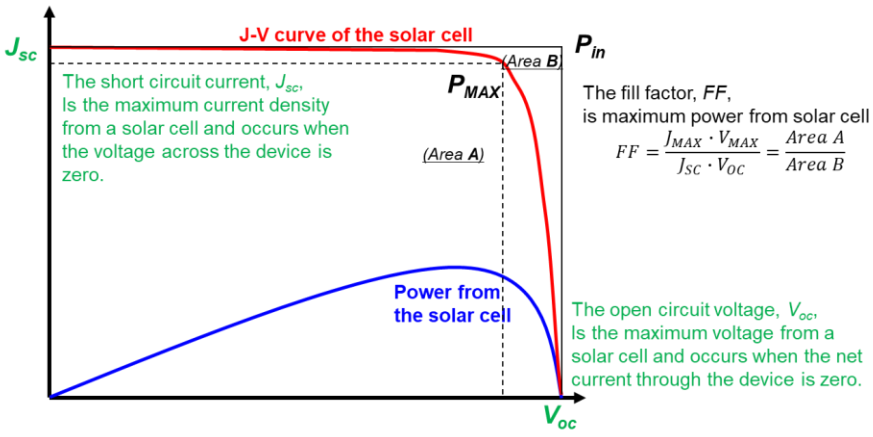

Figure 2.12. Typical J-V curves of PSCs.

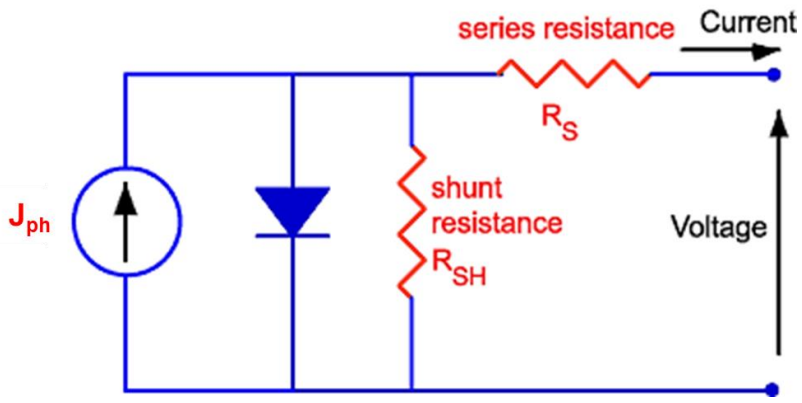

Figure 2.13. Parasitic resistances (series and shunt) in a solar cell circuit.

In addition, one of important factor of measuring PCE is quantum efficiency, which is the ratio of the number of collected carriers in the photovoltaic devices to the number of photons in the energy give to the photovoltaic devices. The quantum efficiency can be provided as an information of wavelength or energy. If all photons of a specific wavelength are absorbed, resulting minority carriers are collected, the quantum efficiency at that particular wavelength is one. The quantum efficiency of the photon having energy less than the bandgap is zero. Two type of quantum efficiency of the solar cell are existed: the external quantum efficiency (EQE) and the internal quantum efficiency (IQE).

The external quantum efficiency (EQE) is the ratio of the number of collected charge carriers by the solar cell to the photon incident from the outside.

$$\mathrm{EQE} = \frac{electons\ /\ sec}{photons\ /\ sec} = \frac{current\ /\ charge\ of\ one\ electron}{total\ power\ of\ photons\ /\ energy\ of\ one\ photon}$$

The internal quantum efficiency (IQE) is the ratio of the number of charge carriers collected by the solar cells to the photons absorbed from the solar cell.

$$\mathrm{IQE} = \frac{electrons\ /\ sec}{absorbed\ photons\ /\ sec} = \frac{EQE}{1 - Reflection - Transmission}$$

The EQE is always lower than the IQE because EQE includes the effects of the optical losses such as reflection and transmission. The difference of EQE and IQE is important to draw a distinction of loss mechanism between the light absorption properties of the entire solar cell and the light conversion properties of the absorber materials. EQE also presented to as incident photon-to-electron conversion efficiency (IPCE), while IPCE is measured with a potentiostatic measurement. The IPCE is described by the following equation [29]:

$$\mathrm{IPCE}\ (\lambda) = \frac{electrons\ /\ cm^2/\ sec}{photons\ /\ cm^2/\ sec} = \frac{J_{ph} \times 1239.8\ (V \cdot nm)}{P_{mono} \times \lambda}$$

Where, 1239.8 V·nm represents a multiplication of Planck's constant, h, and the speed of light, c, P_{mono} is the intensity of calibrated and monochromated illumination power, λ is the wavelength where power of this illumination is measured. Therefore, the IPCE spectrum is proportional to the J_{sc} of the solar cell devices [30].

2.2.3. Benign Properties of Perovskite Solar Cells

2.2.2.1. Advantages of Perovskite Solar Cells

■ Unique Defect Physics

The perovskite solar cells have advantages about excellent defects tolerance. According to first-principle calculation study, the dominant intrinsic defects generate only shallow fermi levels, which is consistent with the long charge diffusion lengths and small loss of open-circuit voltage. Furthermore, it is observed that self-doping mechanism. By change ratio of MAI and PbI_2, p-doped character shown in MAI rich perovskite, whereas n-doped character shown in PbI_2 rich perovskite.

■ High Light Absorption Coefficient and Low Urbach Energy

Perovskite materials are direct bandgap semiconductors with a higher light absorption coefficient than other solar cells in photovoltaic spectrum, as shown in **figure 2.14**. For this reason, perovskite materials effectively reduce thickness of light absorption materials down to below 500 nm. The ideal bandgap of $MAPbI_3$ is calculated to be 1.7 eV by the many-body perturbation theory, which is different from the empirical bandgap value of 1.6 eV. The Shockley-Queisser efficiency limit model predicts that 1.6 eV is very close to the ideal band gap value (1.1 to 1.5 eV) for single junction solar cells under AM 1.5G sunlight irradiation.

Particularly from the rapid onset of absorption, $MAPbI_3$ perovskite materials are revealed a lower Urbach energy of 15 meV, suggesting that $MAPbI_3$ is pure semiconductor with no deeper trap density. All of these remarkable semiconductor properties facilitate the high-performance photovoltaic cell has a high open-circuit voltage and fill factor.

■ Bandgap Tuning in Perovskite Materials

$MAPbI_3$ is a possible candidate for tandem cells due to their bandgaps can be tuned wide spectrum range. Bandgap tuning is performed by compositional substitution in A, B, and/or X site in chemical formula ABX_3. Although halide substitutions (X) have been intensively studied, the mechanism of bandgap tuning through substitution of A and B site is not well known [31, 32]. Two competing mechanisms have recently been identified for the A site cation to affect the bandgap of perovskite materials. In two different perovskite materials, the larger formamidinium (FA, $HC(NH_2)_2$) was replaced by smaller cesium (Cs) and the opposite effect on the bandgap was observed. As a result,

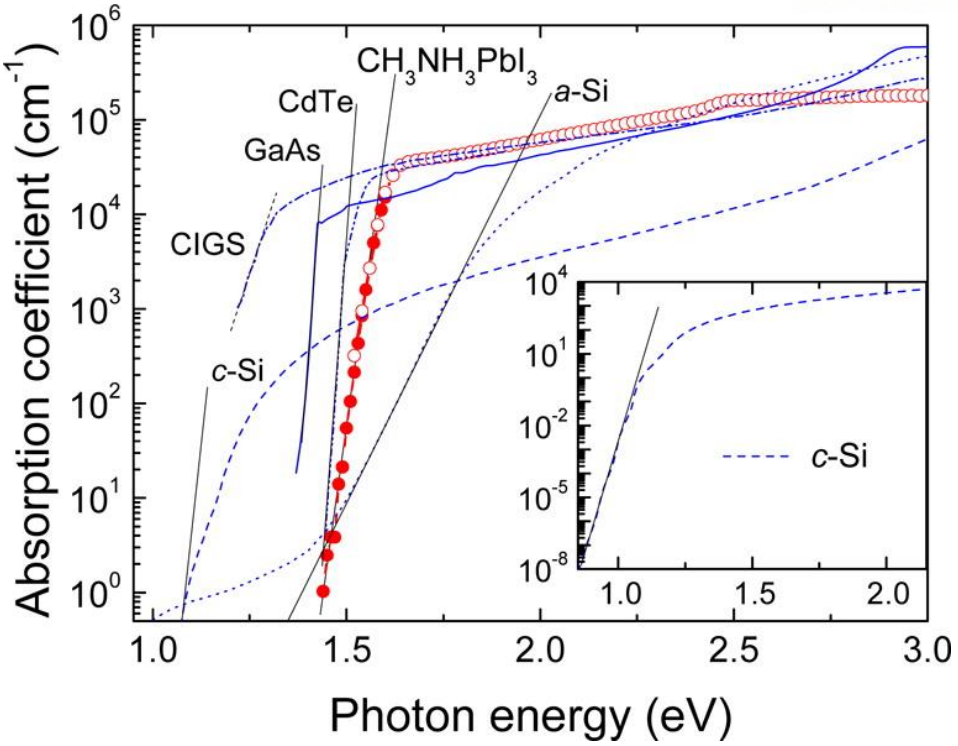

Figure 2.14. Effective absorption coefficient of various photovoltaic materials, resulting a sharp edge of absorption and high absorption coefficient for $MAPbI_3$. Reprinted with permission from [33]. Copyright 2014 Springer Nature.

substitution of Cs for A site in formamidinium tin iodide ($FA_{1-x}Cs_xSnI_3$) showed a decrease in bandgap, whereas, substitution of Cs for A site in formamidinium lead iodide ($FA_{1-x}Cs_xPbI_3$) was observed to increase the bandgap. This was done by performing grazing incidence x-ray diffraction (GIXD) measurements on SSRL Beam Line 11-3 and found that the perovskite crystal structure reacts differently to existence of Cs in these two materials. At Cs-substitution, the tin-based perovskite maintains a cubic structure, and the detected change is the isotropic shrinkage of the lattice only. However, in the lead-based perovskite, new x-ray diffraction (XRD) peaks are detected, indicating that the BX_6 octahedron is tilted besides the lattice contraction. According to electronic structure calculations, valence band maximum (VBM) of these materials is sensitive to B-X orbital overlap because antibonding orbital is formed with s orbitals for metal and p orbitals for halide [34]. This indicates that different bandgap responses observed in tin-based and lead-based perovskites. The former case, the antibonding VBM is stabilized and bandgap is decreased because orbital overlap increased by lattice contraction. The latter case, whereas, antibonding VBM is destabilized and bandgap is increased because orbital overlap decreased by octahedral tilting. Direct band energy measurements using ultraviolet and X-ray photoelectron spectroscopy (XPS) support this concept. The competitive effects of octahedral tilt and lattice shrinkage defined in this study provide a new insight for expertly tuning the bandgap of various perovskite materials.

■ **Long Charge Diffusion Length**

Compared to other semiconductor devices, perovskite material shows long charge diffusion length with ~175 μm in single crystal $MAPbI_3$, making them well suited for use in high performance solar cells. Hole mobility of 100 $cm^2/V{\cdot}s$ or greater was obtained in the SCLC and Hall effect measurement. Likewise, electron mobility of ~24 $cm^2/V{\cdot}s$ was verified by SCLC and time-of-flight measurement. The excellent coincidence of hall mobility with time-of-flight and SCLC in a single crystal indicates that the band-tail states are negligible [35].

Therefore, the carrier diffusion length of the perovskite, which is very different from the organic semiconductor, is sufficient to enable planar heterojunctions with charge-selective interfaces. This allows perovskite to be directly coupled between p-type and n-type interfaces, which form very simple planar n-i-p or p-i-n device architectures with performances comparable to the mesoporous structures. Then, planar perovskite solar cell is not only an excellent light absorber that harvests solar radiation until 800 nm, but also remarkable delivery factor of holes and electrons.

■ **Low Costs**

The high-quality perovskite crystals can form at low temperature, below 140℃, due to the low energy barrier to crystal formation. The low temperature process provides the scalability of this technology when large-area modules are required at faster print speeds in roll-to-roll process [36]. As a result, material and manufacturing cost are greatly decreased, but high performance can be sustained. All of this makes perovskites a low-cost semiconductor that could never be seen in other low-cost semiconductors (GaAs, Si, CdTe, etc.).

2.2.2.2. Limits of Perovskite Solar Cells

■ Hysteresis in Current-Voltage Behavior

One of the important factors of PSCs is that voltage-current scans produce uncertain PCE values. The PCE of the photovoltaic devices is commonly measured by the current-voltage (IV), or current density-voltage (JV), behavior under artificial solar illumination. The perovskite solar cell is different from the other solar cell devices, which has been observed hysteresis in current-voltage behavior that is depended on scanning conditions, such as scan direction, speed, light soaking, and biasing. It is including scanning from forward bias to short circuit (FB-SC) and from short circuit to forward bias (SC-FB). Numerous causing factors, such as polarization, ferroelectric effect, ion migration, and trap state filling, have been suggested, but the exact origin of hysteresis has not been determined yet [37]. However, determining the solar cell efficiency from the I-V curve appears to be at risk of generating an inflated value when the scanning parameters excess the time-scale required by the perovskite system for reaching the electronic steady-state. Two solutions have been developed, namely an extremely slow voltage scan and the introduction of a new indicator 'stabilized power output'. Both methods have been proven to provide lower PCE values than PCE values determined by faster scan. However, early studies have been posted the surface passivation of perovskite absorbing materials can stabilize the efficiency value very close to the face scan efficiency. These reports suggest that little or no-hysteresis is observed in the 'inverted structure' with a transparent cathode [38]. This means that the main difference between the inverted structure and conventional structure is that the interface can play important role in terms of hysteresis I-V behavior in that organic n-type contact is used replacing the metal oxide.

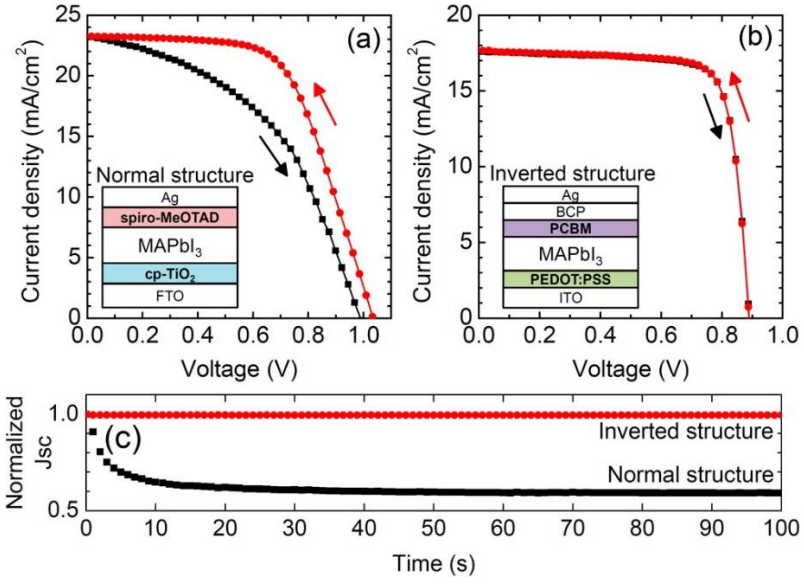

Figure 2.15. J-V hysteresis and time-dependent photocurrent of two-type perovskite solar cell structures. Reprinted with permission from [39]. Copyright 2015 American Chemical Society.

■ **Long- / Short-term Stability in Perovskite Solar Cells**

The biggest challenge with PSCs is the long-term and short-term stability aspects. This instability of PSCs is mostly because environmental effects (H_2O, O_2) [40, 41], thermal effects (intrinsic stability) [42], heating under applied voltage, optical effects (UV) [43], and **mechanical fragility**. Several studies have been accomplished on the stability of PSCs and some of the important factors in the stability of PSCs have been proven. However, the PSCs does not have a standard 'operational' stability protocol. But a method has recently been proposed for quantifying the intrinsic chemical stability of perovskite materials.

The water-soluble organic component of perovskite absorbing materials leads to rapidly degrade the device in humid environment. Water is strongly reacting to common perovskite materials for PSCs [44]. In typical perovskite materials, $MAPbI_3$, when films are exposed to humid air, resulting in decomposition into solid PbI_2 and CH_3NH_2 ion, and HI [45, 46]. This decomposition process is permanent reaction and causing severe breakdown on devices. Degradation caused by moisture, can be overcome by optimizing the functional materials, cell structure, interfaces and environmental conditions during the fabrication steps. The substitution of smaller Br atom for larger I atom would decrease lattice constant and the lattice changes into tetragonal to cubic structure, so that the Pb-Br bond becomes more difficult to break than the Pb-I bond [47]. Encapsulation methods for the perovskite materials with the carbon nanotube composites and the inert polymeric matrix have been demonstrated to prevent immediate degradation of the materials during exposed humid atmosphere at elevated temperatures. Another possible route for stability is to change organic cations. Formamidinium (FA, $HC(NH_2)_2^+$) with slightly lager ionic radius, can be used to replace methylammonium (MA, $CH_3NH_3^+$) [48, 49]. It was found that $FAPbI_3$ exhibits excellent thermal stability. The theoretical mechanism may be due to an increase in the number of hydrogen bonds between the hydrogen atoms of cations and iodide ions [50]. Apart from the perovskite layer, other components of device also affect degradation of device. In general, PEDOT:PSS, which used as hole-transfer layers, damages ITO electrode and decomposes the perovskite layer due to its own acidity and hygroscopicity [51]. To prevent this, various attempts have been made to develop a new HTL or to add a GO in PEDOT:PSS [52]. In addition, studies are being conducted to prevent the influence of external environment in advance by using encapsulation [53-55]. Furthermore, it has been found that embodiments of the apparatus wherein the mesoporous TiO_2 layer is sensitized with a perovskite materials exhibit instability caused by UV light. The cause for the observed degradation in performance of PSCs is related to the interaction between photo-generated holes inside the TiO_2 and oxygen radical on the interface of TiO_2. This can be solved simply by replacing TiO_2 to another ETL.

Due to development of interface engineering, 2D/3D mixed perovskite, which enable the fabrication of the PSCs over 10,000 hours (more than 1 year) stable performance without degradation,

point towards the viability of commercialization. Likewise, there has been rapid studied in long-term stability issues, but precious few theoretical and experimental studies have been reported on mechanical properties. To commercialize, especially flexible devices, reasonable comprehension of mechanical response is urgent priority due to stress state has affect strongly on the device performance and reliability, but it is still the unknown waters in intrinsic mechanical reliability.

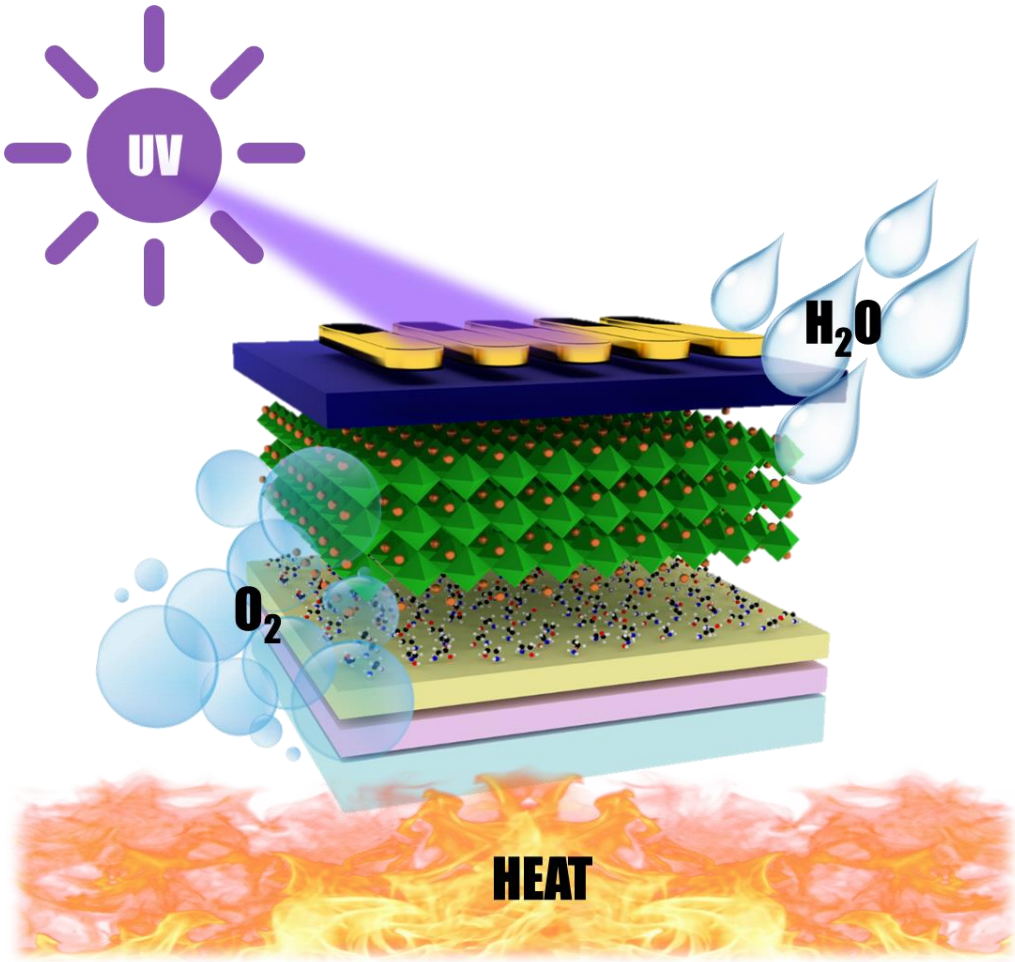

Figure 2.16. Environmental factor affecting on degradation of perovskite solar cells.

2.3. Mechanical Reliability of Perovskite Solar Cells

2.3.1. Previous Studies for Mechanical Reliability

As mentioned above, the value of the perovskite solar cell as a next-generation solar cell is endless. There are some issues to be solved, hysteresis and stability, but they are nearly complemented by many previous studies. However, because materials are easily damaged in the air and sampling for mechanical experiments is difficult, studies on mechanical damage or durability are still lacking both qualitatively and quantitatively. A brief review of these areas will discuss what more needs to be done.

2.3.1.1. Mechanical Testing Methods

In order to measure the mechanical reliability, it is necessary to establish the preparation and test method of test specimens. In the case of perovskite material, since the materials are easily decomposed in atmospheric environment and phenomenon occurs, and a very thin film is produced through the solution process, there is a difficulty. Therefore, the research using nanoindentation technology was the most preferred for the experimental method that can easily measure the mechanical properties. In order to perform nanoindentation experiments [56-59], single-crystal perovskites ($MAPbI_3$, $MAPbBr_3$, and $MAPbCl_3$) of several mm size were precipitated by solution-growth method. In the previous studies using DFT simulation [60], the anisotropy tendency of perovskite materials, especially $MAPbI_3$, was measured and the elastic modulus and hardness were measured by performing nanoindentation for different crystallographic directions. As a result, the elastic modulus was measured in the order of perovskite using $E_{Cl} > E_{Br} > E_I$, and on the contrary, the hardness was measured as the tendency of $H_I > H_{Br} > H_{Cl}$. The tendency of the material's stiffness, i.e. elastic modulus, can be attributed to three reasons: (i) the bond strength of Pb-X, (ii) the packing density, and (iii) the hydrogen bonding between the halide ion and MA^+. The atomic radius decreases in the order of Cl > Br > I, and as a result, a close-packed lattice structure is formed. In the case of hardness, whereas, H_{Br} and H_{Cl} is showing similar values. The reason for this is that tetragonal structure in case of I-based perovskite at room temperature and cubie structure in case of Br- and Cl-based perovskite at room temperature. Generally, since the number of slip system of tetragonal structure is smaller than that of cubic structure, this is because dislocation propagation is reduced [56].

In another study, $CsPbBr_3$ was further tested to investigate the effect of cations on mechanical properties through nanoindentation. A comparison between $MAPbBr_3$ and $CsPbBr_3$ confirmed that the organic groups make the overall structure stiffer (higher elastic modulus). However, in the previous study, the (100) direction of $MAPbBr_3$ is stronger than the (110) direction, so that there is also a difference in the crystallographic direction between crystals. Therefore, the similarity between the modulus of elasticity of PbI_2 (c-plane) and $MAPbI_3$, the elastic modulus of $PbBr_2$ and the elastic

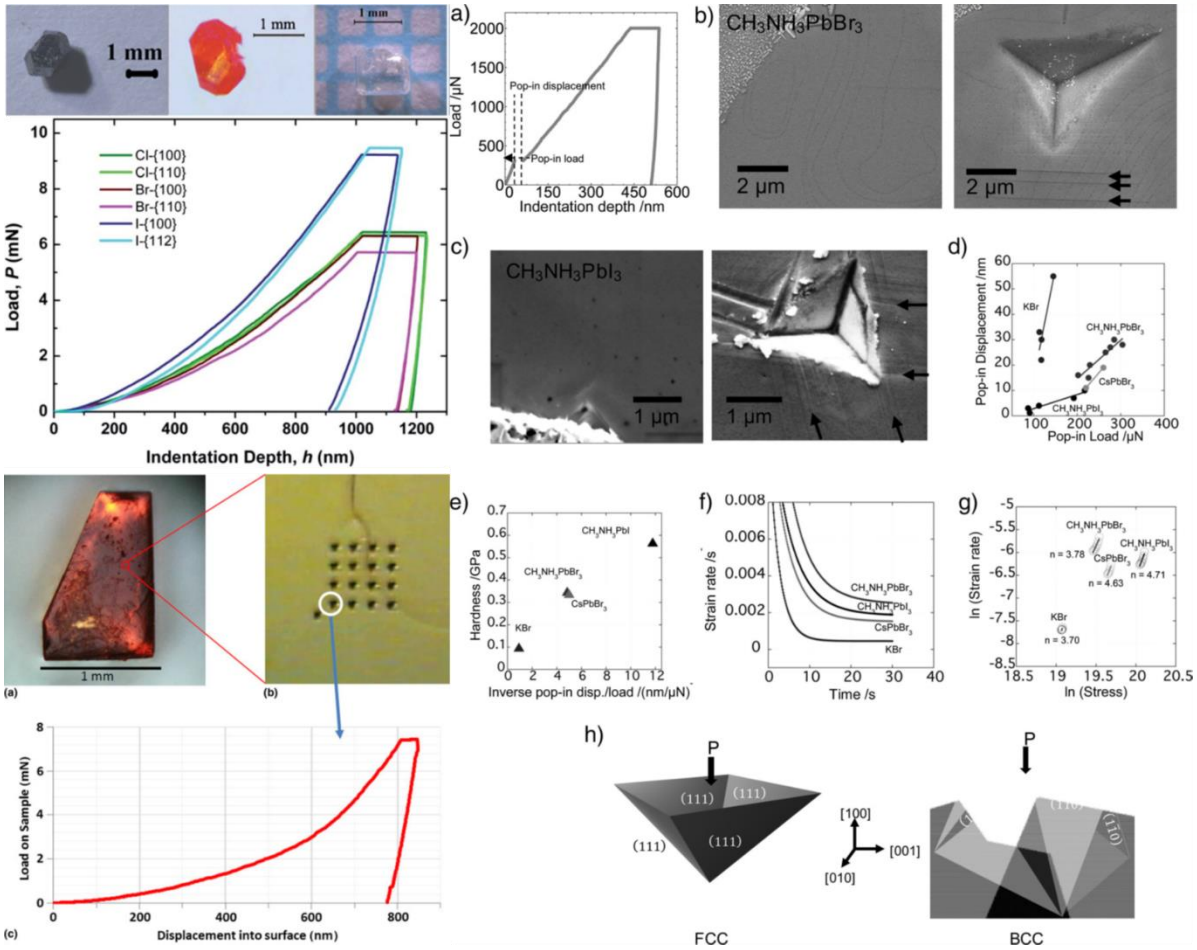

Figure 2.17. Various experimental results using nanoindentation techniques. Reproduced with permission from [56-58]. Copyright 2015 Royal Society of Chemistry, Copyright 2015 Materials Research Society, and Copyright 2017 John Wiley and Sons.

modulus of $APbBr_3$ is dominated by the Pb-X framework [57].

The bulk-to-shear modulus ratio (B/G, ductility index) can be obtained through the ratio of the bulk modulus (B) and the shear modulus (G) obtained by some experimental and computational methods. Perovskite materials have a ductility index of 1.75 or more, regardless of crystal structure. This material has high ductility. Therefore, in order to understand plastic deformation, time-dependent creep behavior was also studied through nanoindentation. The Time-dependent creep behavior and stress relaxation provide an understanding of strain-hardening and response time under constant force/deformation and strain response of different rates of deformation. This dynamic mechanical behavior is critical to design of the device structures for strain-induced application and reveals the limits that can arise from scalable processing with different degrees of deformation. By analyzing the time-dependent behavior of various perovskites ($APbX_3$, A=MA, Cs, X=I, Br), it can see that organic cations have little effect on time- and rate-dependent plastic deformation, and Pb-X frame work is more important. The elastic and viscous properties of a perovskite single crystal can be determined by

modeling creep and relaxation effects using rheological component. Materials with low hardness crystals are expected to creep under the conditions used. The rate-dependent mechanical properties can have a major influence on this material is handled on a large-scale. The reasonable understanding of the effects of plastic deformation on the performance of PSCs is needed for practical applications in flexible devices. Nanoindentation also presents various mechanical properties such as the result of predicting the physical properties of the 2D perovskite material through the indentation test and the method using the spherical indentation [58].

2.3.1.2. Computational Studies

Electrical, optical and crystallographic studies on organic and inorganic halide perovskite materials have been carried out. Through the first principle, the electrical and optical properties of perovskite materials were determined by the calculation method. As a result, it was confirmed that the optical absorption ability was superior to other semiconductor materials. It is very important to measure mechanical properties because the light absorption ability is greatly affected by crystallinity and stress state. However, since it is difficult to measure the mechanical properties of the combination perovskite of various ions in a practical experimental manner, the anisotropy and elastic properties, such as bulk/shear/elastic modulus and Poisson' ratio, etc., of the perovskite crystal were calculated using the first principle based on the density functional theory. As a result, it was confirmed that the elastic properties are determined by the type and strength of the B-X bonding, and the effect of the interaction between organic and inorganic ions has negligible. The calculated result is that the modulus of Br-based material is greater than that of I-based material, the modulus of Sn-based material is greater than that of Pb-based material, and the effect of phase on elastic modulus is unclear. It is believed that the different electronic properties, ionic radius and electronegativity of B^{2+} and X^{-} ions are essential to cause such an observation. The ductility index, ratio of B/G, and Poisson' ratio show that these perovskite materials can be used in compliant devices requiring larger deformations. The main reasons are the lower shear modulus due to heavy anisotropy. The results show that these perovskite materials can be used on flexible polymer substrates due to their "soft nature" and that bandgaps are possible to adjust in strain-induced applications [60].

There is a limit to the comparison of mechanical properties, especially fracture properties, from the various interactions between atoms. Despite the progress of research through nanoindentation and DFT simulation, it is still unclear whether the fundamental understanding and quantification of mechanical properties and fracture mechanisms. Since it is difficult to experimentally perform tensile tests with current technology and DFT simulation is only possible with a scale of below 10 nm, large-scale MD simulation can be used to measure mechanical properties such as fracture toughness and

fracture toughness. To investigate deformation and fracture mechanisms of perfect and notched $MAPbI_3$ using atomic simulation and solid mechanics theory. Based on the three-dimensional surface contours of the elastic modulus of $MAPbI_3$, the tetragonal and orthorhombic phases demonstrate strong elastic anisotropy. Whereas that cubic phase exhibit higher symmetry contributes to weak elastic anisotropy. The simulation result for the initial $MAPbI_3$ is good agreement with nanoindentation results. Furthermore, mechanical properties of polycrystalline $MAPbI_3$ with different grain size measured by MD simulation, the elastic modulus and yield and fracture strength of polycrystalline $MAPbI_3$ were lower than single crystalline. Furthermore, inverse Hall-Petch relationship, yield stress increases along increasing grain size, was revealed in px-$MAPbI_3$. In addition, they show longer yield region during tensile stress states and nanoductility is caused by amorphization process. The plastic deformation regions were presented after the elastic deformation. The stress value after yielding maintains non-zero up to a large plastic deformation region (strain), indicating strong Coulombic attractions between the separated ion components. The measured elastic modulus and fracture toughness indicate that the hybrid perovskite is relatively soft and prone to failure, and mechanically similar to reinforced polymers and glass ceramics. Localized edge dislocations were detected in the vicinity of the crack tip, an observation limited brittleness and significant plastic behavior is due to the nanoductility of the ionic $MAPbI_3$ crystals. Particularly, dislocation slip has cause forming of nanovoids, and limited brittleness is occurred by the increasing nanovoids and its migration. The plastic deformation is mainly due to the expansion of each nanovoids and the merging of neighboring nanovoids. These coarsened nanovoids are gradually

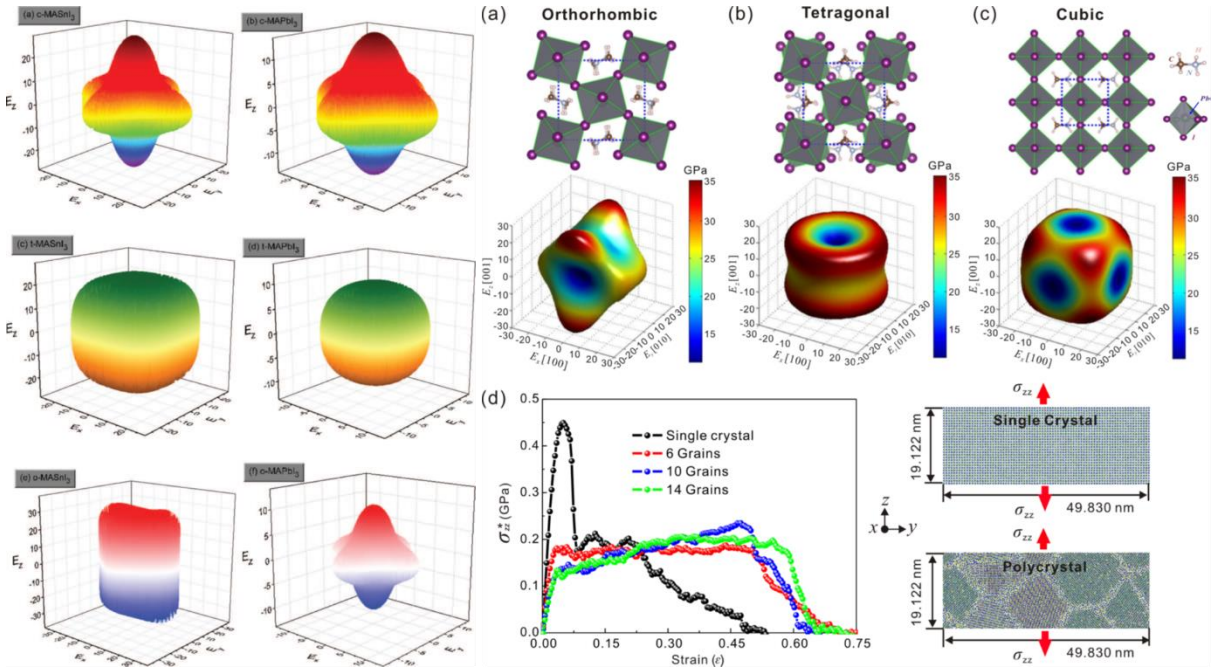

Figure 2.18. Various computational results using DFT, MD, and MM simulations. Reproduced with permission from [60, 61]. Copyright 2014 AIP Publishing, and Copyright 2016 American Chemical Society.

merged and the separated crystalline material, which occurred by crack (merged voids), are connected or retained by ionic bonds only. Completely, the crack propagates near the tip of the crack as some ionic chains begin to collapse and occur failure [61].

2.3.2. Flexible Perovskite Solar Cells

2.3.2.1. Suitability of Flexible Solar Cells

Table 2.1. Cubic phase-transition temperature of various perovskite materials.

Materials	Temperature, K	Materials	Temperature, K
$CH_3NH_3PbCl_3$	~ 179	$HC(NH_2)_2PbI_3$	~ 360
$CH_3NH_3PbBr_3$	~ 237	$CsPbBr_3$	~ 403
$CH_3NH_3PbI_3$	~ 327	$CsPbI_3$	~ 589

Recently, thin PSCs hold promising for flexible solar cells because of light-weight, portability, and low temperature process below 150℃. The phase-transition temperature of various perovskite materials is shown in **table 2.1** [62, 63]. The stable cubic phase is commonly obtained at relatively lower temperature than fully inorganic perovskite materials. It means that organic-inorganic perovskite materials are more adaptable with flexible devices comparing with fully inorganic perovskite materials. Furthermore, annealing temperature of perovskite materials after spin-coating is lower than fully inorganic perovskite materials with under 150℃. The low-temperature crystallization is first reason for promising candidate of flexible device of PSCs.

Secondly, to fabricate of flexible PSCs, mechanical properties of perovskite materials have to consider in flexibility. Based on previous study, which used to first principles, expected the flexibility of various perovskites, which are evidenced by B-X bonding and ratio of bulk to shear modulus of perovskite materials [60]. This study aimed to the ratio of bulk to shear modulus is larger than 2.0, it means that perovskite materials bear various deformation state under external stress, such as tensile, compressive, and flexure, etc. In other words, the conclusion that it can be drawn from a larger B/G ratio is possible to fabricate thin absorbing layers operating at room temperature. Furthermore, larger Poisson' ratio with over 0.3 is larger than Poisson' ratio of common ductile materials (> 0.26) also indicated their suitable flexibility.

Thirdly, organic-inorganic perovskite materials are easily dissolved in polar solvents [64-66], it allows fabricated high-quality thin films via simple solution process. The point that such a uniform thin film can be produced easily makes it possible to fabricate a flexible device while minimizing the performance decrease even in a fluctuating flexible substrate.

Lastly, perovskite materials have high light adsorption coefficient, it means that perovskite materials can be fabrication with thinnest thickness without performance decreasing. And, therefore, flexible PSCs can accomplish high power-per-weight ratio, which is prerequisite for special applications.

2.3.2.2. Stability of Flexible Perovskite Solar Cells

■ Mechanical Stability

Generally, Indium Tin Oxide (ITO) coated flexible polymeric substrate is replace as bottom electrode and substrate instead of rigid ITO coated glass substrate. The major demerits of ITO coated the flexible polymeric substrates as compared to glass substrates are their lower conductivity, transmittance and poor mechanical stability [67, 68]. There is widely notified that common flexible polymeric substrates get damaged at high temperature over 250℃. Accordingly, all fabrication processes have to be carried out at low temperature, but it is occurring low resistance of ITO (over 20 Ω sq^{-1}) [69]. To complement low conductivity, thick ITO coated onto substrates for improving conductivity. Actually, the thickness of commercial ITO on flexible substrates are thicker than 350 nm, whereas ITO on glass is nearly 150 nm. The thicker ITO-coated flexible substrates have lower photovoltaic performance due to low transmittance.

A flexure of substrate after device fabrication usually results in a performance loss. As a result, PCE of the flexible PSCs is lower than rigid PSCs. On the other hand, bending durability is significant factor in flexible PSCs. Many studies of flexible perovskite solar cells have evaluated mechanical degradation using repeatable bending tests and then measuring decreasing PCE [70-73]. However, using metal oxide electrode, such as ITO, FTO, etc., on flexible substrates have several disadvantages as degradation of device performance due to severe cracking in metal oxide electrode during the repeatable bending tests [70].

Furthermore, flexible polymeric substrates, such as PET, PEN, are hindered high-quality ETL materials, such as compact TiO_2, due to its low glass transition temperature. Therefore, to solve these issues, many studies of flexible PSCs have complemented the bottom electrode through using flexible composite electrode, such as AgNWs, graphene, conductive polymer, etc. Moreover, to solve large hysteresis of PCE during reverse and forward scanning, many studies used newly HTL and ETL, and inverted structure of devices because processing temperature of most HTLs are lower than ETLs [74].

Nevertheless, there are many such improvements, but direct research into the flexibility of flexible PSCs has yet to be conducted. The reason for this is that mechanical properties data and measurement techniques of the components are insufficient to directly derive the flexibility and it is very challenging to measure the mechanical properties experimentally because the perovskite material is easily decomposed in the atmosphere.

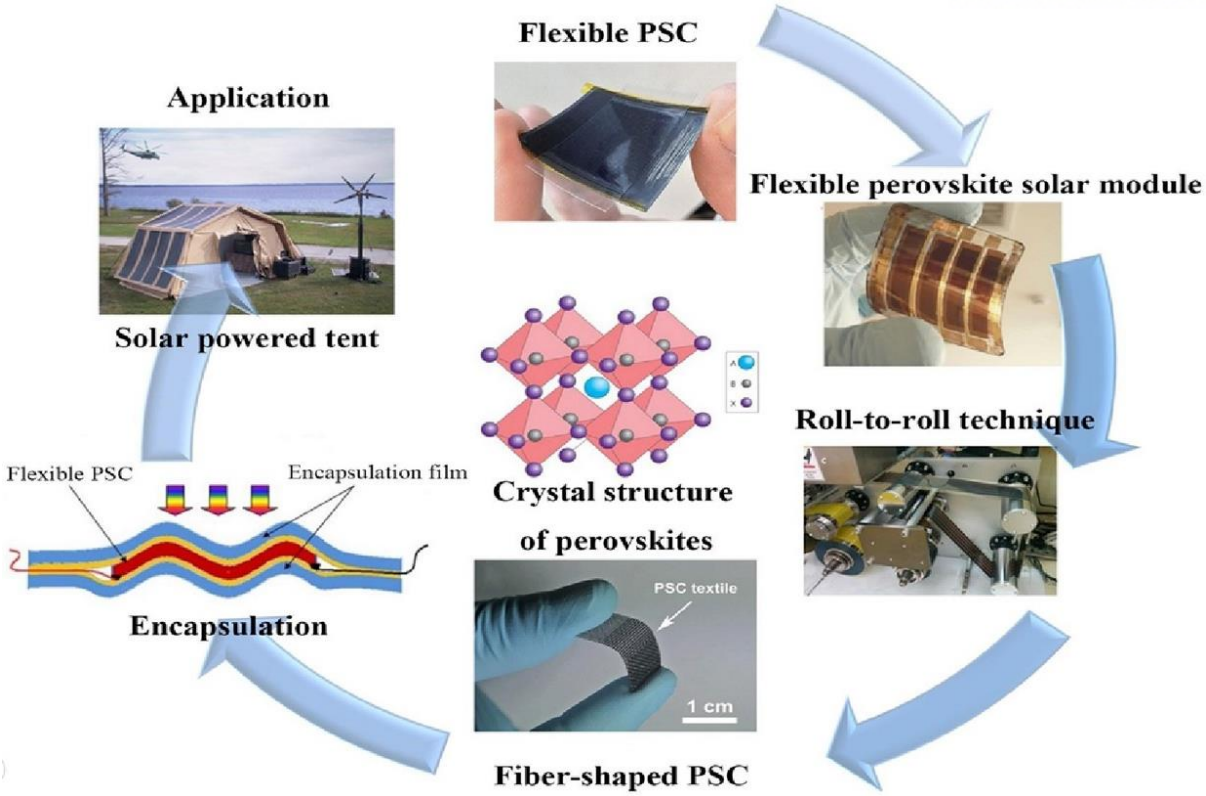

Figure 2.19. The development of flexible perovskite solar cell devices for various special application. Reprinted with permission from [75]. Copyright 2018 Elsevier.

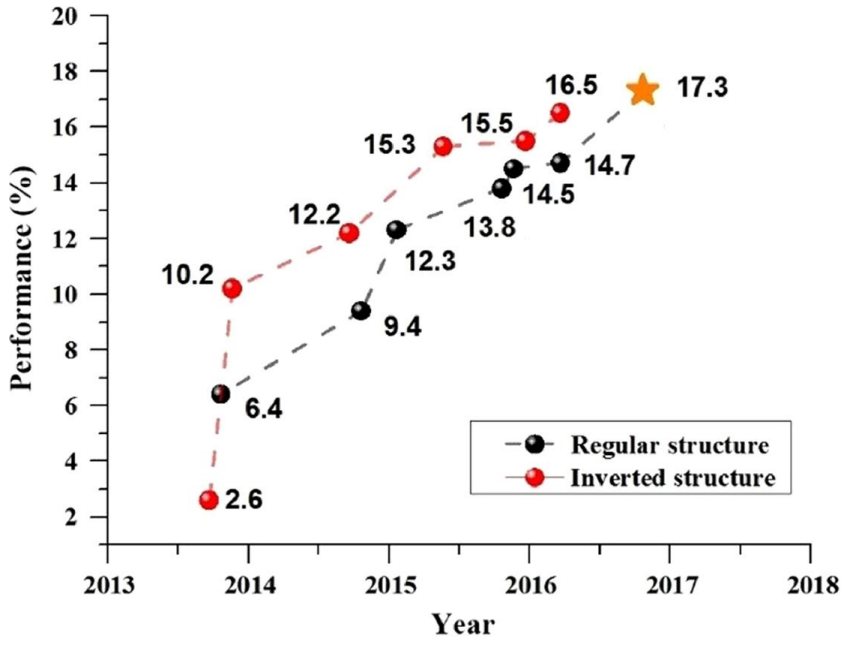

Figure 2.20. The performance evolution of flexible PSCs until 2017. Reproduced with permission from [75]. Copyright 2018 Elsevier.

■ **Environmental Stability**

Long-term environmental stability is an important criterion for practical solar cell devices evaluation. Unfortunately, PSCs remain a challenge to so far. In general, weak stability of PSCs is derived by the instability of HTLs and degradation of PSCs. The spiro-MeOTAD, PTAA, PEDOT:PSS are commonly used as HTLs in flexible PSCs due to easy fabrication in low temperature. To enhance conductivity and to improve device performance, some additive is used in HTLs [75]. Nevertheless, perovskite materials are corroded and degraded by some additives [76, 77]. Furthermore, hydrophilic PEDOT:PSS is causing instability in flexible PSCs, and hurt to perovskite materials due to its acidity [78]. Therefore, stable HTLs developed at low temperatures, such as NiO, Cul, P3HT, etc., have been replaced the common HTLs. The performance and stability of flexible PSCs have been enhanced using replacing HTLs [79-82].

Furthermore, perovskite materials are highly susceptive to moisture, UV radiation and oxygen, occurring degradation and phase-transition in flexible PSCs. Especially, commonly used $MAPbI_3$ is decomposed to PbI_2 and MAI even it is exposed to normal atmosphere due to breaking hydrogen bonding between organic and inorganic ions [83]. While $FAPbI_3$ undergoes a phase transition from black α-phase to yellow δ-phase. While many studies have been complementing the materials itself, encapsulation technique is an essential tool to isolating sensitive devices from corrosive environments. In flexible PSCs, encapsulation methods are huge challenge because polymer-based substrate exhibit not only higher water vapor transmission rate (WVTR), but also severe oxygen penetration rate (this lower factor is, the better). Therefore, flexible PSCs require encapsulation on both front and back sides. On the face of entire active area, flexible sealing film with low WVTR and oxygen penetration ratio can be used to cover the surface [75, 84]. The bottom side, especially, should be encapsulated via flexible encapsulation materials with high transmittance, and need to low WVTR and oxygen penetration. This has been demonstrated by atomic layer deposition (ALD), plasma enhanced chemical vapor deposition (PECVD), physical vapor deposition (PVD), and other techniques of uniform metal oxides in an efficient way to seal the bottom of substrate.

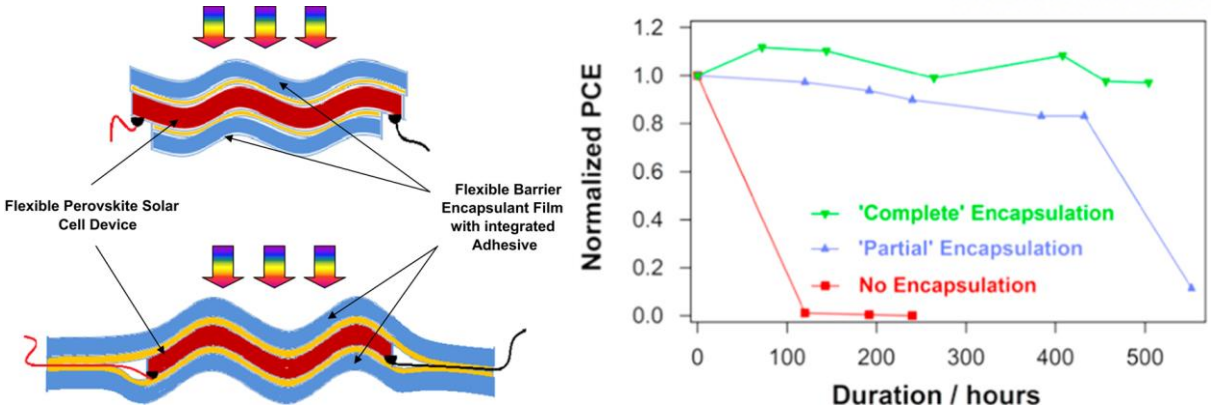

Figure 2.21. The schematic image of encapsulation both side for flexible perovskite solar cells and normalized PCE. Reproduced with permission from [53]. Copyright 2015 Elsevier.

2.3.3. Limits of Previous Studies in Mechanical Properties

As mentioned above, perovskite materials have three main problems to be solved (hysteresis, long term stability, and mechanical stability). Hysteresis and long-term stability issues, which are the problems of materials and devices, have been complemented and resolved through many previous studies about intrinsic materials. However, mechanical stability is only an unknown area, only a fraction of which has been studied. In particular, for the commercialization of devices, the first issue to be solved with long - term stability is mechanical reliability. The most cited and acknowledged researches are computational simulation and nanoindentation. As a result of these two studies, the elastic limit and the result of ductility of the material show similar results. However, there is not convinced that it can be applied to thin and defective materials actually used in devices.

The actual material used for perovskite solar cell is composed of a very thin film (about 300 nm). It also consists of a lot of grains through the growth of crystals, and grain boundaries, which are the boundaries between the grains, play role as electrical, optical and mechanical defects. However, in the case of the computer simulation and the nanoindentation technique, it is difficult to assume that the mechanical properties of the material to be actually used are measured because the mechanical properties are measured based on the material in which such defects are hardly present. In the case of nanoindentation, mechanical properties are measured by applying a load to a very local portion. The mechanical properties vary depending on the presence or absence of defects. In most cases of previous studies, mechanical properties were overestimated because there were not considered several defects.

The most common used measurement method of flexibility for flexible devices is to verify that the device is degraded during repeated bending tests. This is the simplest experimental method to measure the actual critical bending radius to determine how much endured by repeated bending. In the case of a flexible PSCs, it usually consists of six components (substrate, bottom transparent electrode, ETL, perovskite active layer, HTL, top metal electrode), and shape and size are all different. Therefore, flexibility may depend on the constituent conditions. Particularly, the most affected factors are the presence of metal oxide electrodes and the thickness of the substrate. However, studies on the flexibility of the device itself and the critical bending radius of each device have not been studied yet.

Generally, flexible devices are subjected to tensile deformation at top-surface under bending deformation. Therefore, measuring the tensile properties of the device is the most crucial method. However, the tensile test is very challenging since the perovskite materials are easily decomposed in ambient environment and difficulty of producing test pieces. The previous study has been predicted tensile properties, grain size effect using tensile testing through MD and MM simulation. It also has investigated the phenomena occurring at grain boundaries during fracture. However, it is also difficult to predict the fracture behavior when materials failure because it is only atomic scale prediction.

Reference

[1] V. M. Goldschmidt, "Die Gesetze der Krystallochemie," *Naturwissenschaften*, vol. 14, no. 21, pp. 477-485, 1926.

[2] H. D. Megaw, "Crystal structure of barium titanate," *Nature*, vol. 155, no. 3938, pp. 484-485, 1945.

[3] C. K. MØLLER, "Crystal structure and photoconductivity of caesium plumbohalides," *Nature*, vol. 182, no. 4647, p. 1436, 1958.

[4] D. Weber, "CH3NH3PbX3, ein Pb (II)-System mit kubischer Perowskitstruktur/CH3NH3PbX3, a Pb (II)-system with cubic perovskite structure," *Zeitschrift fur Naturforschung B*, vol. 33, no. 12, pp. 1443-1445, 1978.

[5] D. B. Mitzi *et al.*, "Conducting tin halides with a layered organic-based perovskite structure," *Nature*, vol. 369, no. 6480, p. 467, 1994.

[6] A. Kojima *et al.*, "Organometal halide perovskites as visible-light sensitizers for photovoltaic cells," *Journal of The American Chemical Society*, vol. 131, no. 17, pp. 6050-6051, 2009.

[7] H.-S. Kim *et al.*, "Lead iodide perovskite sensitized all-solid-state submicron thin film mesoscopic solar cell with efficiency exceeding 9%," *Scientific Reports*, vol. 2, p. 591, 2012.

[8] "Best Research-Cell Efficiencies Charts", NREL, https://www.nrel.gov/pv/assets/pdfs/pv-efficiencies-07-17-2018.pdf.

[9] N.-G. Park, "Perovskite solar cells: an emerging photovoltaic technology," *Materials Today*, vol. 18, no. 2, pp. 65-72, 2015.

[10] M. Saliba *et al.*, "Cesium-containing triple cation perovskite solar cells: improved stability, reproducibility and high efficiency," vol. 9, no. 6, pp. 1989-1997, 2016.

[11] W. S. Yang *et al.*, "High-performance photovoltaic perovskite layers fabricated through intramolecular exchange," *Energy & Environmental Science*, vol. 348, no. 6240, pp. 1234-1237, 2015.

[12] N. Elumalai *et al.*, "Perovskite solar cells: progress and advancements," *Energies*, vol. 9, no. 11, p. 861, 2016.

[13] C. Momblona *et al.*, "Efficient vacuum deposited pin and nip perovskite solar cells employing doped charge transport layers," vol. 9, no. 11, pp. 3456-3463, 2016.

[14] H. Zhou *et al.*, "Interface engineering of highly efficient perovskite solar cells," *Energy & Environmental Science*, vol. 345, no. 6196, pp. 542-546, 2014.

[15] E. Edri *et al.*, "Why lead methylammonium tri-iodide perovskite-based solar cells require a mesoporous electron transporting scaffold (but not necessarily a hole conductor)," *Nano Letters*, vol. 14, no. 2, pp. 1000-1004, 2014.

[16] J. S. Shaikh *et al.*, “Perovksite solar cells: In pursuit of efficiency and stability,” *Materials & Design*, vol. 136, pp. 54-80, 2017.

[17] M. A. Green *et al.*, "The emergence of perovskite solar cells," *Nature Photonics*, vol. 8, no. 7, p. 506, 2014.

[18] Q. Lin *et al.*, "Electro-optics of perovskite solar cells," *Nature Photonics*, vol. 9, no. 2, p. 106, 2015.

[19] D. A. Egger *et al.*, "Hybrid organic–inorganic perovskites on the move," *Accounts of Chemical Research*, vol. 49, no. 3, pp. 573-581, 2016.

[20] Y. Hou, "Rational Interfaces Design of Efficient Organic-inorganic Hybrid Perovskite Solar Cells," Friedrich-Alexander-Universität Erlangen-Nürnberg (FAU), 2017.

[21] F. Zheng *et al.*, "Rashba spin–orbit coupling enhanced carrier lifetime in CH3NH3PbI3," *Nano Letters*, vol. 15, no. 12, pp. 7794-7800, 2015.

[22] L. M. Herz, "Charge-carrier dynamics in organic-inorganic metal halide perovskites," *Annual Review of Physical Chemistry*, vol. 67, pp. 65-89, 2016.

[23] N. Marinova *et al.*, "Organic and perovskite solar cells: working principles, materials and interfaces," *Journal of Colloid and Interface Science*, vol. 488, pp. 373-389, 2017.

[24] T. C. Sum *et al.*, “Advancements in perovskite solar cells: photophysics behind the photovoltaics”, *Energy & Environmental Science*, vol. 7, pp. 2518-2534, 2014.

[25] R. Ihly *et al.*, "Efficient charge extraction and slow recombination in organic–inorganic perovskites capped with semiconducting single-walled carbon nanotubes," *Energy & Environmental Science*, vol. 9, no. 4, pp. 1439-1449, 2016.

[26] L. Tsakalakos, *Nanotechnology for photovoltaics*. CRC press, 2010.

[27] F. Kasten and A. T. Young, "Revised optical air mass tables and approximation formula," *Applied Optics*, vol. 28, no. 22, pp. 4735-4738, 1989.

[28] P. Schilinsky *et al.*, "Simulation of light intensity dependent current characteristics of polymer solar cells," vol. 95, no. 5, pp. 2816-2819, 2004.

[29] Z. Chen *et al.*, "Efficiency Definitions in the Field of PEC," in *Photoelectrochemical Water Splitting*: Springer, 2013, pp. 7-16.

[30] W. C. Choy, *Organic solar cells: materials and device physics*. Springer, 2012.

[31] J. H. Noh *et al.*, "Chemical management for colorful, efficient, and stable inorganic-organic hybrid nanostructured solar cells," *Nano Lett,* vol. 13, no. 4, pp. 1764-9, Apr 10 2013.

[32] E. T. Hoke *et al.*, “Reversible photo-induced trap formation in mixed-halide hybrid perovskites for photovoltaics," *Journal of Applied Physics*, vol. 6, no. 1, pp. 613-617, 2015.

[33] S. De Wolf *et al.*, "Organometallic Halide Perovskites: Sharp Optical Absorption Edge and Its Relation to Photovoltaic Performance," *The Journal of Physical Chemistry Letters,* vol. 5, no. 6, pp. 1035-9, Mar 20 2014.

[34] C. Grote *et al.*, "Strain tuning of tin–halide and lead–halide perovskites: a first-principles atomic and electronic structure study," *The Journal of Physical Chemistry C*, vol. 119, no. 40, pp. 22832-22837, 2015.

[35] Q. Dong *et al.*, "Electron-hole diffusion lengths> 175 μm in solution grown CH3NH3PbI3 single crystals," *Science*, p. aaa5760, 2015.

[36] D. Vak *et al.*, "3D printer based slot-die coater as a lab-to-fab translation tool for solution-processed solar cells," *Advanced Energy Materials*, vol. 5, no. 4, p. 1401539, 2015.

[37] H. J. Snaith *et al.*, "Anomalous hysteresis in perovskite solar cells," *The Journal of Physical Chemistry Letters*, vol. 5, no. 9, pp. 1511-1515, 2014.

[38] H. Azimi *et al.*, "A Universal Interface Layer Based on an Amine-Functionalized Fullerene Derivative with Dual Functionality for Efficient Solution Processed Organic and Perovskite Solar Cells," *Advanced Energy Materials*, vol. 5, no. 8, p. 1401692, 2015.

[39] H. S. Kim *et al.*, "Control of I-V hysteresis in CH3NH3PbI3 perovskite solar cell," *The Journal of Physical Chemistry Letters,* vol. 6, no. 22, pp. 4633-9, Nov 19 2015.

[40] S. De Wolf *et al.*, "Organometallic Halide Perovskites: Sharp Optical Absorption Edge and Its Relation to Photovoltaic Performance," *The Journal of Physical Chemistry Letters,* vol. 5, no. 6, pp. 1035-9, Mar 20 2014.

[41] A. Seemann *et al.*, "Influence of oxygen on semi-transparent organic solar cells with gas permeable electrodes," *Organic Electronics*, vol. 10, no. 8, pp. 1424-1428, 2009.

[42] A. Dualeh *et al.*, "Thermal behavior of methylammonium lead-trihalide perovskite photovoltaic light harvesters," *Chemistry of Materials*, vol. 26, no. 21, pp. 6160-6164, 2014.

[43] M. Manceau *et al.*, "Effects of long-term UV–visible light irradiation in the absence of oxygen on P3HT and P3HT: PCBM blend," *Solar Energy Materials and Solar Cells*, vol. 94, no. 10, pp. 1572-1577, 2010.

[44] T.-B. Song *et al.*, "Perovskite solar cells: film formation and properties," *Journal of Materials Chemistry A,* vol. 3, no. 17, pp. 9032-9050, 2015.

[45] G. Niu *et al.*, "Review of recent progress in chemical stability of perovskite solar cells," *Journal of Materials Chemistry A*, vol. 3, no. 17, pp. 8970-8980, 2015.

[46] G. Niu *et al.*, "Study on the stability of CH3NH3PbI3films and the effect of post-modification by aluminum oxide in all-solid-state hybrid solar cells," *Journal of Materials Chemistry A,* vol. 2, no. 3, pp. 705-710, 2014.

[47] M. Benavides-Garcia and K. Balasubramanian, "Bond energies, ionization potentials, and the singlet–triplet energy separations of SnCl2, SnBr2, SnI2, PbCl2, PbBr2, PbI2, and their positive ions," *The Journal of Chemical Physics,* vol. 100, no. 4, pp. 2821-2830, 1994.

[48] Q. Chen *et al.*, "Under the spotlight: The organic–inorganic hybrid halide perovskite for optoelectronic applications," *Nano Today,* vol. 10, no. 3, pp. 355-396, 2015.

[49] G. E. Eperon *et al.*, "Formamidinium lead trihalide: a broadly tunable perovskite for efficient planar heterojunction solar cells," *Energy & Environmental Science,* vol. 7, no. 3, 2014.

[50] A. Binek *et al.*, F"Stabilization of the Trigonal High-Temperature Phase of Formamidinium Lead Iodide," *The Journal of Physical Chemistry Letters,* vol. 6, no. 7, pp. 1249-53, Apr 2 2015.

[51] F. Hou *et al.*, "Efficient and stable planar heterojunction perovskite solar cells with an MoO3/PEDOT:PSS hole transporting layer," *Nanoscale,* vol. 7, no. 21, pp. 9427-32, Jun 7 2015.

[52] J. C. Yu *et al.*, "Highly efficient and stable inverted perovskite solar cell employing PEDOT:GO composite layer as a hole transport layer," *Scientific Reports,* vol. 8, no. 1, p. 1070, Jan 18 2018.

[53] H. C. Weerasinghe *et al.*, "Encapsulation for improving the lifetime of flexible perovskite solar cells," *Nano Energy,* vol. 18, pp. 118-125, 2015.

[54] F. Matteocci *et al.*, "Encapsulation for long-term stability enhancement of perovskite solar cells," *Nano Energy,* vol. 30, pp. 162-172, 2016.

[55] Q. Dong *et al.*, "Encapsulation of Perovskite Solar Cells for High Humidity Conditions," *ChemSusChem,* vol. 9, no. 18, pp. 2597-2603, Sep 22 2016.

[56] S. Sun *et al.*, "Mechanical properties of organic–inorganic halide perovskites, CH3NH3PbX3 (X = I, Br and Cl), by nanoindentation," *Journal of Materials Chemistry A,* vol. 3, no. 36, pp. 18450-18455, 2015.

[57] Y. Rakita *et al.*, "Mechanical properties of APbX 3 (A = Cs or CH3NH3; X = I or Br) perovskite single crystals," *MRS Communications,* vol. 5, no. 04, pp. 623-629, 2015.

[58] M. A. Reyes-Martinez *et al.*, "Time-Dependent Mechanical Response of APbX3 (A = Cs, CH3 NH3 ; X = I, Br) Single Crystals," *Advanced Materials,* vol. 29, no. 24, Jun 2017.

[59] M. Spina *et al.*, "Mechanical signatures of degradation of the photovoltaic perovskite CH3NH3PbI3upon water vapor exposure," *Applied Physics Letters,* vol. 110, no. 12, 2017.

[60] J. Feng, "Mechanical properties of hybrid organic-inorganic CH3NH3BX3 (B = Sn, Pb; X = Br, I) perovskites for solar cell absorbers," *APL Materials,* vol. 2, no. 8, 2014.

[61] J. Yu *et al.*, "Probing the Soft and Nanoductile Mechanical Nature of Single and Polycrystalline Organic-Inorganic Hybrid Perovskites for Flexible Functional Devices," *ACS Nano,* vol. 10, no. 12, pp. 11044-11057, Dec 27 2016.

[62] C. C. Stoumpos *et al.*, "Semiconducting tin and lead iodide perovskites with organic cations: phase transitions, high mobilities, and near-infrared photoluminescent properties," *Inorganic Chemistry*, vol. 52, no. 15, pp. 9019-9038, 2013.

[63] S. Sharma *et al.*, "Phase diagrams of quasibinary systems of the type: ABX3—A′ BX3; ABX3—AB′ X3, and ABX3—ABX′ 3; X= halogen," *Zeitschrift fur Physikalische Chemie*, vol. 175, no. 1, pp. 63-80, 1992.

[64] M. Long *et al.*, "Large-Grain Formamidinium PbI3–xBrx for High-Performance Perovskite Solar Cells via Intermediate Halide Exchange," *Advanced Energy Materials*, vol. 7, no. 12, p.

1601882, 2017.

[65] M. Long *et al.*, "Nonstoichiometric acid–base reaction as reliable synthetic route to highly stable CH 3 NH 3 PbI 3 perovskite film," *Nature Communications*, vol. 7, p. 13503, 2016.

[66] K. Yan *et al.*, "Hybrid halide perovskite solar cell precursors: colloidal chemistry and coordination engineering behind device processing for high efficiency," *Journal of The American Chemical Society*, vol. 137, no. 13, pp. 4460-4468, 2015.

[67] Y. Li *et al.*, "High-efficiency robust perovskite solar cells on ultrathin flexible substrates," *Nature Communications,* vol. 7, p. 10214, Jan 11 2016.

[68] S. T. Williams *et al.*, "Current challenges and prospective research for upscaling hybrid perovskite photovoltaics," *The Journal of Physical Cehmistry Letters*, vol. 7, no. 5, pp. 811-819, 2016.

[69] J. Feng *et al.*, "Record Efficiency Stable Flexible Perovskite Solar Cell Using Effective Additive Assistant Strategy," *Advanced Materials*, vol. 30, no. 35, p. 1801418, 2018.

[70] V. Zardetto *et al.*, "Substrates for flexible electronics: A practical investigation on the electrical, film flexibility, optical, temperature, and solvent resistance properties," *Journal of Polymer Science Part B: Polymer Physics*, vol. 49, no. 9, pp. 638-648, 2011.

[71] D. Yang *et al.*, "High efficiency planar-type perovskite solar cells with negligible hysteresis using EDTA-complexed SnO2," *Nature Communications*, vol. 9, no. 1, p. 3239, 2018.

[72] S. S. Shin *et al.*, "High-performance flexible perovskite solar cells exploiting Zn 2 SnO 4 prepared in solution below 100 C," *Nature Communications*, vol. 6, p. 7410, 2015.

[73] B. J. Kim *et al.*, "Highly efficient and bending durable perovskite solar cells: toward a wearable power source," *Energy & Environmental Science,* vol. 8, no. 3, pp. 916-921, 2015.

[74] L. Qiu *et al.*, "Integrating perovskite solar cells into a flexible fiber," *Angewandte Chemie International Edition*, vol. 53, no. 39, pp. 10425-10428, 2014.

[75] L. Li *et al.*, "Recent advances of flexible perovskite solar cells," *Journal of Energy Chemistry*, 2018.

[76] Y. Yue *et al.*, "Enhanced Stability of Perovskite Solar Cells through Corrosion-Free Pyridine Derivatives in Hole-Transporting Materials," *Advanced Materials*, vol. 28, no. 48, pp. 10738-10743, 2016.

[77] Z. Li *et al.*, "Extrinsic ion migration in perovskite solar cells," *Energy & Environmental Science*, vol. 10, no. 5, pp. 1234-1242, 2017.

[78] J. Niu *et al.*, "Graphene-oxide doped PEDOT: PSS as a superior hole transport material for high-efficiency perovskite solar cell," *Organic Electronics*, vol. 48, pp. 165-171, 2017.

[79] J.-I. Park *et al.*, "Highly flexible InSnO electrodes on thin colourless polyimide substrate for high-performance flexible CH3NH3PbI3 perovskite solar cells," *Journal of Power Sources*, vol. 341, pp. 340-347, 2017.

[80] B. A. Nejand *et al.*, "All-inorganic large-area low-cost and durable flexible perovskite solar cells using copper foil as a substrate," *Chemical Communications*, vol. 53, no. 4, pp. 747-750, 2017.

[81] Z. Liu *et al.*, "Nickel oxide nanoparticles for efficient hole transport in pin and nip perovskite solar cells," *Journal of Materials Chemistry A*, vol. 5, no. 14, pp. 6597-6605, 2017.

[82] H. Zhang *et al.*, "CuGaO2: A Promising Inorganic Hole-Transporting Material for Highly Efficient and Stable Perovskite Solar Cells," *Advanced Materials*, vol. 29, no. 8, p. 1604984, 2017.

[83] J. Yang *et al.*, "Investigation of CH3NH3PbI3 degradation rates and mechanisms in controlled humidity environments using in situ techniques," *ACS Nano*, vol. 9, no. 2, pp. 1955-1963, 2015.

[84] R. Liu *et al.*, "Oxygen-barrier properties of cold-drawn polyesters," *Journal of Polymer Science Part B: Polymer Physics*, vol. 40, no. 9, pp. 862-877, 2002.

3. Aims and Outline of This Thesis

Perovskite solar cells hold promising candidates as a new alternative energy resource. This is because the high light absorption coefficient, bandgap tunability, and power generation cost are lower than other solar cells. Despite these various advantages, there are many fatal disadvantages for practical commercialization. There is hysteresis of material itself, stability that is vulnerable to the atmospheric environment, and mechanical stability issues. Recent efforts have described progress in improving the chemical stability of perovskite solar cell devices intrinsically, such as reconstitution of perovskite materials and replacing several functional materials. However, the field of perovskite solar cells has described insouciance toward mechanical stability, even though it is essential for the commercialization. Although there are several existing studies, it is difficult to determine the quantitative mechanical properties of PSCs due to limits of previous studies, as mentioned in previous chapter.

Therefore, this research work is mainly aimed to the mechanical properties of organic-inorganic metal halide perovskite solar cells based on nanomechanics. The key objective of the study are:

1. To fabricate the ultra-flexible perovskite solar cells via ITO-free transparent bottom electrode
2. To measure the mechanical properties of constituent materials in flexible perovskite solar cell devices
3. To design the innovated mechanical testing method for vulnerable perovskite materials using in-situ nanoindentation system
4. To measure direct tensile properties of organic-inorganic perovskite materials via in-situ tensile testing
5. To suggest enhancing mechanical flexibility of flexible perovskite solar cell devices based nanomechanics

The outline of the thesis is composed of three parts based on relative contents. The first part (Chapter 1, 2, 3) presents an overview of photovoltaic devices along with detailed explanation of the organic-inorganic hybrid perovskite and its application, especially solar cells, and its benign properties, and previous studies and its limits.

The second part (Chapter 4) summarized the research work and achievements, that is investigation of mechanical properties of flexible perovskite solar cell devices using various

nanomechanical tests which are unprecedented in perovskite fields.

The last part (Chapter 5) present the summary and conclusion the research work. And it is suggesting the future ideas that can be explored to further enhance the mechanical flexibility of flexible perovskite solar cells via nanomechanics are also described.

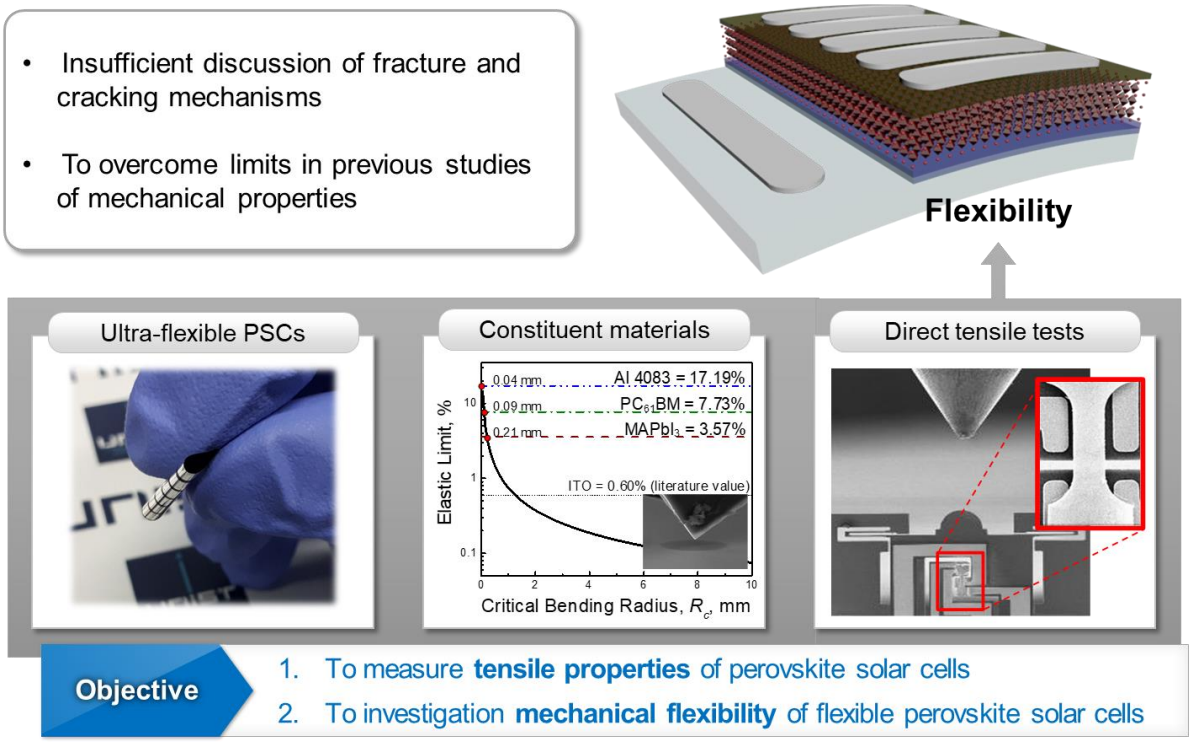

Figure 3.1. The aims of this dissertation.

4. Results and Discussion

4.1. Flexibility of Ultra-flexible Perovskite Solar Cells

4.1.1. Introduction

Exploring alternative energy sources is one of important assignment in the world. The sun is a sustainable, reliable and almost infinite source of energy that can make significant contributions to the global demand for energy [1]. Therefore, photovoltaic energy is currently drawing attention as an upcoming alternative energy source, and organic-inorganic halide perovskite solar cells hold promise for next-generation photovoltaic devices because of their remarkable optical properties, high light-absorption coefficient and good cost-effectiveness. The PCE of PSCs has drastically rise from 3.8% to 23.3% [2-5]. In addition, perovskite devices have promise not only in photovoltaic applications but also in other applications such as luminescent devices and transistors.

The Advanced technology development in the fiddle of electronics industry, the demand of flexible devices, such as portable electronics, electronic textiles, and wearable devices, etc., is consistently rising. Therefore, flexible photovoltaic devices are drawing attention for their attractive properties including flexibility, light-weight, compatible with curved surfaces. More importantly, commercialization of the flexible photovoltaic devices can be accomplished by roll-to-roll process [6]. It is a great advantage which are related to time reduction, simple equipment, and lower cost; comparing batch-to-batch manufacturing for rigid devices. Furthermore, the rigid devices are much thicker and heavier, therefore they are more need costs for storage and transportation. Whereas flexible devices are thinner, lighter, and more flexible for storage, transportation and installation which enormously reduce related costs [7].

The organic-inorganic metal halide perovskite solar cells (PSCs) hold promising candidate for flexible photovoltaic devices. All of precursor materials of flexible PSCs are plentiful and fabrication process can be carried out at low temperature nearly 100℃. Strong light absorbing ability is main figure-of-merits demanded for high performance absorbing material. The hybrid perovskite materials have determined great light absorbing ability in this regard, only about 300 nm-thick is enough to light-absorption at all range of visible light. Furthermore, its absorption range can be tuned by substitution and composition change in perovskite structure [8, 9]. The bandgap of the perovskite materials can be modified by simple mixing process, resulting it can be matched with charge transport layers for enhancing performance [10]. Meanwhile, many previous studies exhibited that high quality perovskite materials with uniform morphology, great crystallinity, pin hole-free, and they were possible to fabricate flexible PSCs in lower temperature process, indicating these materials and procedures are prospective candidates for fabrication onto flexible polymeric substrates. Recently many studies have focused on

designing low-cost, light weight, high performance, and mechanically flexible PSCs.

In the following contents, in this work, I fabricated ultra-flexible perovskite solar cell devices using special transparent bottom electrode and substrate alternating commonly used PET (PEN) / ITO. The flexible PSCs are composed of polyethyleneimine (PEI) / Au as bottom electrode on Norland Optical Adhesive 88 (NOA 88) substrate, AI 4083 (PEDOT:PSS, Clevious) as hole transport layer, $MAPbI_3$ and $MAPb(I_{0.87}Br_{0.13})_3$ as perovskite layer, phenyl-C61-butyric acid methyl ester ($PC_{61}BM$) as electron transport layer, silver as top electrode. I carried out repeatable bending tests using specific bending apparatus, resulting it shows that critical bending radius with 0.5 ~ 1 mm.

4.1.2. Experimental Procedure

4.1.2.1. Materials

Norland Optical Adhesive 88 (NOA 88) was purchased from Norland Optics. and PEDOT:PSS solution (Clevious AI 4083) was purchased from OSM. Methylammonium iodide (MAI) purchased from Dyesol. Lead iodide (PbI_2, 99.9%) was purchased from Alsa Aesar. Polystyrene (PS, Mw ~ 35,000), Polyethylenimine (PEI, Mw ~25,000), Dimethyl Sulfoxide (DMSO, anhydrous, 99.8%), γ-Butyrolactone (GBL, anhydrous, > 99.0%), N,N-dimethylformamide (DMF, anhydrous, 99.8%), 2-propanol (IPA, anhydrous, 99.5%), chlorobenzene (anhydrous, 99.8%), and Zonyl FS-300 were purchased from Sigma Aldrich. [6,6]-Phenyl-C61-butyric acid methyl ester ($PC_{61}BM$, > 99%) was purchased from 1-materials.

4.1.2.2. Solar Cell Fabrication

The configuration of perovskite solar cell was PEI / Au / AI 4083 / Perovskite / $PC_{61}BM$ / Ag on NOA 88 substrate. The bottom electrode is composed of laminated structure with substrate, NOA88 / PEI / Au). Glass substrate were sequentially cleaned with distilled water, acetone, and IPA. PS was deposited on oxygen-plasma-treated glass via spin-coating at 5,000 rpm for 40 s, which help to detaching flexible substrates, i.e., NOA 88 / PEI / Au. NOA 88 was spin-coated on PS coated glass at 5,000 rpm and UV curing with 15 minutes. PEI was spin-coated on NOA 88 / Glass substrate at 5,000 rpm for 40 s and annealed at 120℃ for 15 minutes. Au was deposited on glass / PS / PEI / NOA 88 laminated substrate via thermal evaporation at a based pressure of ~10^{-6} torr at a deposition rate of 1.0 Å s^{-1}. Afterward, AI 4083 solution was filtered through a 0.45 μm PVDF filter, and spin-coated onto laminated electrode on substrate at 5,000 rpm for 40 s and annealed at 150℃ for 10 minutes. To deposit the perovskite layer, the $MAPbI_3$ precursor solution (45 wt.% MAI and PbI_2 1:1 molar ratio in GBL and DMSO (7:3 v/v) co-solvent kept at 100℃) was spin-coated at 5,000 rpm for 25 s, and 0.5 mL chlorobenzene (CB) solvent was dripped onto the substrates 10 s after spin-coating. The samples were annealed at 100℃ for 30 min. The PC61BM solution in CB (2.2 wt.%) was spin-coated at 2,000 rpm for 45 s onto the samples. Finally, Ag counter-electrodes were deposited by thermal evaporation at a based pressure of ~10^{-6} torr at a deposition rate of 0.1 Å s^{-1} for initial thickness of 10 nm and at a deposition rate of 0.5 Å s^{-1} for the remaining 90 nm, which defines the active cell area of 0.135 cm^2.

4.1.2.3. Solar Cell Characterization

The PCE of the PSCs was determined through J-V measurements using an Ivium-n-Stat Source

meter under AM 1.5G solar simulator. All of the J-V measurements of the PSCs were conducted in low humidity air without encapsulation. The illumination intensity of the light source was calibrated before measurement using a standard silicon reference solar cell, with a value of 100 mW cm^{-2}. The voltage scanning rate and step were 0.3 V s^{-1} and 10 mV, respectively. The external quantum efficiency (EQE) spectra were measured by a certified incident photon to current efficiency (IPCE) measurement system. Sheet resistance of bottom transparent electrode was measured with four-point probe surface resistance measuring equipment (CMT 2000N) and measuring resistance of electrode after repeatable bending tests was measured with digital multimeter using two proves at the same points of electrode before and after bending. Scanning electron microscopy (SEM) images were obtained using Nova NanoSEM 230 operated at 10 ~ 15 kV.

4.1.2.4. Repeatable Bending Test

The repeatable bending tests were carried out the manual type using specific apparatus with different radius. Entire covered bending radius are 8, 4, 2, 1, 0.5 mm. Despite of hold the repeatable bending test machine based on M-403.42S precision transition stage (PI), in this work, performed the bending tests on manual operation. This is because size of sample is too smaller (15 mm, square) and inaccurate sample shape, omega shape, at smallest bending radius (R_c = 0.5 mm).

4.1.3. Results and Discussion

4.1.3.1. Flexible Perovskite Solar Cells

The device configuration of flexible PSCs is composed with NOA 88 / PEI / Au / AI 4083 / $MAPbI_3$ / $PC_{61}BM$ / Ag, as shown in **figure 4.1**. The most common reason of rapidly degradation in flexible PSCs at smaller bending radius is broken metal oxide electrode, such as ITO, FTO. Therefore, this work fabricated new polymer-metal flexible transparent electrodes. It is laminated of PEI and Au on thinner NOA 88 substrates, substrate effect is demonstrated in latter part. PEI is a polymer with abundant amine-based groups that is consist of ethylenimine moieties as the repeating unit, which is possible to protonate to form polycation. Therefore, this material which functional amine-based group forms molecular dipole and shifts the work function of metallic cathode, resulting play role of nucleation inducer. The metal electrode deposition, Au in this study, was heavily affected by PEI. The functional amine groups in PEI have perform like ligands and provide electron pairs that are not shared to make covalent bonds with Ag-sharing atoms [11]. Therefore, the Au atoms are initially deposited, and is fixed by the formation of a coordination complex of the PEI-coated substrate. This coordination reaction produces Au nuclei uniformly and densely distributed over surface of PEI coated-substrate without undergoing irregular Au migration and agglomeration, which is responsible for the growth of metal island of the grain, as shown in **figure 4.2**.

Particularly, the key point of this new structure is due to the density of Au nuclei generated by such coordinate bonding. If the atomic spacing of the amine-based groups of the PEI repeat units is about 4 Å, resulting Au nuclei can be intensely dense at this angstrom-scale interval. Furthermore, since the coordination bond nature ensures the strong bonding between first deposited Au atoms and amines, the subsequent Au deposition is centered throughout uniformly distributed Au nuclei with high density.

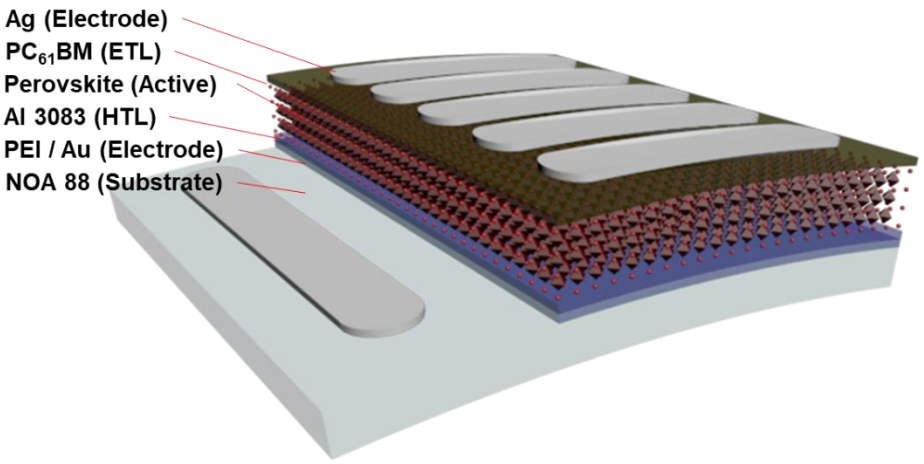

Figure 4.1. Device configuration of flexible PSCs.

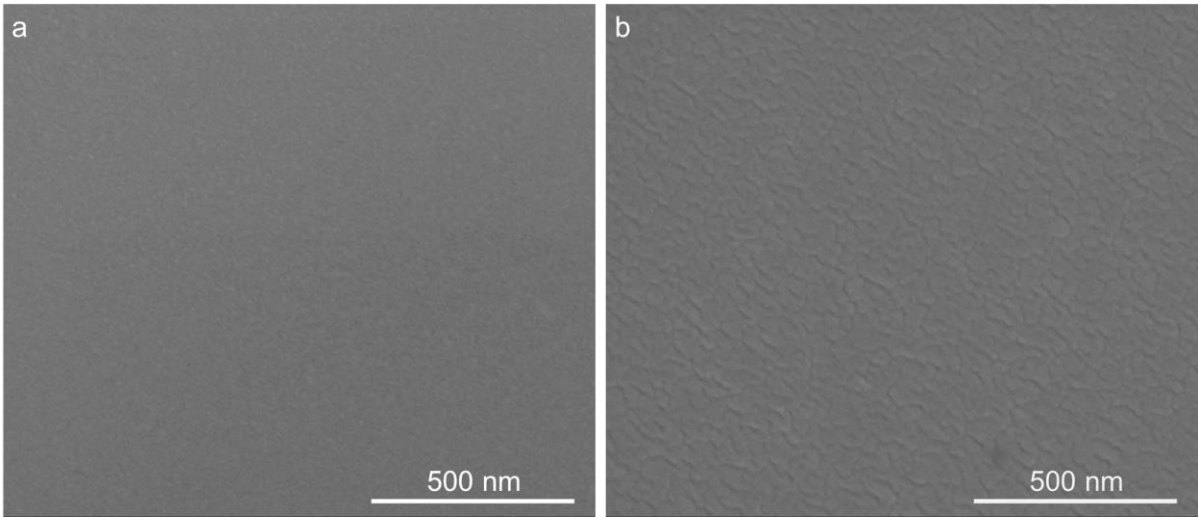

Figure 4.2. Scanning electron microscopy images of (a) PEI / Au, and (b) Au.

The deposition process maintains with two steps of coarsening and increasing thickness, resulting in uniform Au film is thinner than 15 nm, i.e. visible light). The sheet resistance of this composite electrodes is 15.16 (0.47) Ω sq.$^{-1}$ which is similar to ITO sheet resistance of ITO electrode with 12.00 (0.39) Ω sq.$^{-1}$, measured by four-probe surface resistance measurement system. It means that the composite electrodes have similar electric properties with much thinner thickness than ITO electrode, as shown in **figure 4.3**.

The photovoltaic characteristic of flexible PSCs is shown in **figure 4.4** comparing with rigid solar cells which are used to ITO electrode and PEI / Au electrode on glass substrates, which is described cells with 0.135 cm^2 active area under light intensities of 100 mW cm^{-2}. As results, PCE and photovoltaic parameters of PSCs with flexible and rigid devices are summarized in **table 4.1**. Despite of similar sheet resistance, PEI / Au electrode-based PSCs were exhibited lower PCE value than ITO electrode-based PSCs in rigid glass substrate. There may be multiple complex effect, but the most directly influencing factor is low transmittance of composite electrode, which is directly affected in short circuit current density, J_{sc}, as shown **figure 4.5**. This is expected as less light is penetrated and as less absorbed in active perovskite layers. Consequently, fewer charges can be photogenerated. This trend is also seen in the EQE graph (**figure 4.6**) which shows similar proportional ratio with difference of transmittance [12]. Meanwhile, PCE of flexible PSCs are slight lower than rigid PSCs using same electrodes, which revealed in low J_{sc} and V_{oc} in **figure 4.4**. The possible reason of this issue is that the flexible substrate, NOA 88 in this work, has more rough surface than rigid substrate, resulting less uniform film quality during fabrication procedures. It is well known that most PSCs are greatly influenced by morphology and crystallinity of perovskite layer due to existence of trap site and pin hole, etc. Furthermore, the flexible device used in this work has lower efficiency than the previous studies due to using standard structure of PSCs, inverted $MAPbI_3$, in order

Table 4.1. The photovoltaic properties of various PSCs.

PSCs type	J_{sc} (mA cm^{-2})	V_{oc} (V)	FF (%)	PCE (%)
Glass / ITO	16.60	0.88	76.42	11.16
Glass / PEI / Au	12.34	0.86	73.12	7.76
NOA 88 / PEI / Au	11.66	0.78	73.87	6.72

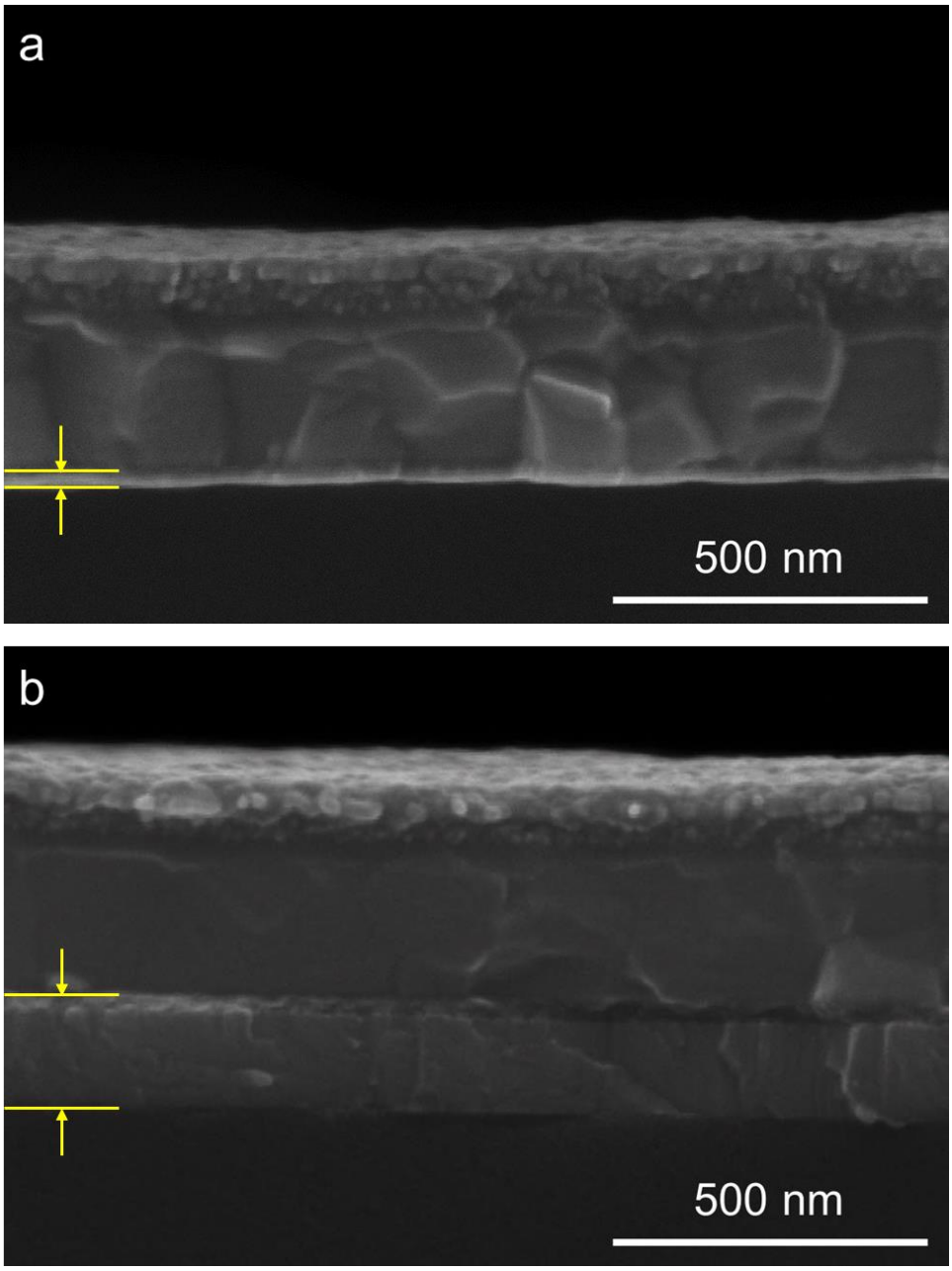

Figure 4.3. Cross-section images of flexible PSCs measured by scanning electron microscopy, (a) PEI / Au electrode based-, and (b) ITO electrode based-devices.

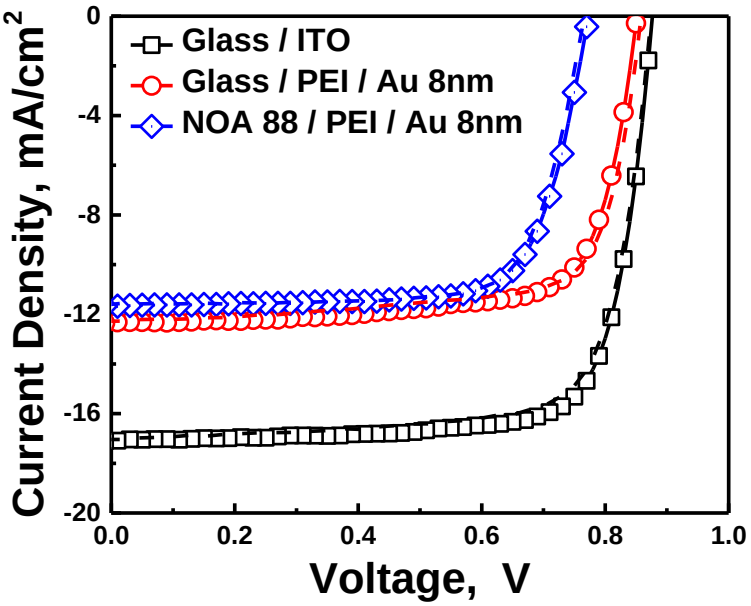

Figure 4.4. Typical J-V curves of rigid and flexible PSCs with different electrodes and substrates of Glass-ITO, Glass-PEI/Au, and NOA 88-PEI/Au.

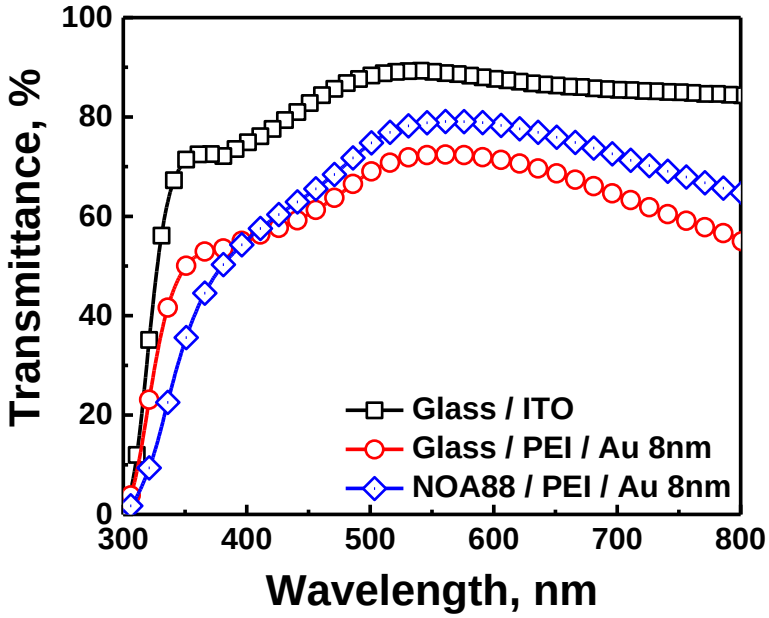

Figure 4.5. Typical transmittance data of rigid and flexible PSCs with different electrodes and substrates of Glass-ITO, Glass-PEI/Au, and NOA 88-PEI/Au.

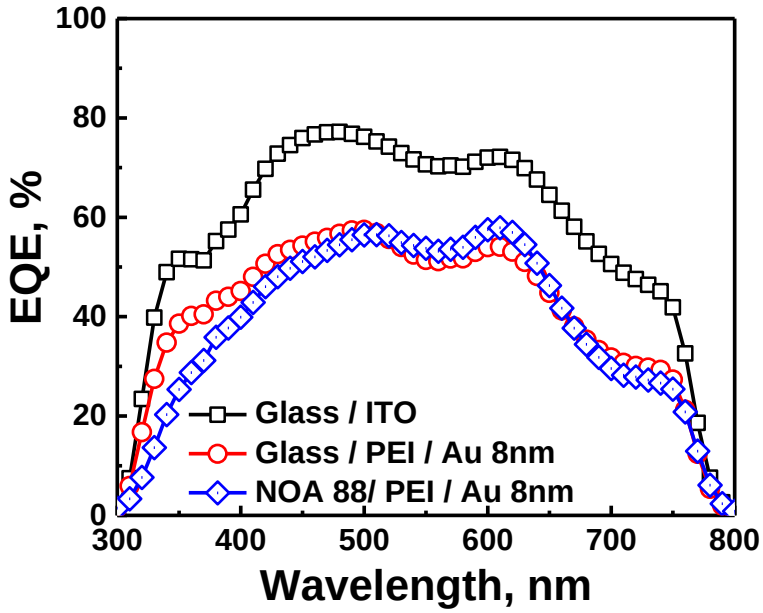

Figure 4.6. External quantum efficiency of rigid and flexible PSCs with different electrodes and substrates of Glass-ITO, Glass-PEI/Au, and NOA 88-PEI/Au.

to investigate mechanical flexibility only. If the advanced structure perovskite, such as mixed cation and halide, is used and the charge transport layer is replaced, the efficiency can be increased sufficiently.

4.1.3.2. Repeatable Bending Tests

To evaluate the mechanical flexibility of flexible PSCs, the changes in photovoltaic properties of devices were measured by repeatable bending tests with different bending radius, *R*. Typically reported studies for flexibility of flexible PSCs were measured by degradation of PCE after bending tests only. Almost previous studies bent until failure, which is beginning to initiate crack in ITO electrode. Therefore, several studies replaced ITO electrode to graphene and AgNWs and polymeric complex electrode, they revealed more flexible under bending deformation. The composite electrode used in this work has ultimate bending durability under bending deformation. The repeatable bending tests were carried out manually via special bending apparatus (as shown in **figure 4.7**) because of small samples and incorrect bending radius, which is not "U" shape but "Ω" shape in small bending radius. **Figure 4.8** shows the normalized resistance of two electrode on flexible substrate, NOA 88 / PEI / Au and PEN / ITO, with different bending radius of 8, 4, 2, 1, 0.5 mm. Bending tests were performed at 100 cycles each bending radius, unlike previous studies with 1,000 cycles or more, since it is not to measure fatigue behavior bun sufficient to confirm the crack initiating. As a result, NOA 88 / PEI / Au electrode-substrate had not changed until smallest bending radius of 0.5 mm, whereas, PEN / ITO electrode-substrate were rapidly increased normalized resistance at 8 mm bending radius due to occurring catastrophic fracture on ITO electrode, as shown in **figure 4.9**, which is different with

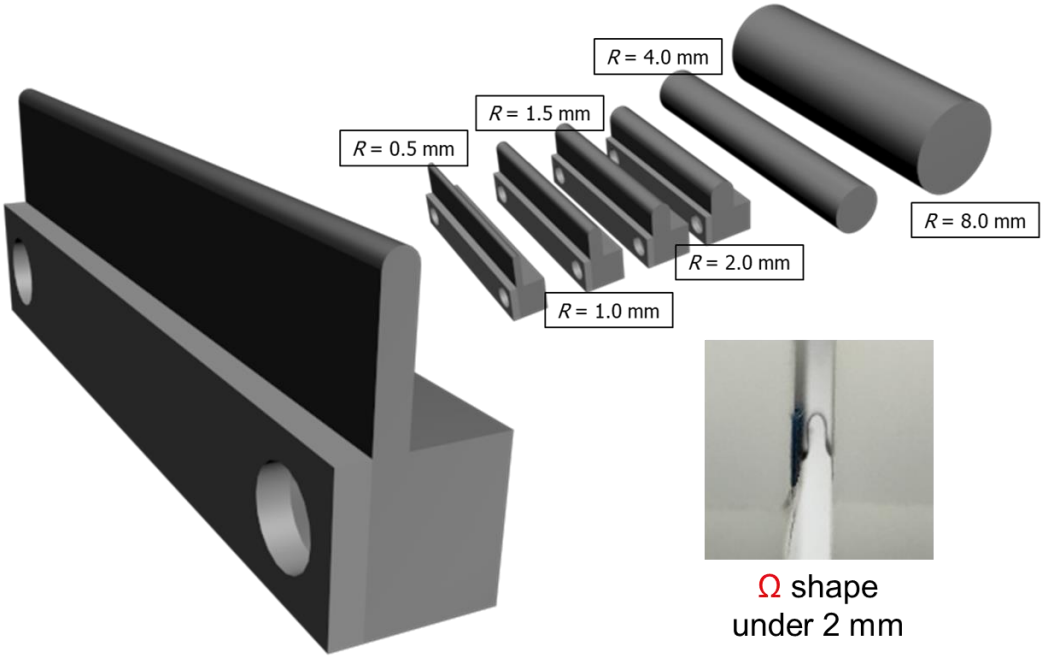

Figure 4.7. Manual bending apparatuses with different bending radius.

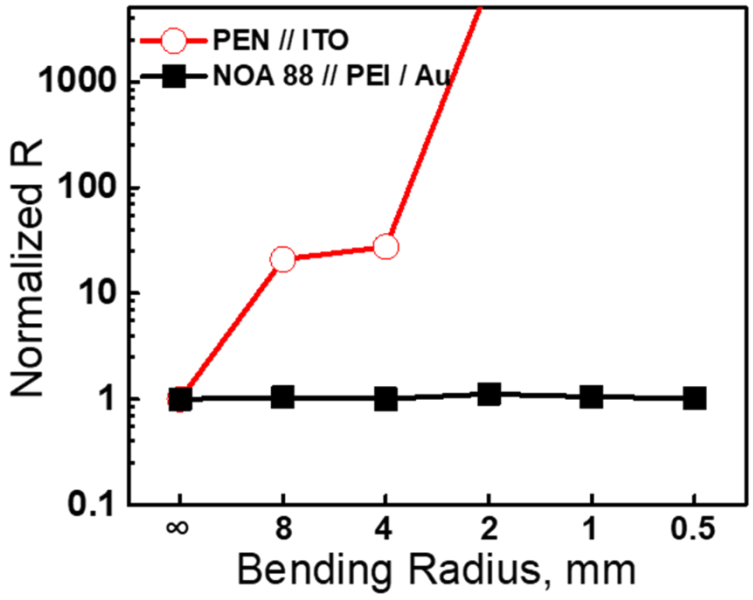

Figure 4.8. Normalized resistance of NOA 88 / PEI / Au and PEN / ITO electrodes with different bending radius of 8, 4, 2, 1, 0.5 mm.

previous studies of bending radius 4 mm for ITO electrode [13] due to thickness of PEN substrate is too thick of 150 μm. The critical bending radius, R_c, has enormously affected by thickness of materials in bending deformation. To apply extremely severe deformation on flexible electrode, I carried out

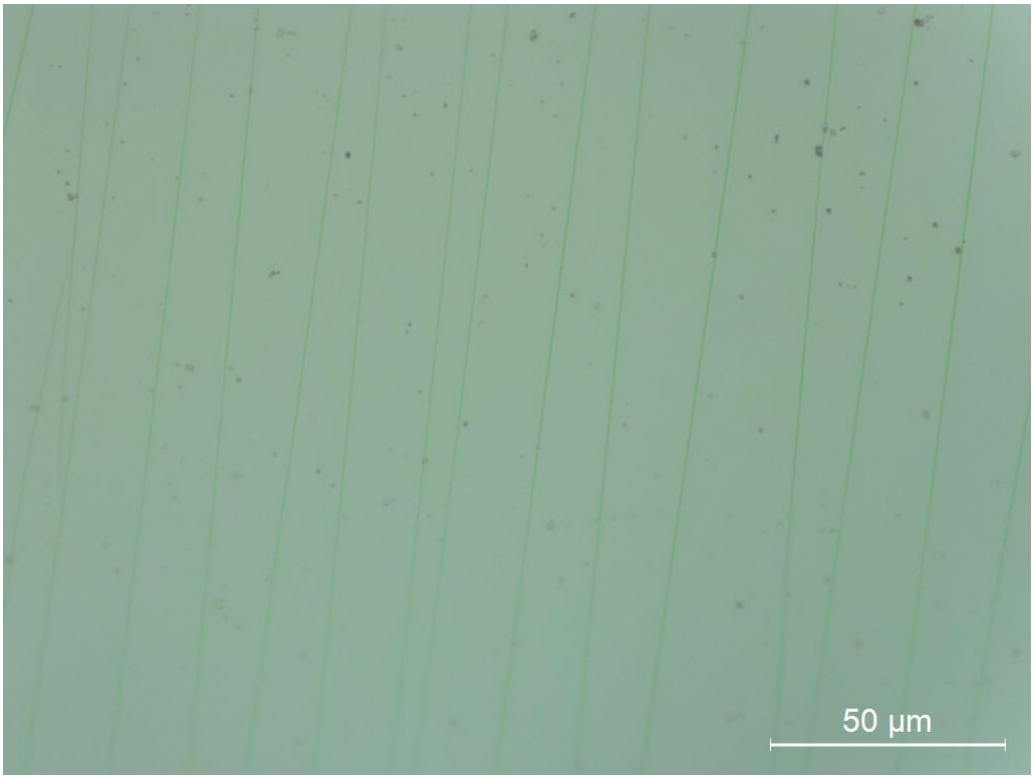

Figure 4.9. Optical microscopy image of crack initiating on ITO electrode on 150 μm-thick PEN substrate with bending radius of 8 mm.

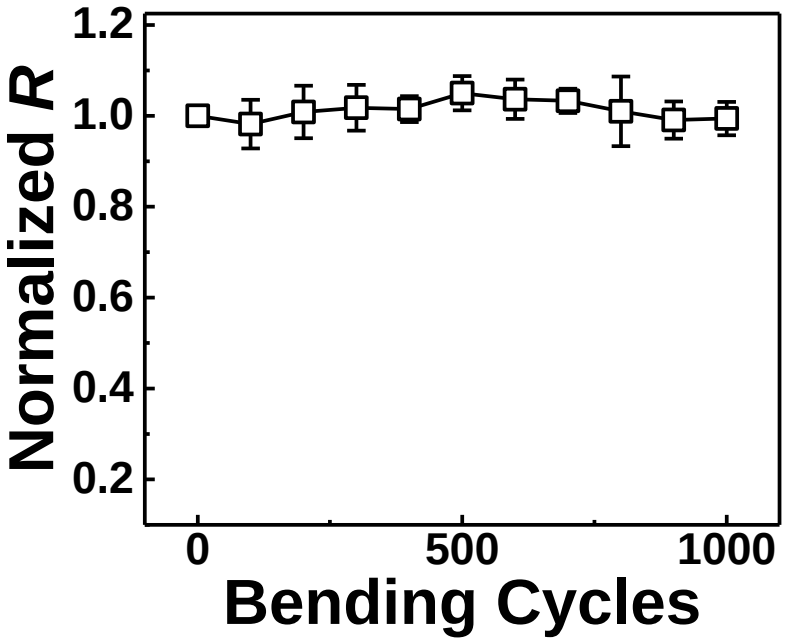

Figure 4.10. Normalized resistance of NOA 88 / PEI / Au electrodes with different bending cycles up to 1,000 cycles, bending radius of 0.5 mm.

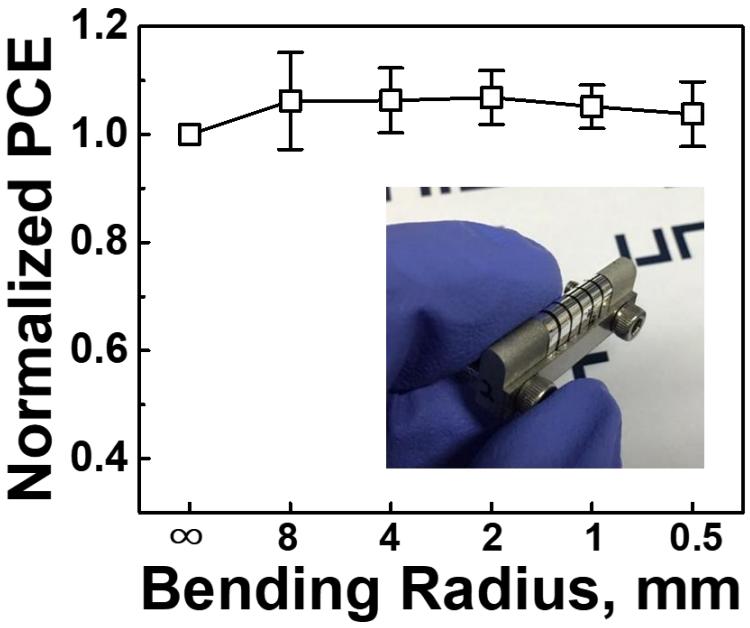

Figure 4.11. Normalized PCE of flexible PSCs after 100 cycles bending deformation with different bending radius of flat, 8, 4, 2, 1, 0.5 mm.

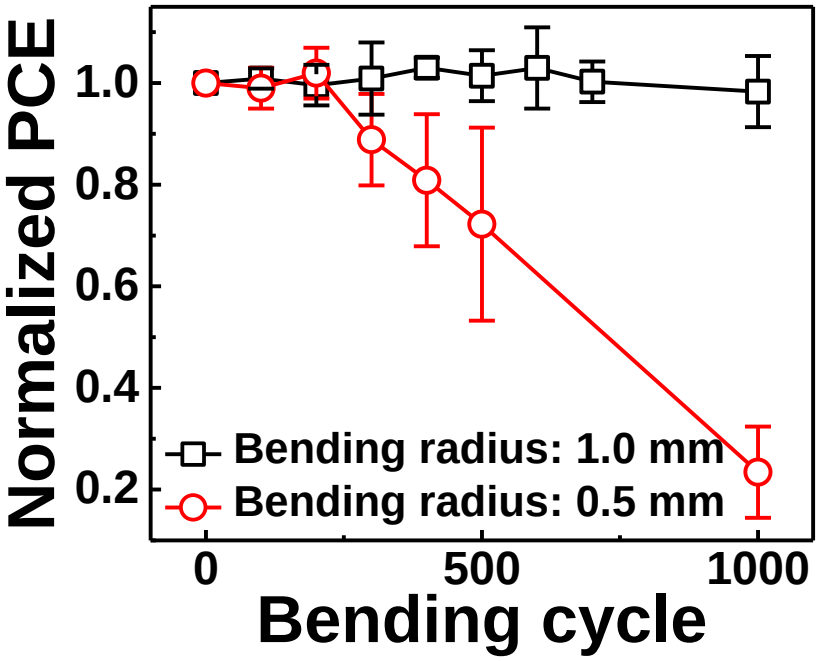

Figure 4.11. Normalized PCE of flexible PSCs after repeatable bending deformation with different bending cycles, bending radius of 1, 0.5 mm.

repeatable bending tests with increasing bending cycles in 0.5 mm bending radius, as shown in **figure 4.10**. The results of the bending tests were also not significantly changed. In other words, this electrode

has a great advantage in manufacturing a flexible device.

Figure 4.11 shows normalized PCE were bent around bending apparatus and cylindrical rods under 8, 4, 2, 1, and 0.5 mm. Bending tests were performed at 100 cycles each bending radius that is same to bending tests of electrode. The PCE of bent PSCs was shown nearly 100% of initial PCE at 0.5 mm bending radius with other electrical properties. It means that the critical bending radius of PSCs is under 0.5 mm which is no change of PCE from flat surface to 0.5 mm during 100 cycles bending tests. In order to measure more precise critical bending radius, I had performed repeatable bending tests with different bending cycles in bending radius with 0.5, and 1 mm. **Figure 4.12** shows normalized PCE of flexible PSCs with two bending radius of 0.5 and 1 mm, resulting of drastically decreasing of normalized PCE after 300 cycles bending at 0.5 mm bending radius, whereas no significant change in bending radius of 1 mm. The most effective factor of degradation of flexible PSCs during severe bending deformation, I have expected to failure of perovskite materials, $MAPbI_3$, because other constituent materials are well known that is ductile materials. To confirm this expectation, I had checked fracture behavior of perovskite materials. **Figure 4.13** shows SEM images of cracking on perovskite thin films with different bending cycles of 100 and 500 cycles. In the first 100 bending cycles, linear fine crack is generated on the surface, in which the device is normally operated, which shown **figure 4.12**, it because of no significant failure on vertical direction. However, bending cycle more than 500 cycles causes severe cracks on the surface, which negatively influence the operation of the device. The flexibility of PSCs has been studied in previous research through repeatable bending tests, but the PSCs were composed of various constituent materials, structure, and thickness. Therefore, repeatable bending tests are difficult to quantitative results for measuring typical flexibility of PSCs without clear variable due to it can be diverse as much as the structure of PSCs.

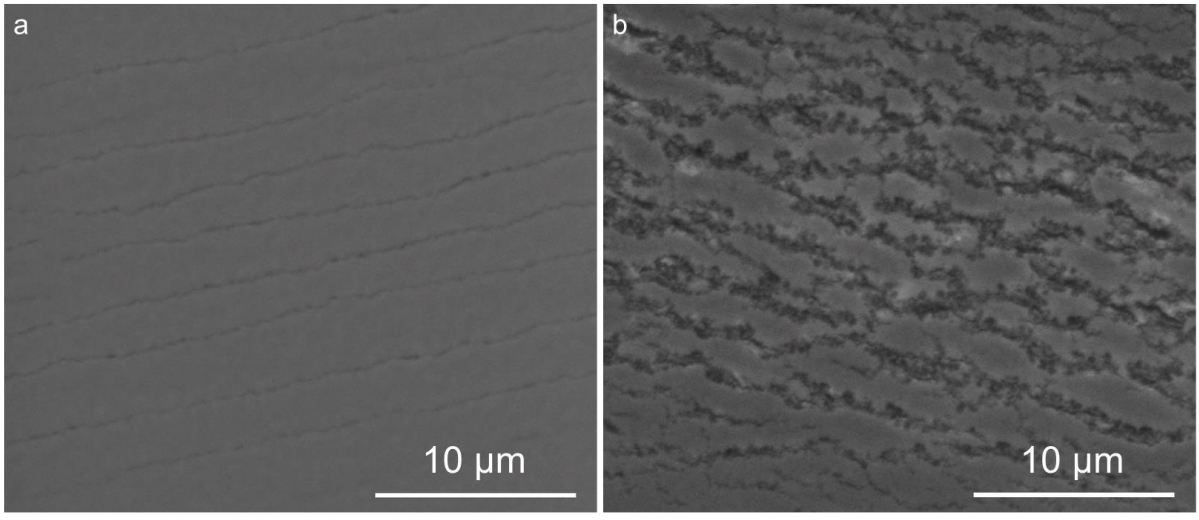

Figure 4.12. Scanning electron microscopy images of crack-initiated perovskite materials after (1) 100 cycles, and (2) 500 cycles with bending radius of 0.5 mm.

4.1.4. Summary

To measure flexibility of flexible perovskite solar cells, I have fabricated flexible PSCs using special electrode and substrate. The polymer-metal composite electrode shows great recoverable properties during extremely severe bending deformation. It was confirmed by repeatable bending tests with different bending radius using specific bending apparatus. The bending tests were performed manually because bending tests via automatic system have concerned from smaller device size and incorrect device shape. The composite electrodes shown similar sheet resistance with ITO electrode, and also shown no change of resistance after severe bending deformation, it indicated suitable candidates for ultra-flexible electronic devices. However, this electrode has lower transmittance than ITO electrode, resulting in lower PCE values than ITO based PSCs. Nevertheless, it needs to complement transmittance, it was enough to demonstrate flexibility of flexible PSCs. Furthermore, this work performed repeatable bending tests on flexible PSCs with different bending radius and cycles. First 100 cycles bending tests shown no degradation of flexible PSCs, but smallest bending radius of 0.5 mm shown crack initiating after repeatable bending tests on perovskite materials. And then photovoltaic performances were rapidly decreased after 300 cycles bending radius due to severe crack occurring. But photovoltaic properties were not decreased after 1,000 cycles bending of 1 mm bending radius with no significant cracking. Therefore, results of this work were expected that possible reason of performance degradation is most vulnerable materials, perovskite materials in this work, in severe bending deformation. And this argument will be aimed to following section.

Reference

[1] N. Armaroli and V. Balzani, "The future of energy supply: challenges and opportunities," *Angewandte Chemie International Edition*, vol. 46, no. 1-2, pp. 52-66, 2007.

[2] "Best Research-Cell Efficiencies Charts", NREL, https://www.nrel.gov/pv/assets/pdfs/pv-efficiencies-07-17-2018.pdf.

[3] A. Kojima *et al.*, "Organometal halide perovskites as visible-light sensitizers for photovoltaic cells," *Journal of the American Chemical Society*, vol. 131, no. 17, pp. 6050-6051, 2009.

[4] N. J. Jeon *et al*, "Solvent engineering for high-performance inorganic–organic hybrid perovskite solar cells," *Nature Materials*, vol. 13, no. 9, p. 897, 2014.

[5] S. S. Shin *et al.*, "Colloidally prepared La-doped BaSnO3 electrodes for efficient, photostable perovskite solar cells," *Science*, vol. 356, no. 6334, pp. 167-171, 2017.

[6] L. Li *et al.*, "Recent advances of flexible perovskite solar cells," *Journal of Energy Chemistry*, 2018.

[7] D. Vak *et al.*, "3D printer based slot-die coater as a lab-to-fab translation tool for solution-processed solar cells," *Advanced Energy Materials*, vol. 5, no. 4, p. 1401539, 2015.

[8] N. Rolston *et al.*, "Effect of Cation Composition on the Mechanical Stability of Perovskite Solar Cells," *Advanced Energy Materials,* vol. 8, no. 9, 2018.

[9] A. Binek *et al.*, "Stabilization of the Trigonal High-Temperature Phase of Formamidinium Lead Iodide," *The Journal of Physical Chemistry Letters,* vol. 6, no. 7, pp. 1249-53, Apr 2 2015.

[10] J. H. Noh *et al.*, "Chemical management for colorful, efficient, and stable inorganic-organic hybrid nanostructured solar cells," *Nano Letters,* vol. 13, no. 4, pp. 1764-9, Apr 10 2013.

[11] H. Kang *et al.*, "Polymer-metal hybrid transparent electrodes for flexible electronics," *Nature Communications,* vol. 6, p. 6503, Mar 19 2015.

[12] D. Yang *et al.*, "Recent Advanced in Flexible Perovskite Solar Cell: Fabrication and Application," *Angewandte Chemie International Edition,* Oct 17 2018.

[13] K. Poorkazem *et al.*, "Fatigue resistance of a flexible, efficient, and metal oxide-free perovskite solar cell," *Journal of Materials Chemistry A,* vol. 3, no. 17, pp. 9241-9248, 2015.

4.2. Mechanical Properties of Constituent Materials

4.2.1. Introduction

Organic-inorganic halide perovskite solar cells (PSCs) hold promise for next-generation photovoltaic devices because their remarkable optical properties and high-absorption coefficient [1]. Furthermore, there were demonstrated many advantages for possible candidate of flexible electronics [2]. Mechanical flexibility of the perovskite solar cells together with high photovoltaic efficiency has been attracting attentions because processing temperature are so low that all the constituent materials can be flexible unlike rigid inorganic solar cells. While various flexible materials used for transparent electrodes and hole- and electron-transport layers have been introduced, irreplaceable perovskite materials have organic-inorganic crystalline structures that can be brittle. In most previous studies, flexibility of the flexible PSCs has been evaluated empirically, for example, decrease in photovoltaic performance by cyclic bending deformation for a certain bending radius. Beyond the empirical studies determining flexibility of the flexible PSCs based on repeatable bending tests, investigation on mechanical properties of constituent materials on entire flexible PSCs.

The flexible PSCs using composite electrode were shown great bending durability on bending deformations, and expectation of previous section is that perovskite materials which can be the weakest material among the constituent materials [3]. However, this prediction has not been proven yet. Unlike perovskite materials, electrodes and hole- and electron transport layers for flexible PSCs can be easy handling and sampling. Therefore, many previous studies expected their mechanical properties, but studies of perovskite materials are still insufficient, which have been conducted by nanoindentations and computational simulations [4-9]. Because nanoindentations are evaluated only for local volume of single crystalline perovskite precipitates fabricated by solution-growth method. Therefore, these previous studies may not by represent mechanical properties of film-type perovskite materials including various defects. Furthermore, computation studies are also insufficient to represent mechanical properties of perovskite materials because most computational simulation methods are deal with only atomic scale range, but minimum grain size of most perovskite materials is greater than 150 nm. It is means that most computational methods cannot demonstrate fracture mechanism arise from defects such as grain boundary, and cups between grains.

The many electronic devices are composed with laminated structure of various materials. The flexible PSCs are also composed with laminated structure. In the stressed state, laminated structure has been occurring various deformation, such as delamination and cracking, etc., due to difference of mechanical or thermomechanical properties of each layers. Therefore, investigation of mechanical properties of constituent materials in laminated structure devices is important to measure mechanical reliability for commercialization. But, thickness of constituent materials in flexible PSCs is too thin of

sub-100 nm, exceptional perovskite materials of about 300 nm-thick. Therefore, many previous studies have not been performed direct mechanical testing on these thinner materials. To evaluate mechanical properties of thinner materials, some studies used experimental methods using atomic force microscopy (AFM) indentation on the suspended materials [10]. It is widely used in two-dimensional materials, such as graphene, MoS_2, etc., but this method has limitation of conversion measurement of mechanical properties [11-13].

In the following contents, in this work, I fabricated thinner functional constituent materials of AI 4083, $MAPbI_3$, and $PC_{61}BM$ exception of electrode and substrate. These thin films coated on hole-patterned substrate, and then performed nanoindentation tests via in-situ nanoindentation system. As a result, I can be obtained mechanical properties of entire functional materials and measured elastic limit which is index of mechanical flexibility of reversible process in deformation state. I show that critical bending radius of flexible PSCs using elastic limit via hole-nanoindentation, resulting some unmatched with repeatable bending tests performed previous section. Among them, despite of overestimated mechanical properties vis hole-nanoindentation, perovskite material is suggested as the mechanically-weakest layer.

4.2.2. Experimental Procedure

4.2.2.1. Materials

Polymethyl methacrylate (PMMA, C4) was purchased from Micro Chem. and PEDOT:PSS solutions (Clevious AI 4083 and PH 1000) was purchased from OSM. Methylammonium iodide (MAI) purchased from Dyesol. Lead iodide (PbI_2, 99.9%) was purchased from Alsa Aesar. N,N-dimethylformamide (DMF, anhydrous, 99.8%), Dimethyl Sulfoxide (DMSO, anhydrous, 99.8%), γ-Butyrolactone (GBL, anhydrous, > 99.0%), 2-propanol (IPA, anhydrous, 99.5%), chlorobenzene (anhydrous, 99.8%), hexamethyldisilazane (HMDS) and Zonyl FS-300 were purchased from Sigma Aldrich. [6,6]-Phenyl-C61-butyric acid methyl ester ($PC_{61}BM$, > 99%) was purchased from 1-materials.

4.2.2.2. Thin Films Fabrication

The functional materials are fabricated on sacrificial layer for wet-transfer. The sacrificial layer was conducted to solubility of functional constituent materials. Glass substrate were sequentially cleaned with distilled water, acetone, and IPA. Sacrificial layer was coated on oxygen-plasma treat glass via spin coating. PMMA was spin coated at 2,000 rpm for 45 s and annealing at 110℃ for 5 min. PH 1000 was deposited via spin coating at 5,000 rpm for 45 s and annealing at 150℃ for 10 min. AI 4083 solution was filtered through a 0.45 μm PVDF filter, and spin-coated onto PMMA coated glass substrate at 5,000 rpm for 40 s and annealed at 150℃ for 10 min. To deposit the perovskite layer, the $MAPbI_3$ precursor solution (45 wt.% MAI and PbI_2 1:1 molar ratio in GBL and DMSO (7:3 v/v) co-solvent kept at 100℃) was spin-coated at 5,000 rpm for 25 s, and 0.5 mL chlorobenzene (CB) solvent was dripped onto PMMA coated substrates 10 s after spin-coating and then the samples were annealed at 100℃ for 30 min. The $PC_{61}BM$ solution in CB (2.2 wt.%) was spin-coated at 2,000 rpm for 45 s onto PH 1000 coated glass substrate. The functional films on sacrificial layer were immersed on suitable solvents, which are selective etched only sacrificial layers. And then floating materials was transferred on to hole-patterned silicon substrate.

4.2.2.3. Hole-nanoindentation Tests

The hole-nanoindentation tests were performed to measure mechanical properties of each constituent materials of PSCs. The hole-nanoindentation tests were performed nanoindentation on suspended functional materials, AI 4083, $MAPbI_3$, and $PC_{61}BM$, via in situ nanoindentation system (PI-87 SEM PicoIndenter). This in situ nanoindentation system had installed in scanning electron microscopy (Quanta 200 SEM). The entire tests had holding time for calibration of thermal drift under

0.05 nm s^{-1}. And then nanoindentation tests was performed on center of hole-pattern with a sample-thickness dependent displacement rate.

4.2.3. Results and Discussion

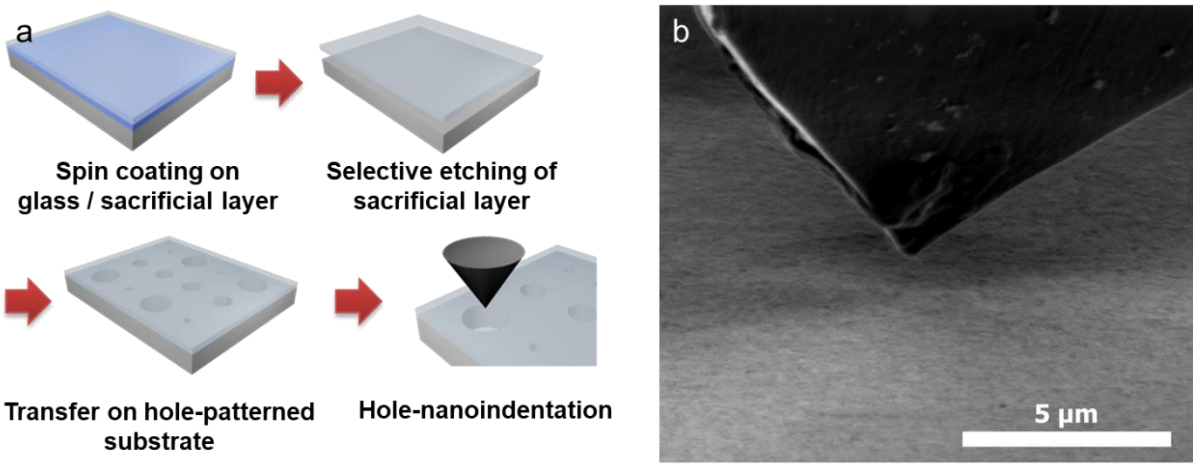

Figure 4.14. (a) Schematics of experimental method of hole-nanoindentation, (b) Typical scanning electron microscopy image of before testing.

The measurement of mechanical properties of functional constituent materials in flexible PSCs are too challenging due to thickness of each materials are below 100 nm, except perovskite material. Accordingly, many studies carried out nanoindentation on precipitation and thick films. To investigate whether flexibility of flexible PSCs is dominated by perovskite materials, we carried out hole-nanoindentation tests for measurement of mechanical properties in constituent materials of flexible PSCs. Unlike nanoindentation on bulk materials which is restricted substrate effect, called 1/10 rule, it is performing nanoindentation on ultra-thin films which is suspended on hole-patterned Si substrate, as shown **figure 4.14** [10]. The hole-pattern was fabricated by photo-resist (PR) process and Deep reactive-ion etching (Deep RIE) process, as shown in **figure 4.15**. The pattered hole sizes were different, which dependent on different sample thickness. The hole diameters were set to be below 1% due to prevention of stress concentration on hole edge. Because of this, AI 4083, $PC_{61}BM$, $MAPbI_3$ thin films were transferred on to 4, 8, 50 μm-diameter hole patterned substrate as shown **figure 4.16**.

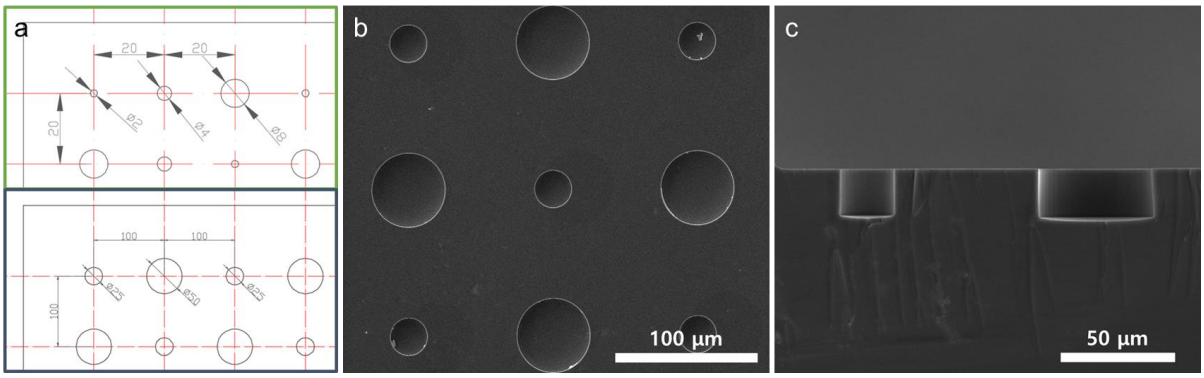

Figure 4.15. (a) the Blueprints of hole patterned mask, (b) Scanning electron microscopy image of hole-patterned substrate, and (c) cross-section SEM image of hole-patterned substrate.

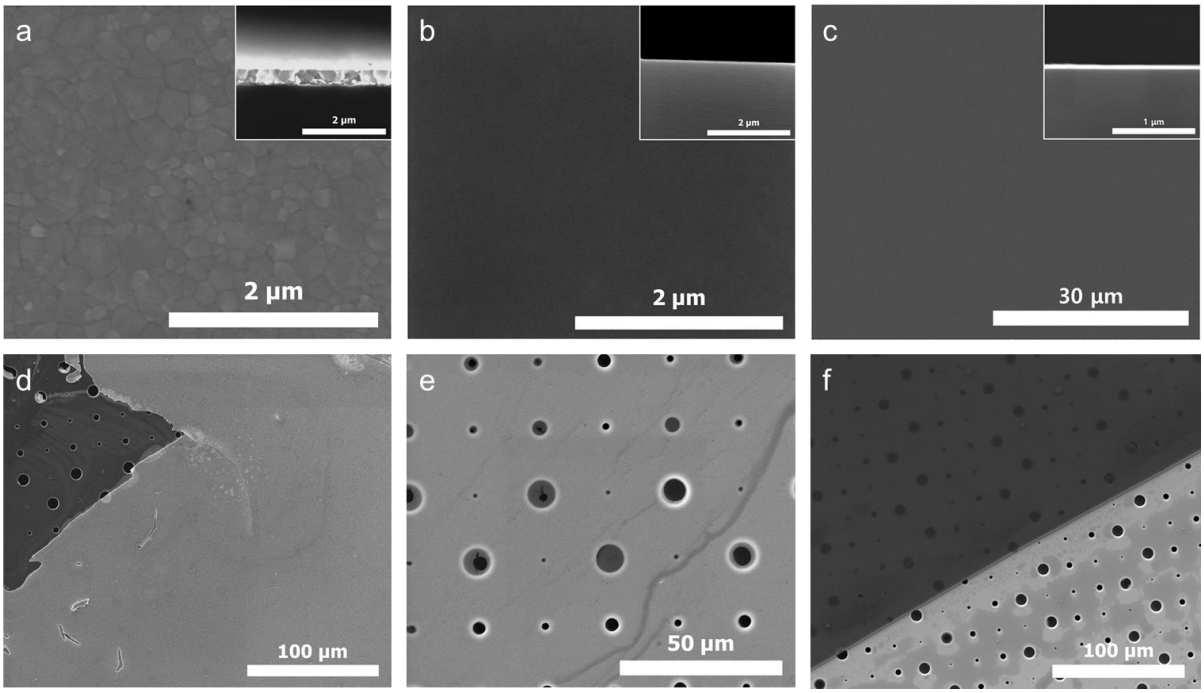

Figure 4.16. The configuration of samples and transferred on hole-patterned substrates, (a) and (d) are $MAPbI_3$, (b) and (e) are AI 4083, (c) and (f) are $PC_{61}BM$.

Figure 4.17 shows typical force-indentation depth curves for AI 4083, $MAPbI_3$, and $PC_{61}BM$. Unlike previous studies of nanoindentation, these were prepared by same conditions and procedures for as the fabrication process of flexible PSCs, and then transferred onto hole-patterned substrate which is assisted by suitable sacrificial layers. It was expected to have identical microstructure and thickness with flexible PSCs. From **figure 4.17**, the fracture strength and elastic modulus of each layers are measure using:

$$F = \sigma_0(\pi a)\left(\frac{\delta}{a}\right) + E(q^3 a)\left(\frac{\delta}{a}\right)^3$$

$$\sigma_f = \left(\frac{FE}{4\pi R}\right)^{\frac{1}{2}}$$

Where F and δ are indentation force and displacement at center point of hole, respectively, σ_0 is the pretension in the film, a is the patterned hole radius, $q = 1/(1.05\text{-}0.15\nu\text{-}0.16\nu^2) = 1.02$ with $\nu = 0.33$ [6] is a dimensionless constant based on Poisson' ratio, ν, R is the indenter tip ratius, E is the elastic modulus, and σ_f is the maximum stress at the center point [10-12]. The elasic modulus and fracture stress were divided by thin film thickness with 40 nm for AI 4083, 300 nm for $MAPbI_3$, 60 nm for $PC_{61}BM$. The fracture strength of each layers was estimated to be 0.87 (±0.09) GPa for AI 4083, 0.49 (±0.01) GPa for $MAPbI_3$, and 0.92 (±0.09) GPa for $PC_{61}BM$, respectively. The elastic modulus was measured as 5.06 (±0.61) GPa for AI 4083, 13.67 (±1.85) GPa, and 11.90 (1.63) GPa for $PC_{61}BM$, respectively.

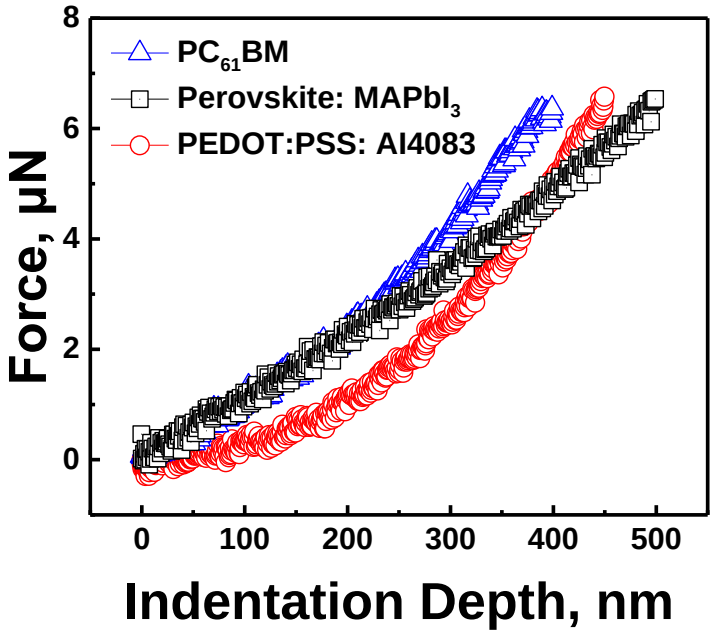

Figure 4.17. Typical force-indentation depth curves of $MAPbI_3$, AI 4083, and $PC_{61}BM$.measured by hole-nanoindentation.

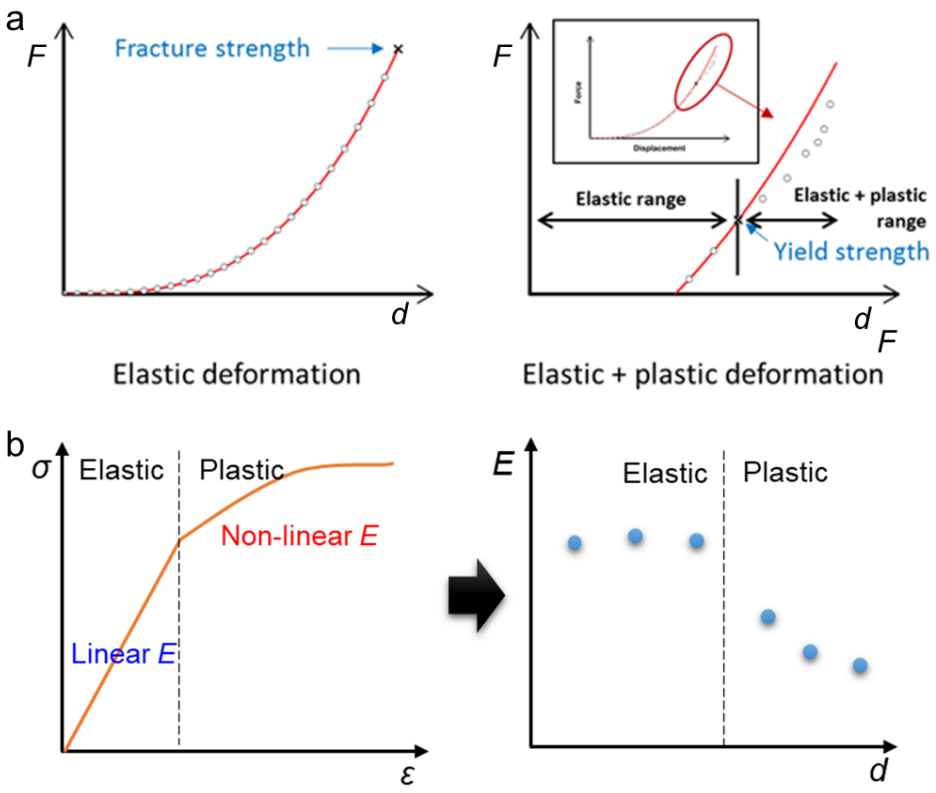

Figure 4.18. Schematics of separation method about elastic and plastic deformation in hole-nanoindentation methods, (a) using fitting curves, and (b) using linear elasticity.

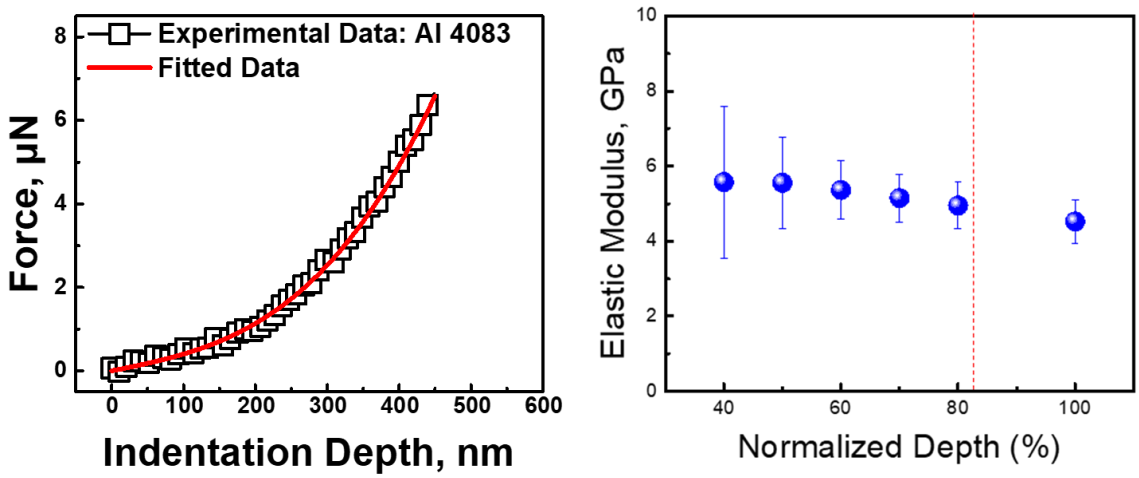

Figure 4.19. Typical hole-nanoindentation curve and linear elasticity of AI 4083.

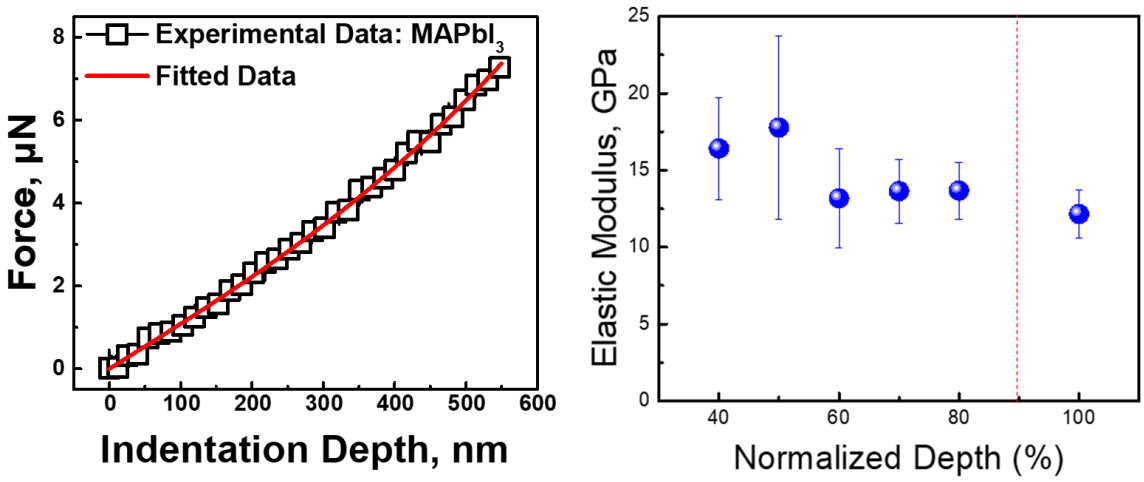

Figure 4.20. Typical hole-nanoindentation curve and linear elasticity of $MAPbI_3$.

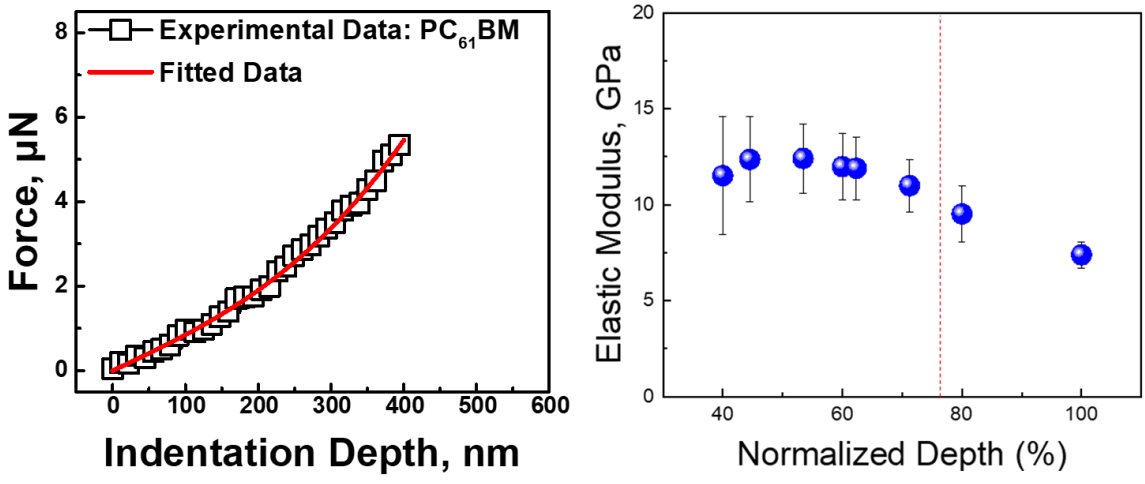

Figure 4.21. Typical hole-nanoindentation curve and linear elasticity of $PC_{61}BM$.

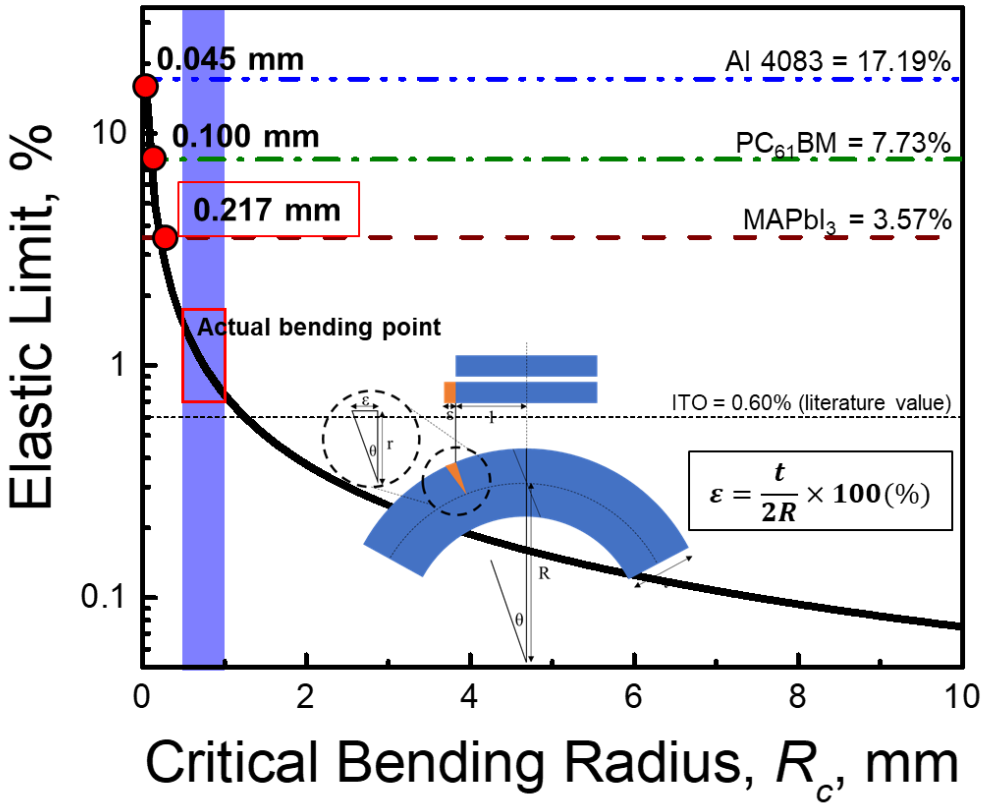

Figure 4.22. Calculation of critical bending radius based on elastic limit measured by hole-nanoindentation of constituent materials in flexible PSCs.

The mechanical flexibility has represented to elastic limit which is separation point between elastic and plastic deformation and revealed recoverable properties after deformation. It was described to **figure 4.18**. In the hole-nanoindentation tests, however, it is difficult to distinguish the brittle/ductile behavior of the materials. Therefore, I can be established that the change of linearity of elastic modulus at a certain proportional of indentation depth as a start of plastic deformation, as shown **figure 4.19 ~ 21**. Coincidentally, it was also confirmed that the fitting of above equation begins to shift from that point. By simple assumption for linear elasticity and fracture, fracture strain is 17.19% for AI 4083, 3.58% for $MAPbI_3$, and 7.73% for $PC_{61}BM$. As previously mentioned, perovskite material is the weakest of all the constituent materials of flexible PSCs. **Figure 4.22** shows calculated critical bending radius based on elastic limit of constituent materials using following equation

$$R_c = \frac{t}{2 \times \varepsilon} \times 100(\%)$$

where t is the total thickness of devices and ε is elastic limit (i.e. yield/fracture strain). Based on the elastic limit of constituent materials by hole-nanoindentation tests, the calculated critical bending radius is 0.05 mm for AI 4083, 0.10 mm for $PC_{61}BM$, and 0.22 mm for weakest $MAPbI_3$ with 15 μm-thick

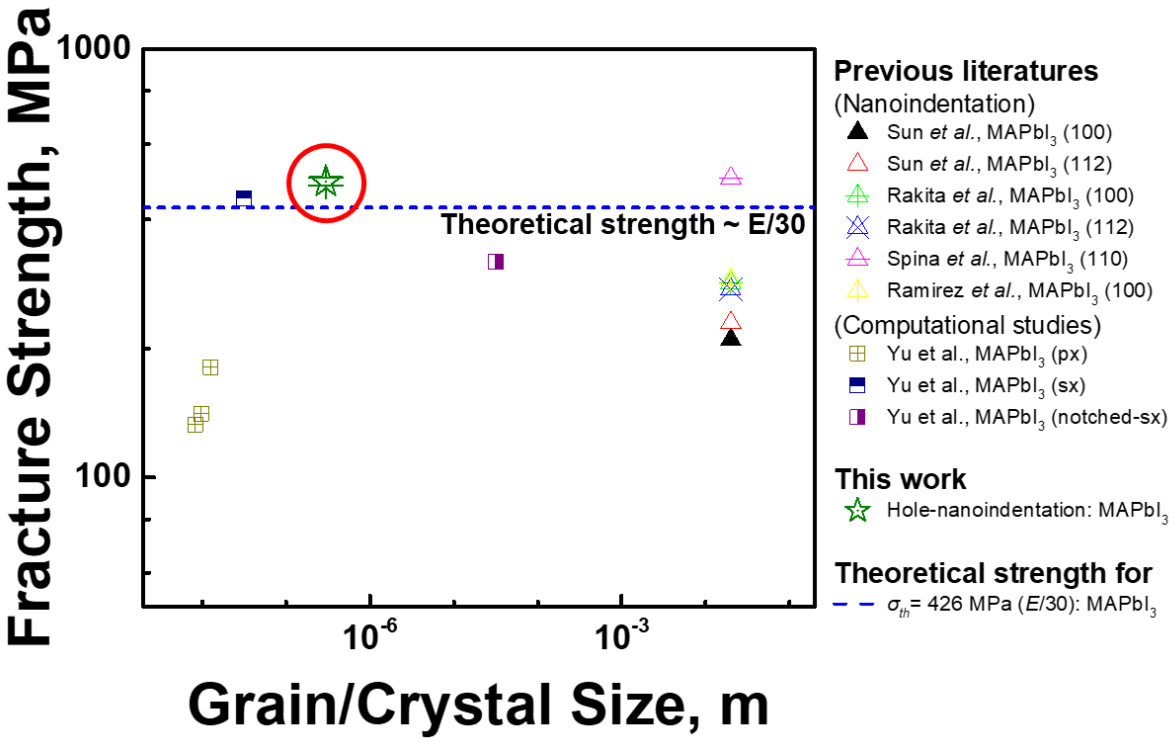

Figure 4.23. Distribution of fracture strength of perovskite materials with previous studies and hole-nanoindentation results.

NOA 88 substrate. It has a difference with repeatable bending tests with critical bending radius of above 0.5 mm. It is means that hole nanoindentation tests were overestimated mechanical properties rather than actual mechanical properties. **Figure 4.23** show fracture strength of the perovskite materials studied so far [4, 5, 7-9]. Previous results by nanoindentations and computational simulations are similar to hole-nanoindentation results approaches 426 MPa for theoretical strength defined by $E/30$.

The possibly reasons of overestimation of hole-nanoindentation are (1) nanoindentation tests are measured only local volume, rarely contained various defects in underneath indenter tip, and the constituent materials in PSCs are brittle manner, so its stress depends on the probability that it contains crack with high stress concentration. (2) in uniaxial tensile state, it is that occur catastrophic failure after crack nucleation near multiple defects due to uniform stress field, but hole-nanoindentation is insufficient driving force to occur catastrophic failure after crack nucleation due to less existence of defects [12]. For these reasons, it is too hard to represent flexibility of constituent materials measured by hole-nanoindentation due to its overestimation. However, it is distinctly indicated that perovskite material is weakest layer in flexible PSCs since it was performed same testing method. This indicate that perovskite materials have dominate mechanical flexibility of flexible PSCs.

4.2.4. Summary

To measure mechanical flexibility of flexible PSCs, I have performed hole-nanoindentation tests for suspended functional constituent materials on hole-patterned substrate. As results, I had obtained the fracture strength of each layers was estimated to be 0.87 (±0.09) GPa for AI 4083, 0.49 (±0.01) GPa for $MAPbI_3$, and 0.92 (±0.09) GPa for $PC_{61}BM$, respectively. The elastic modulus was measured as 5.06 (±0.61) GPa for AI 4083, 13.67 (±1.85) GPa, and 11.90 (1.63) GPa for $PC_{61}BM$, respectively. It was converted to elastic limit because these results was obtained from the range of linear elastic modulus, this indicated the measured in elastic deformation sections. Therefore, fracture (or yield) strain is 17.19% for AI 4083, 3.58% for $MAPbI_3$, and 7.73% for $PC_{61}BM$, and conveted critical bending radius of 0.05 mm, 0,10 mm, and 0.22 mm of each materials, respectively. It was different to critical bending radius measured by repeatable bending tests of 0.5 mm due to mechanical properties measured by hole-nanoindentation is overestimated. The possible reasons of this, hole-nanoindenation is mesurement on local defect-free area and low driving force for occuring catastriphic failure. However, hole-nanoindentation results sugest that cracks initiate in the perovskite materials rather than other constituent materials, indicating perovskite materials dominate mechanical flexibility of flexible PSCs. Therfore, it need to measure acture tensile properties for determining flexibility, this argument will be aimed to following section.

Reference

[1] S. De Wolf *et al.*, "Organometallic Halide Perovskites: Sharp Optical Absorption Edge and Its Relation to Photovoltaic Performance," *The Journal of Physical Chemistry Letters,* vol. 5, no. 6, pp. 1035-9, Mar 20 2014.

[2] L. Li *et al.*, "Recent advances of flexible perovskite solar cells," *Journal of Energy Chemistry*, 2018.

[3] B. J. Kim *et al.*, "Highly efficient and bending durable perovskite solar cells: toward a wearable power source," *Energy & Environmental Science,* vol. 8, no. 3, pp. 916-921, 2015.

[4] S. Sun *et al.*, "Mechanical properties of organic–inorganic halide perovskites, CH3NH3PbX3 (X = I, Br and Cl), by nanoindentation," *Journal of Materials Chemistry A,* vol. 3, no. 36, pp. 18450-18455, 2015.

[5] Y. Rakita *et al.*, "Mechanical properties of APbX 3 (A = Cs or CH3NH3; X = I or Br) perovskite single crystals," *MRS Communications,* vol. 5, no. 04, pp. 623-629, 2015.

[6] J. Feng, "Mechanical properties of hybrid organic-inorganic CH3NH3BX3 (B = Sn, Pb; X = Br, I) perovskites for solar cell absorbers," *APL Materials,* vol. 2, no. 8, 2014.

[7] J. Yu *et al.*, "Probing the Soft and Nanoductile Mechanical Nature of Single and Polycrystalline Organic-Inorganic Hybrid Perovskites for Flexible Functional Devices," *ACS Nano,* vol. 10, no. 12, pp. 11044-11057, Dec 27 2016.

[8] M. Spina *et al.*, "Mechanical signatures of degradation of the photovoltaic perovskite CH3NH3PbI3upon water vapor exposure," *Applied Physics Letters,* vol. 110, no. 12, 2017.

[9] M. A. Reyes-Martinez *et al.*, "Time-Dependent Mechanical Response of APbX3 (A = Cs, CH3 NH3 ; X = I, Br) Single Crystals," *Advanced Materials,* vol. 29, no. 24, Jun 2017.

[10] C. Lee *et al.*, "Measurement of the elastic properties and intrinsic 1strength of monolayer graphene," (in English), *Science,* vol. 321, no. 5887, pp. 385-388, Jul 18 2008.

[11] S. Bertolazzi *et al.*, "Stretching and breaking of ultrathin MoS2," *ACS Nano,* vol. 5, no. 12, pp. 9703-9, Dec 27 2011.

[12] J. Han *et al.*, "Nanoindentation cannot accurately predict the tensile strength of graphene or other 2D materials," *Nanoscale,* vol. 7, no. 38, pp. 15672-9, Oct 14 2015.

[13] N. R. Kang *et al.*, "Wall-thickness-dependent strength of nanotubular ZnO," *Scientific Reports,* vol. 7, no. 1, p. 4327, Jun 28 2017.

4.3. Quantitative Tensile Properties of Perovskite Materials

4.3.1. Introduction

Organic-inorganic halide perovskite solar cells hold promise for flexible PSCs due to its remarkable optical properties [1], thinner fabrication ability, and low temperature manufacturing ability [2, 3]. Therefore, many previous studies had fabricated flexible PSCs and they measured flexibility using only repeatable bending tests [4-7]. Therefore, there has been a continuing demand for tensile properties that can directly predict flexibility [8]. However, perovskite is very vulnerable to moisture and oxygen, making it difficult to fabricate and handle samples [9, 10].

To investigate mechanical properties of perovskite materials which can be the most vulnerable materials among the functional constituent materials have been conducted by nanoindentation and computational simulation methods. Because nanoindentations are measured only for local volume, mechanical properties measured by nanoindentations may not represent mechanical properties of thin film-type perovskite materials including various defects [9, 11-14]. Elastic properties of perovskite materials, $MABX_3$ (B=Pb, Sn; X=I, Br) have been investigated by first principle theory based on density functional theory (DFT) [15], which can be restrict to perfect crystallin structures. The best way to overcome limitations of nanoindentation and DFT studies is to measure uni-axial tensile properties of fee-standing perovskite materials because (1) gauge section can include all possible defects that tensile properties represent real mechanical properties of the perovskite materials and (2) deformation and fracture behavior of the perovskite materials at any deformed states of the solar cell can be predicted by solid mechanics with their tensile properties [16].

There has been a computational study on tensile behavior of single- and poly-crystalline perovskite materials, but experimental measurement of tensile properties of free-standing perovskite materials has not been reported so far as far as known [8]. This is possibly because perovskite materials have limits in the long- and short-term environmental stability issues, resulting the various atomistic interactions. Direct measurements of deformation behaviors based on mechanical properties are challenging due to the high sample quality and large samples, including a lot of defects, are required. The previous work of hole-nanoindentation results was directly measured fracture strength and elastic modulus, but it is cannot be include various defects which are affected actual fracture response.

As a mentioned previous works, the perovskite layer is suggested as the mechanically-weakest layer. Here, the last work in this thesis, I report uni-axial tensile properties of four perovskite materials, $MAPbI_3$, $MAPb(I_{0.87}Br_{0.13})_3$, and two solvent annealed $MAPb(I_{0.87}Br_{0.13})_3$. The perovskite materials were synthesized by the same conditions and procedures as fabrication processes of the flexible PSCs. They all show linear elasticity followed by brittle fracture. The elastic modulus and fracture strength

are correlated with microstructures of the perovskite materials. The doping of Br atoms in halide site, it was enhancing photovoltaic performance and stability, but mechanical properties is decreasing due to its lattice distortion. Smaller Br atoms play role of point defects it was occurring lattice distortion. Furthermore, this work was demonstrated the grain size effect on mechanical properties. Unlike Br doping, increasing grain size is enhancing both photovoltaic properties and mechanical properties. However, mechanical flexibility along grain sizes is nearly constant due to non-linear elastic modulus values.

4.3.2. Experimental Procedure

4.3.2.1. Materials

Polymethyl methacrylate (PMMA, C4) was purchased from Micro Chem. Methylammonium iodide (MAI) and Methylammonium bromide (MABr) were purchased from Dyesol. Lead iodide (PbI_2, 99.9%) was purchased from Alsa Aesar. N,N-dimethylformamide (DMF, anhydrous, 99.8%), Dimethyl Sulfoxide (DMSO, anhydrous, 99.8%), γ-Butyrolactone (GBL, anhydrous, > 99.0%), 2-propanol (IPA, anhydrous, 99.5%), chlorobenzene (anhydrous, 99.8%) were purchased from Sigma Aldrich.

4.3.2.2. Perovskite Thin Films Fabrication

The perovskite materials are fabricated on sacrificial layer of PMMA for wet-transfer. The PMMA sacrificial layer were selective dissolved in chlorobenzene. Glass substrate were sequentially cleaned with distilled water, acetone, and IPA. PMMA was deposited on oxygen-plasma-treated glass via spin-coating at 2,000 rpm for 45 s and annealed at 110℃ for 5 min. To deposit the perovskite layer, the $MAPbI_3$ precursor solution (45 wt.% MAI and PbI_2 1:1 molar ratio in GBL and DMSO (7:3 v/v) co-solvent kept at 100℃) was spin-coated at 5,000 rpm for 25 s, and 0.5 mL chlorobenzene was dripped onto the substrates 10 s after spin-coating. The samples were annealed at 100℃ for 30 min. the $MAPb(I_{0.87}Br_{0.13})_3$ precursor solution (45 wt% MAI, MABr, and PbI_2 0.6:0.4:1 molar ratio in GBL and DMSO (7:3 v/v) co-solvent kept at 100℃) were made by stoichiometric mixing, and spin-coated at 5,000 rpm 25 s, and 0.5 mL chlorobenzene was dripped onto the substrates 10 s after spin-coating. The samples were annealed also at 100℃ for 30 min. The large grain samples were prepared via solvent annealing methods. The perovskite films were covered by a glass petri dish around 20 μL of DMF solvent was added at the opposite of petri dish during thermal-annealing process with different temperature of 50℃ and 80℃ for 30 min. The DMF vapor was expected to be able to contact perovskite films and lead to growth of grain of perovskite material.

4.3.2.3. Uni-axial Tensile Tests

Preparation of tensile samples were illustrated in **figure 4.24**. $MAPbI_3$ and $MAPb(I_{0.87}Br_{0.13})_3$ layers were spin-coated onto PMMA coated glass substrate at same conditions and procedures as the fabrication process of the solar cell devices. In order to analyze the effect of grain size, solvent annealing processes were performed in DMF atmosphere as suggested in previous study. The PMMA layers play role as a sacrificial layer without affecting perovksite layer. To remove PMMA sacrificial layer, samples immersed in anhydrous chlorobenzene, and the free-standing perovksite layer were transffered onto 50

μm-diameter hole-patterned Si substrates. Dog-born shaped tensile samples with gauge length of 10 μm and gauge width of 5 μm were fabricated by focus ion beam (Quanta 3D FEG) milling and transferred onto push-to-pull device using micro-manipulator system. In situ tensile tests were performed by in situ SEM nanoindenter systme (PI-87 SEM PicoIndenter) at a constant displacement rate of 10 nm s^{-1}. The machine compliance including stiffness of the push-to-pull devices was calibrated by tensile testing without samples and was corrected for caculation of stress-strain values.

4.3.3. Results and Discussion

Figure 4.24 shows the schematic of uni-axial tensile testing for perovskite materials using in-situ nanoindentation system. the perovskite materials were spin-coated onto PMMA coated glass substrate at same conditions and procedures as the fabrication process of the flexible PSCs. The tensile sample of perovskite materials were fabricated by focus ion beam, and transferred onto push-to-pull devices, as shown in **figure 4.25**. **Figure 4.26** shows the typical true stress-stain curves for two perovskite materials; tensile strain was estimated by image correlation method as shown **figure 4.27**. The elastic modulus was measured to be 5.54 (±0.73) GPa for $MAPbI_3$, 4.54 (±0.51) GPa for $MAPb(I_{0.87}Br_{0.13})_3$, and tensile fracture strength was measured to be be 63.23 (±7.76) MPa for $MAPbI_3$, 47.4 (±4.95) MPa for $MAPb(I_{0.87}Br_{0.13})_3$. Many previous studies have been studied mixed halide to enhance stability and tune bandgap. In the mixed halides, substitution of smaller Br atoms with larger I atoms causes reduction of lattice parameter and transition from tetragonal phase to cubic phase [17-19]. To investigate effect of substitution of Br atoms with I atoms on mechanical properties, in-situ tensile

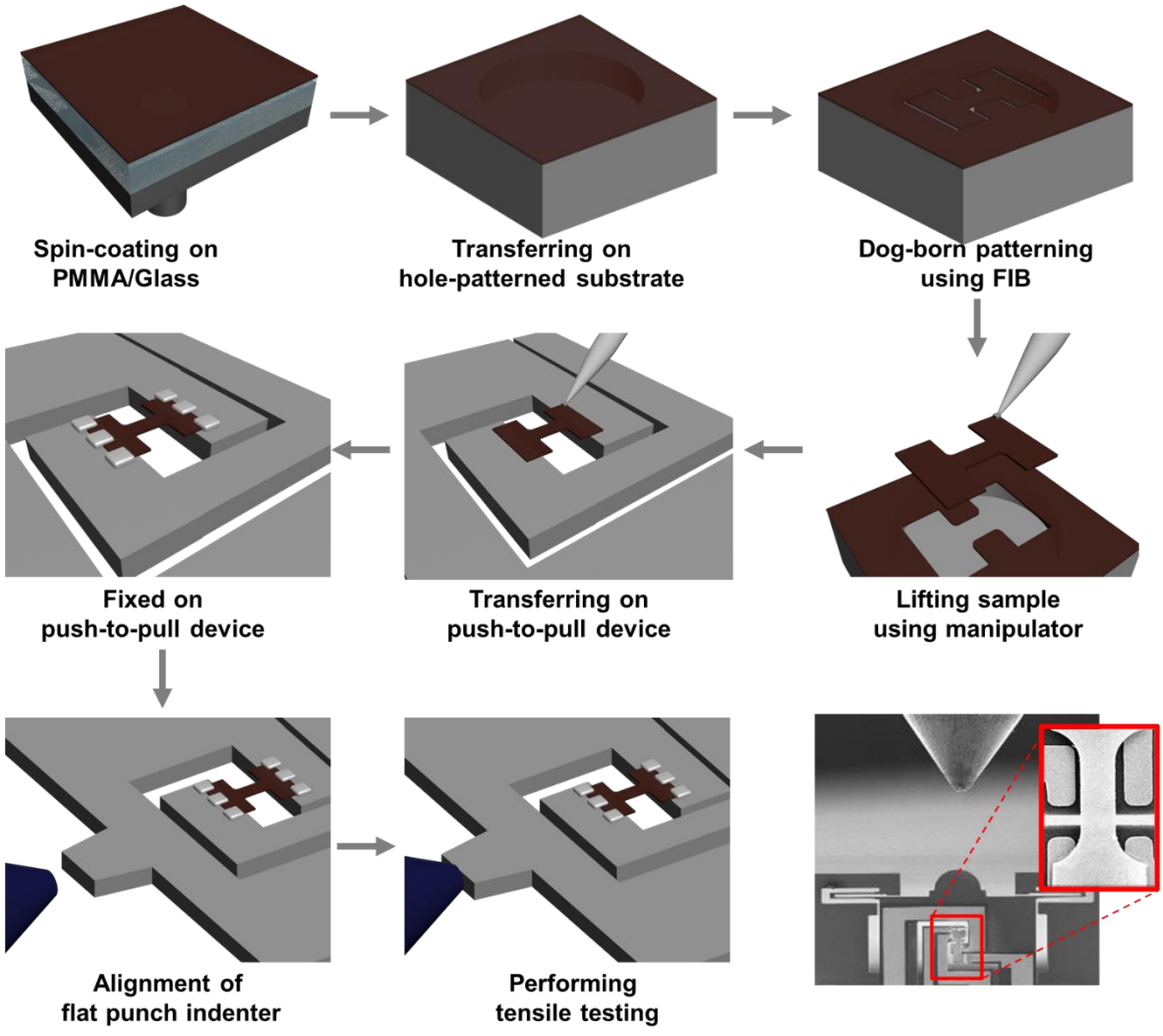

Figure 4.24. Schematics of in situ SEM tensile tests methods.

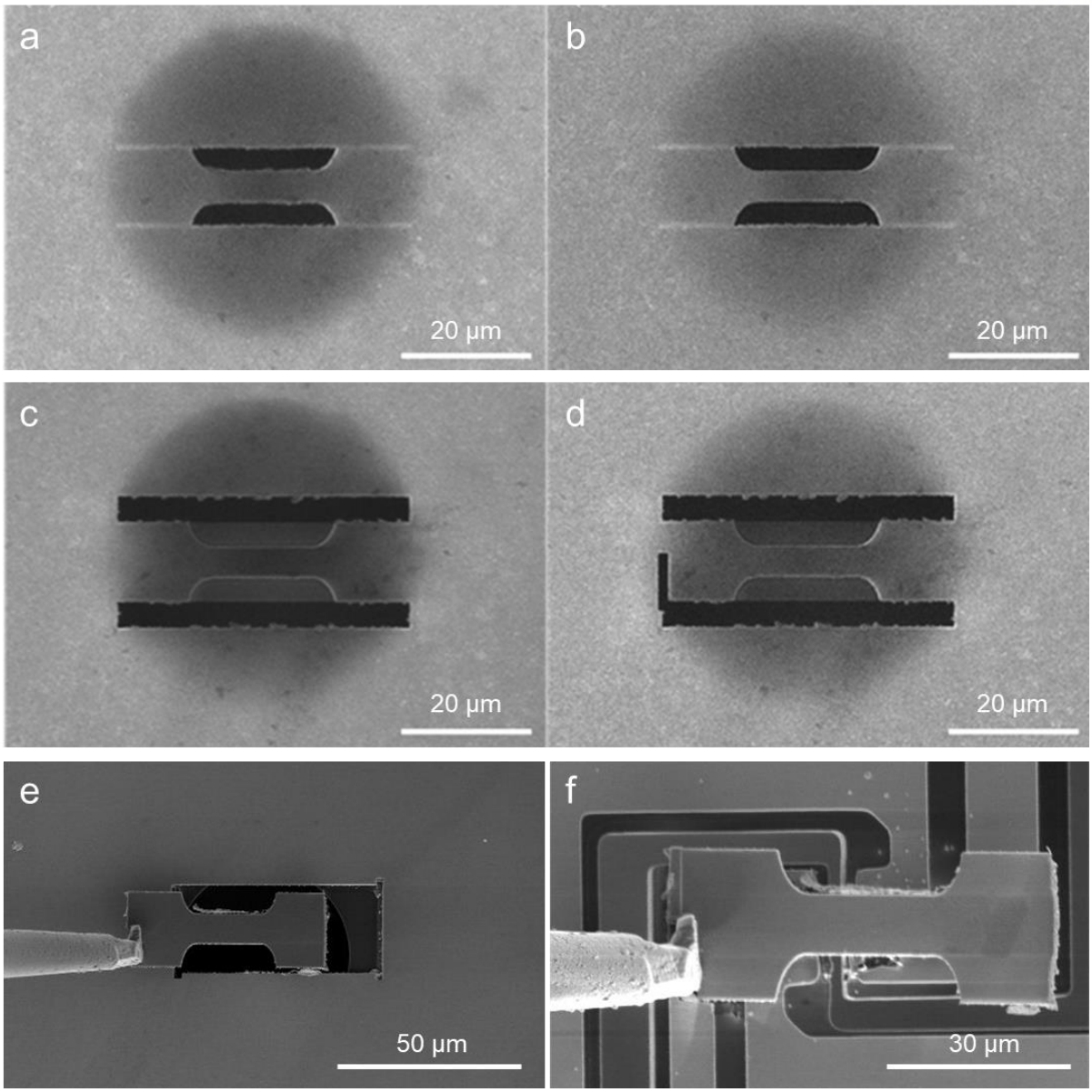

Figure 4.25. Preparation of tensile samples via focus ion beam system.

testing was performed for two perovskite materials, $MAPbI_3$ and $MAPb(I_{0.87}Br_{0.13})_3$. The elastic modulus of $MAPbI_3$ is greater than that of $MAPb(I_{0.87}Br_{0.13})_3$ by 22%. By previous DFT simulations and nanoindentations for single crystalline $MAPbX_3$ (X=I and Br), elastic modulus of $MAPbBr_3$ is greater than that of $MAPbI_3$ because bonding strength of Pb-Br is greater than that of Pb-I [11, 12, 15]. While $MAPbI_3$ has tetragonal structure and $MAPbBr_3$ has cubic structure at room temperature, both $MAPbI_3$ and $MAPb(I_{0.87}Br_{0.13})_3$ are expected to have tetragonal structures because transition from tetragonal structure to cubic structure occurs when X in $MAPb(I_{1-X}Br_X)_3$ is greater than 0.20. In $MAPb(I_{1-X}Br_X)_3$, however, begin to transit to pseudo-cubic (pc) structure because perovskite structure is slight rotation of PbX_6 cages along the <001> axis in substitution of Br atom instead of I atom over 13%. It was certified to X-ray diffraction patterns in previous study that (004) tetragonal plane is

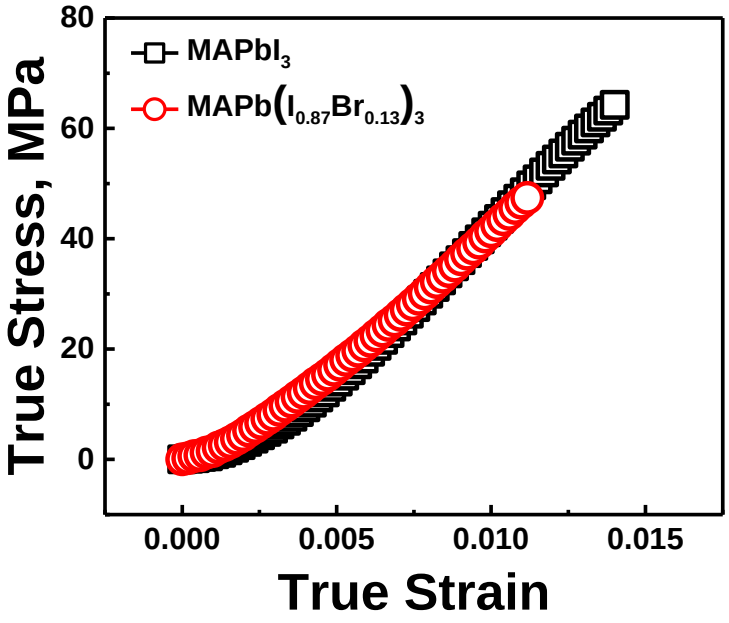

Figure 4.26. Typical true stress-strain curves of $MAPbI_3$ (open-black squares) and $MAPb(I_{0.87}Br_{0.13})_3$ (open-red circles).

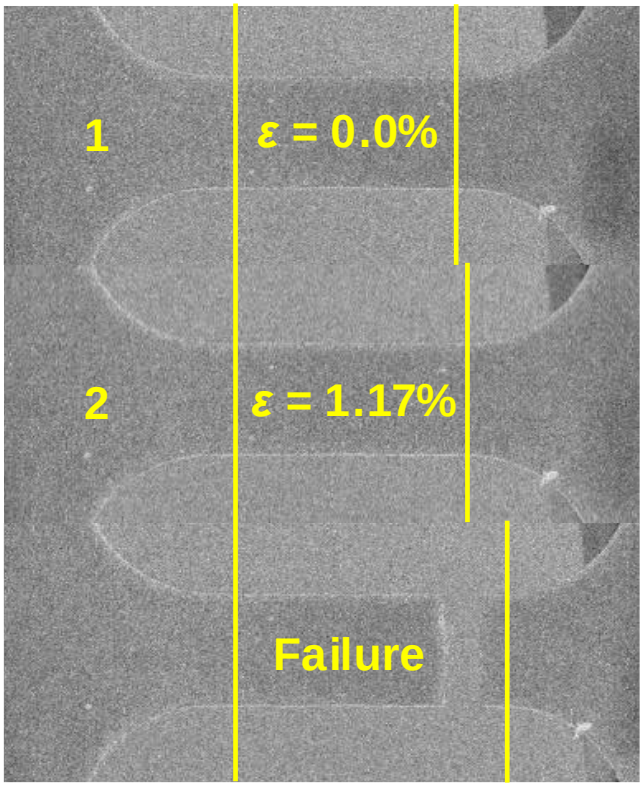

Figure 4.27. Image correlation methods for measurement of true strain during in situ SEM tensile tests.

gradually disappeared with increasing fraction of Br atoms, and finally merges into (200) cubic plane around 20% fraction of Br atoms. In 13 ~ 20% Br atoms, therefore, (100) pseudo-cubic plane can match

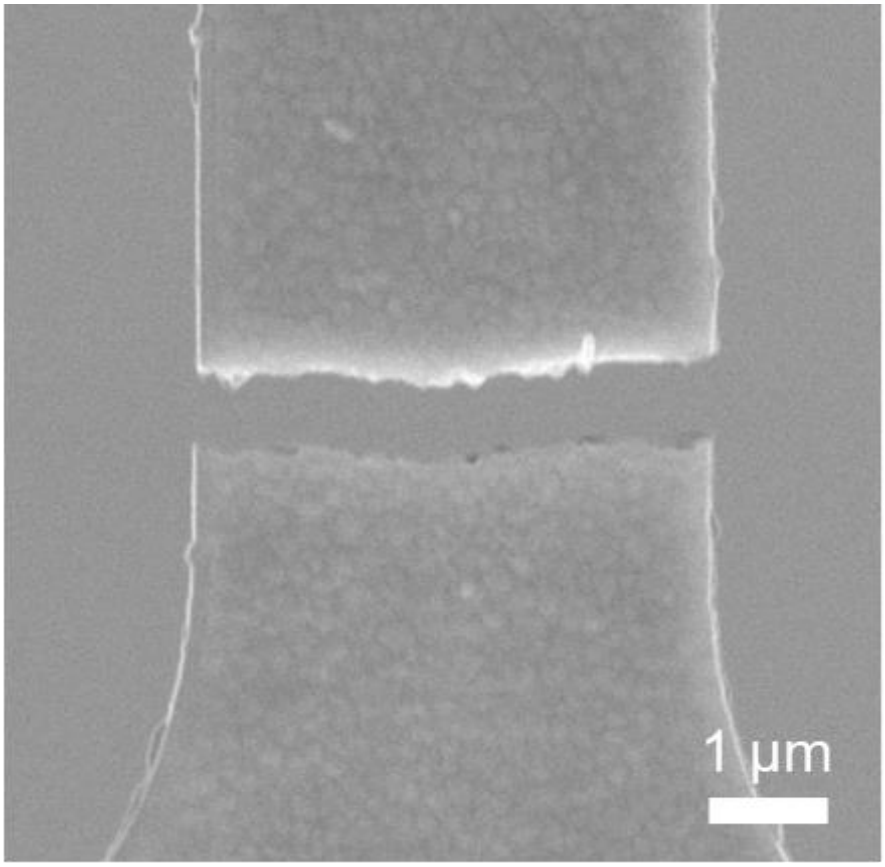

Figure 4.28. Scanning electron microscopy image of $MAPbI_3$ after failure, which occurred intergranular fracture.

with (100) tetragonal plane, which means, despite tetragonal phase, that is arranged in a cubic shape through a lattice tilting [17]. The cubic structure has more slip systems than tetragonal structure, and therefore more dislocation systems may be active in cubic structure [20]. As results, the tensile fracture strength of $MAPbI_3$ is greater than $MAPb(I_{0.87}Br_{0.13})_3$ by 33% [11, 12]. Strength is more affected by defects while elastic modulus tends to depend on atomic bonding.

Important parameter determining flexibility of materials is tensile elastic limit because elastic deformation within elastic limit is recoverable. The tensile stress-strain cures for both $MAPbI_3$ and $MAPb(I_{0.87}Br_{0.13})_3$ show linear elasticity followed by negligible plasticity, and catastrophic failure. The tensile elastic limit is 1.17 (±0.13) % for $MAPbI_3$ and 1.05 (0.10) % for $MAPb(I_{0.87}Br_{0.13})_3$. As shown in **figure 4.28**, failure occurred by intergranular fracture owing to rapid crack propagation along grain boundaries. More stress concentrates at grain boundaries than interior of grains, so crack initiates at a grain boundary and propagates rapidly along with grain boundaries. This indicates that the stress required to initiate crack at the weakest grain boundary is directly related with tensile fracture strength of the perovskite materials.

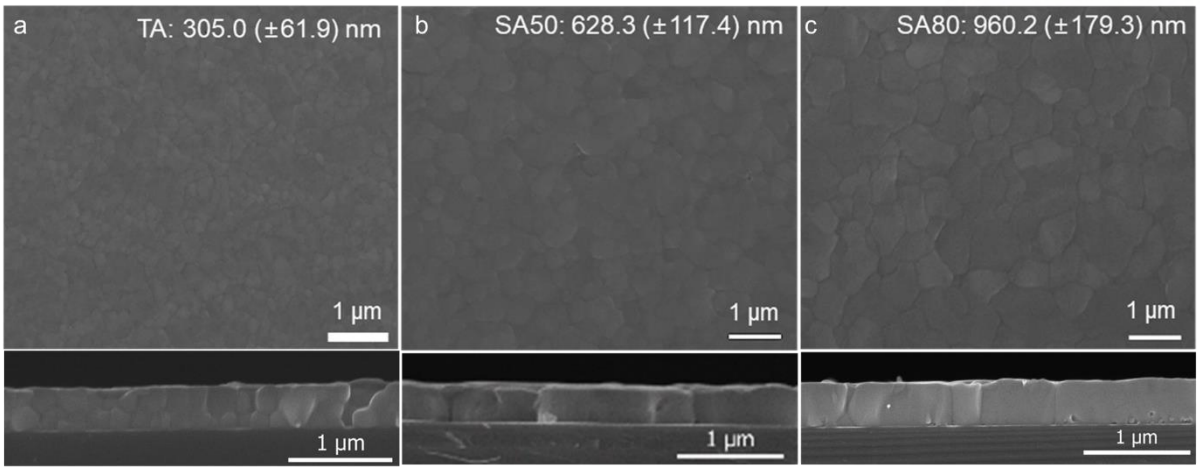

Figure 4.29. Scanning electron microscopy image of $MAPbI_3$ with different grain size samples, (a) thermal-annealed sample, (b) 50°C solvent-annealed sample, and (c) 80°C solvent-annealed sample.

It is well known that crystallinity and grain size have an enormous effect in performance of electronic devices due to decreasing trap site and improving charge mobility. A lot of researcher puts a lot of effort into increase the crystallinity and grain size [21-23]. There are easily controlled by heat-treatment condition and molar concentration of precursor solutions. I found grain boundaries are crack initiation site and propagation path, which implies that grain size could be important factor to determine tensile fracture strength of the perovskite materials. To investigate effect of grain size on tensile properties, three $MAPb(I_{0.87}Br_{0.13})_3$ samples with different grain sizes with 305.0 (±61.9) nm for as-

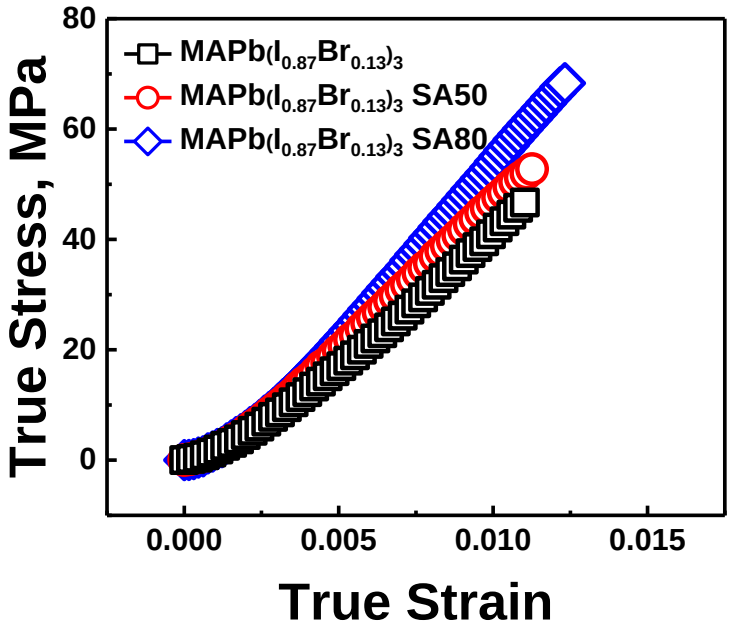

Figure 4.30. Typical true stress-strain curves for three different grain size samples of $MAPb(I_{0.87}Br_{0.13})_3$, with TA sample (open-black squares), SA50 (open-red circles), and SA80 (open-blue diamond rhombuses).

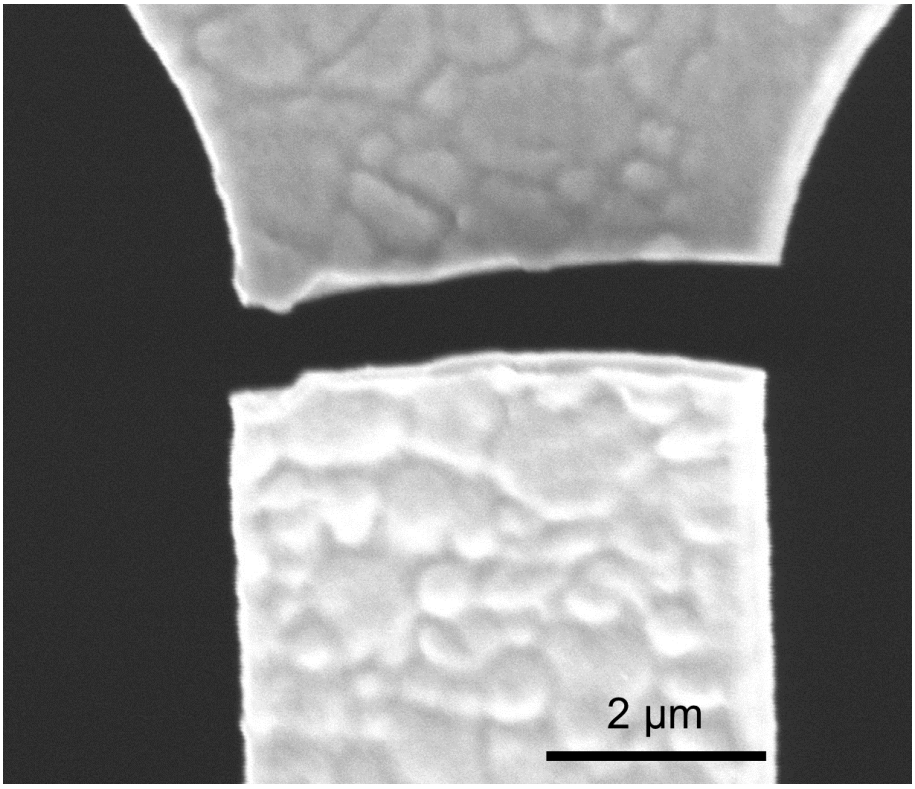

Figure 4.31. Scanning electron microscopy image of $MAPb(I_{0.87}Br_{0.13})_3$ with 80°C solvent annealing after failure, which occurred intergranular fracture.

thermal annealing samples, 628.3 (±117.4) nm for 50°C solvent-annealed samples, and 960.2 (±179.3) nm for 80°C solvent-annealed samples as shown in **figures 4.29**. Grain sizes were determined from at least 100 measurements in SEM images on the basis of diameter of grains. **Figure 4.30** shows typical true stress-strain curves for three samples with different grain size. All the stress-strain curves show linear elasticity, followed by negligible plasticity and failure. Unlike typical polycrystalline materials, Hall-Petch relationship, it is revealed that tensile mechanical properties of perovskite materials are improved when increasing grain size. This phenomenon can be described in amorphization process of grain boundary cause by lattice distortion of Pb-X. These amorphic grain boundaries play role of weakening of fracture strength and crack-propagation path which is occurring intergranular fracture [8, 24]. It is well known density of grain boundaries are linearly decrease with increasing grain size which imply that decrease crack propagation path in larger grain size samples. Interestingly, large grain size samples were occurring different fracture behavior with small grain size sample. Crack initiating on tensile state of polycrystalline thin film, which have seen inverse Hall-Petch relation, is occurring in grain boundary junction which is then propagating along grain boundary [25]. However, crack generated in large grain sample was propagating on grain interior which is transgranular fracture as shown in **figure 4.31**. The distribution of low-angle boundaries of large grain samples is higher than small grain size samples. It is reported that low misorientation is demonstrated through less hysteresis of ion migration system with increasing grain size due to most grain boundaries were aligned

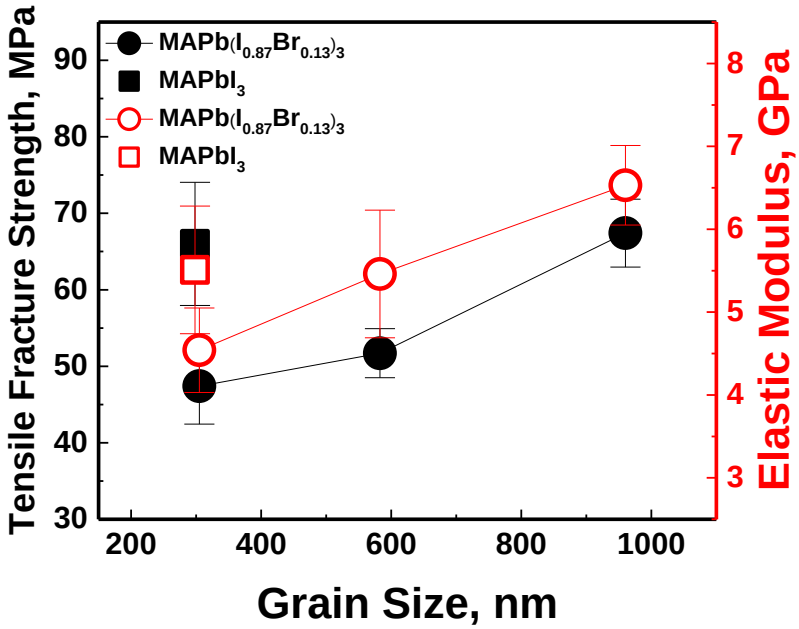

Figure 4.32. Relation between mechanical properties and grain size, yield stress (filled black circles and square) and elastic modulus (dot-centered red circles and square).

perpendicular to substrate [26]. The low- angle grain boundaries are resistant to intergranular fracture, which occurred transgranular fracture due to high resistance of fracture in grain interior [27]. **Figure 4.32** shows that both tensile fracture strength and elastic modulus increase with increasing grain size. Increase in elastic modulus with increasing elastic modulus is possibly because atomic defects interior grains are annihilated during additional solvent annealing. Strengthening of grain boundaries during solvent annealing process is accomplished possibly because (1) excess volume in grain boundaries shrank and (2) cusps became so blunt that stress concentrations at cusps are reduced, as shown **figure 4.33**.

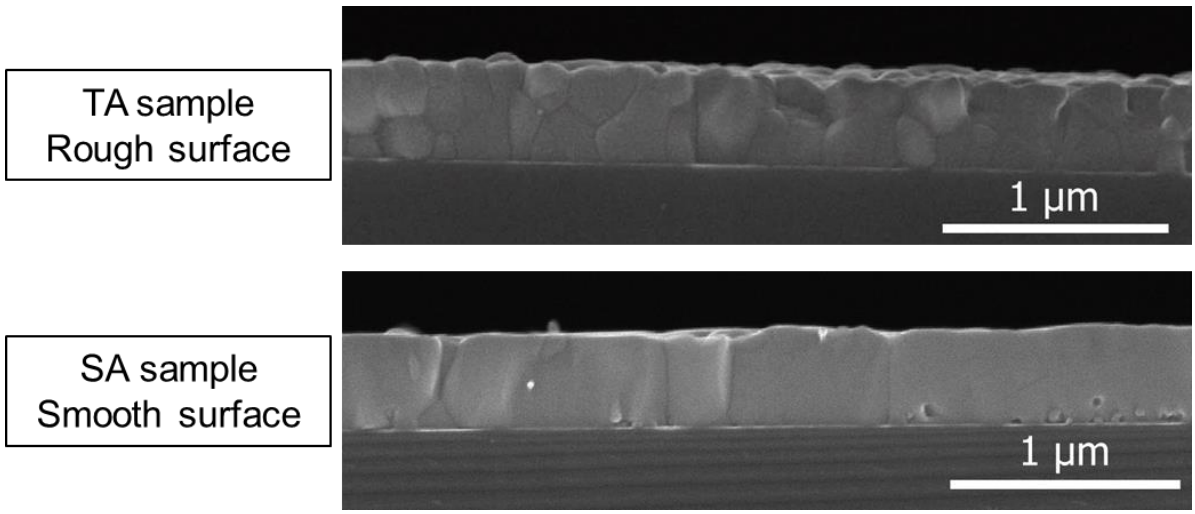

Figure 4.33. Cross-section SEM image of TA and SA samples comparing cusps and surfaces.

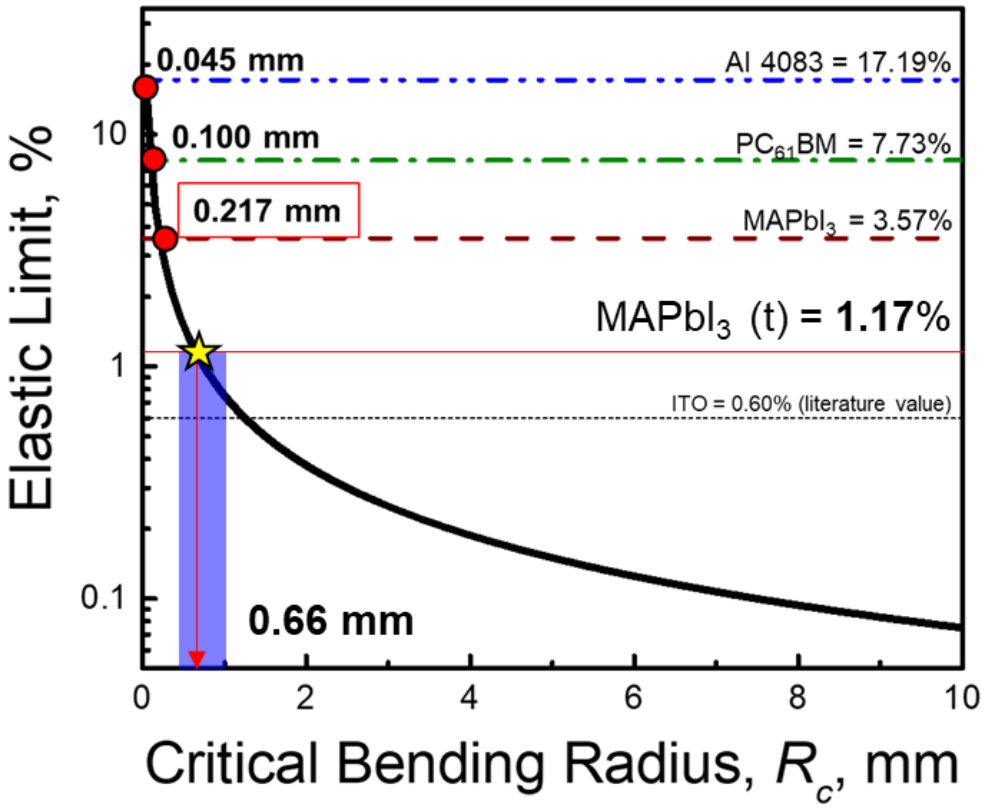

Figure 4.34. Relationship between elastic limit and critical bending radius measured by hole-nanoindentation and uni-axial tensile tests.

As a mentioned previous work, the mechanical flexibility is determined by elastic limit measure by tensile tests. The critical bending radius was over 0.5 mm determined by repeatable bending tests. **Figure 4.34** show calculated critical bending radius based on elastic limit of $MAPbI_3$ and results of hole-nanoindentation using following equation

$$R_c = \frac{t}{2 \times \varepsilon} \times 100(\%)$$

where t is the total thickness of devices and ε is elastic limit. Based on the elastic limit of $MAPbI_3$ by uni-axial tensile tests, the calculated critical bending radius is 0.66 mm with 15 μm-thick NOA 88 substrate. It is well-agreement with critical bending radius of above 0.5 mm measured by repeatable bending tests as shown in **figure 4.34**. While coarsening grains increase elastic modulus and tensile fracture strength as described above, tensile elastic limit, important parameter for flexibility, is similar for three samples regardless of grain size as shown in **figure 4.35,** because strain is given by stress over elastic modulus, $\varepsilon = \sigma/E$ and both tensile strength and elastic modulus increase with increasing grain size.

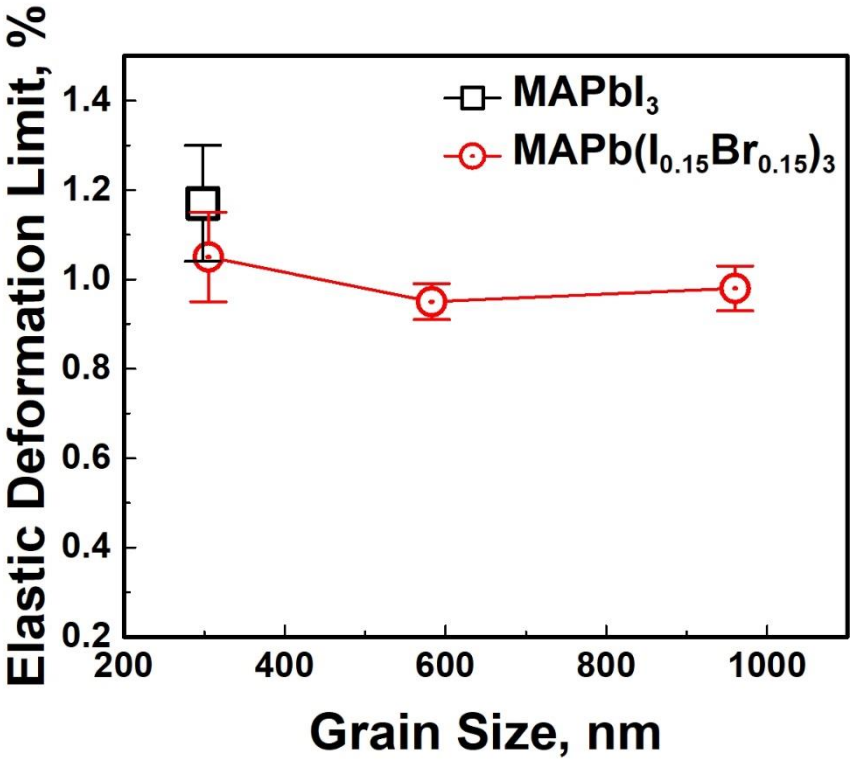

Figure 4.35. Elastic deformation limit of $MAPbI_3$ and three $MAPb(I_{0.87}Br_{0.13})_3$ samples with different grain size.

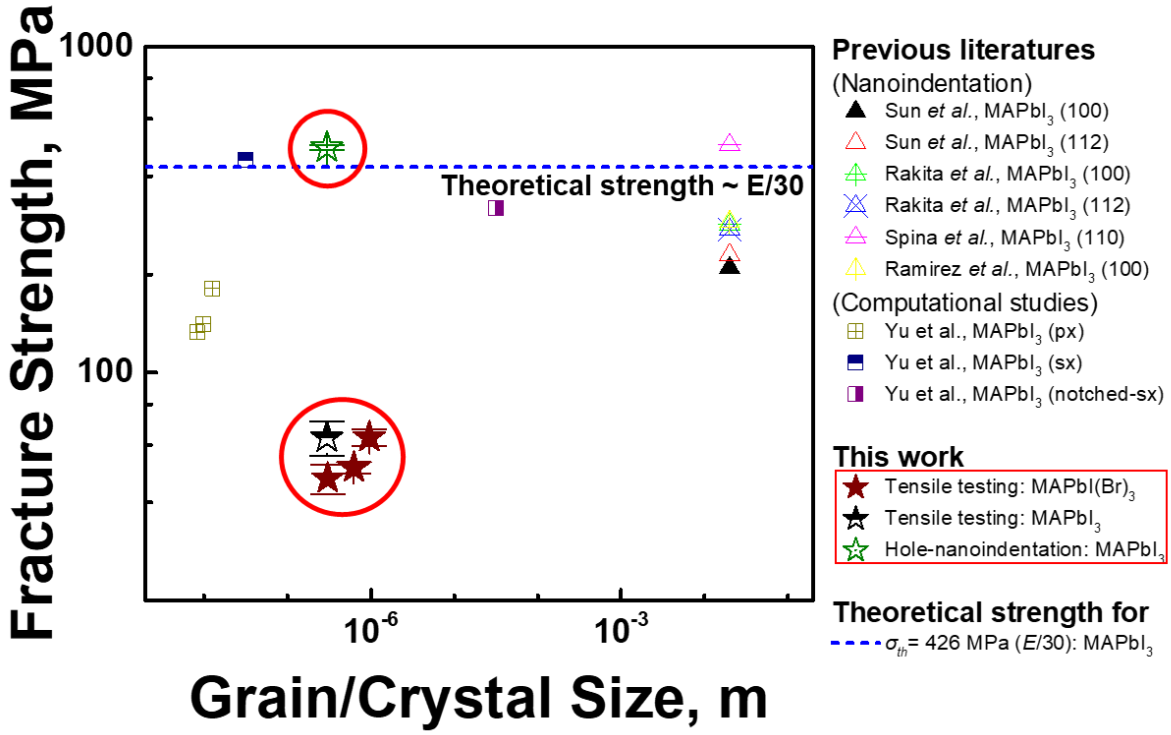

Figure 4.36. Distribution of fracture stress and grain/crystal size of perovskite materials obtained by previous studies and experimental data of this study (shows star symbols).

Figure 4.36 shows fracture strength of the perovskite materials studies so far [8, 9, 11-15]. Previous results by nanoindentations and computational simulations, even though hole-nanoindentation performed in this work, are much higher than this work measured by uni-axial tensile tests as summarized in **table 4.2**. This is because gauge section in tensile test samples includes all possible defects as in the flexible PSCs, which is close to real strength of the perovskite materials. The results of this work are expected to be used as important indicator for mechanical reliability of flexible perovskite devices.

Table 4.2. Mechanical properties of perovskite materials.

Materials	Structure	*E* (GPa)	*H* (GPa)	σ (MPa)	E.L.	Ref.
$MAPbI_3$	Tetragonal	10.4~10.78	0.42~0.46			[11]
$MAPbBr_3$	Cubic	17.7~15.6	0.31~0.26			[11]
$MAPbCl_3$	Cubic	19.8~17.4	0.29~0.25			[11]
$MAPbI_3$	Tetragonal	12.8				[14]
$MAPbBr_3$	Cubic	29.1				[14]
$MAPbI_3$	Tetragonal	14.3~14.0	0.57~0.55			[12]
$MAPbBr_3$	Cubic	19.6	0.36			[12]
$MAPbI_{2.93}Cl_{0.07}$	Tetragonal	13.5				[28]
$MAPbI_3$	Tetragonal	11.6	0.55			[9]
$MAPbBr_3$	Cubic	18.9	0.36			[14]
$MAPbI_3$	Tetragonal	20.0	1.00			[14]
$MAPbI_3$	Tetragonal	17.8~12.7	0.58~0.48			[8]
$MAPbI_3$	Tetragonal	14.94/5.08~7.89		449/133~181	5/3.4~4.6	[8]
$MAPbI_3$	Tetragonal	5.44		63.23	1.17	This work
$MAPb(I_{0.87}Br_{0.13})_3$	Tetragonal	4.53~6.43		47.4~63.41	0.95~1.05	This work

4.3.4. Summary

To measure direct tensile properties, I occurred uni-axial tensile tests for four samples of $MAPbI_3$ and three $MAPb(I_{0.87}Br_{0.13})_3$ with different grain size fabricated by solvent annealing. Because of challenging sampling and handing issues for measuring mechanical properties of perovskite materials, this uni-axial tensile testing and sampling were carried out in isolated high vacuum state. All of results of tensile tests revealed linear elasticity, followed by negligible plasticity and failure. It is means that perovskite materials are brittle nature, which can be confirmed in fracture behavior of intergranular fracture. This means grain boundaries are weaker than grain interiors, which is possibly because (1) grain boundaries naturally contain excess volume, (2) stress concentrates more at cusps, and (3) amorphous structure in grain boundaries caused by lattice distortion of Pb-X bonding. Interestingly, failures for solvent-annealed samples are accomplished by transgranular fracture. this indicates load-bearing ability of grain boundaries is similar to that of grain interiors for solvent-annealed samples. strengthening of grain boundaries during solvent annealing process is accomplished possibly because (1) excess volume in grain boundaries shrank and (2) cusps became so blunt that stress concentrations at cusps are reduced. Furthermore, the critical bending radius calculated by elastic limit, which is measured by tensile tests, is well-agreement with critical bending radius measured by repeatable bending radius. This indicates that mechanical flexibility of flexible PSCs, which are used in this work, is dominated by perovskite materials, especially tensile properties.

Reference

[1] S. De Wolf *et al.*, "Organometallic Halide Perovskites: Sharp Optical Absorption Edge and Its Relation to Photovoltaic Performance," *The Journal of Physical Chemistry Letters,* vol. 5, no. 6, pp. 1035-9, Mar 20 2014.

[2] L. Li *et al.*, "Recent advances of flexible perovskite solar cells," *Journal of Energy Chemistry*, 2018.

[3] D. Yang *et al.,* "Recent Advanced in Flexible Perovskite Solar Cell: Fabrication and Application," *Angewandte Chemie International Edition,* Oct 17 2018.

[4] B. J. Kim *et al.*, "Highly efficient and bending durable perovskite solar cells: toward a wearable power source," *Energy & Environmental Science,* vol. 8, no. 3, pp. 916-921, 2015.

[5] K. Poorkazem *et al.*, "Fatigue resistance of a flexible, efficient, and metal oxide-free perovskite solar cell," *Journal of Materials Chemistry A,* vol. 3, no. 17, pp. 9241-9248, 2015.

[6] J.-I. Park *et al.*, "Highly flexible InSnO electrodes on thin colourless polyimide substrate for high-performance flexible CH 3 NH 3 PbI 3 perovskite solar cells," *Journal of Power Sources,* vol. 341, pp. 340-347, 2017.

[7] Y. Li *et al.*, "High-efficiency robust perovskite solar cells on ultrathin flexible substrates," *Nature Communications,* vol. 7, p. 10214, Jan 11 2016.

[8] J. Yu *et al.*, "Probing the Soft and Nanoductile Mechanical Nature of Single and Polycrystalline Organic-Inorganic Hybrid Perovskites for Flexible Functional Devices," *ACS Nano,* vol. 10, no. 12, pp. 11044-11057, Dec 27 2016.

[9] M. Spina *et al.*, "Mechanical signatures of degradation of the photovoltaic perovskite CH3NH3PbI3upon water vapor exposure," *Applied Physics Letters,* vol. 110, no. 12, 2017.

[10] J. Yang *et al.*, "Investigation of CH3NH3PbI3 degradation rates and mechanisms in controlled humidity environments using in situ techniques," *ACS Nano*, vol. 9, no. 2, pp. 1955-1963, 2015.

[11] S. Sun *et al.*, "Mechanical properties of organic–inorganic halide perovskites, CH3NH3PbX3 (X = I, Br and Cl), by nanoindentation," *Journal of Materials Chemistry A,* vol. 3, no. 36, pp. 18450-18455, 2015.

[12] Y. Rakita *et al.*, "Mechanical properties of APbX 3 (A = Cs or CH3NH3; X = I or Br) perovskite single crystals," *MRS Communications,* vol. 5, no. 04, pp. 623-629, 2015.

[13] M. A. Reyes-Martinez *et al.*, "Time-Dependent Mechanical Response of APbX3 (A = Cs, CH3 NH3 ; X = I, Br) Single Crystals," *Advanced Materials,* vol. 29, no. 24, Jun 2017.

[14] C. Ramirez *et al.*, "Thermo-mechanical behavior of organic-inorganic halide perovskites for solar cells," *Scripta Materialia*, vol. 150, pp. 36-41, 2018.

[15] J. Feng, "Mechanical properties of hybrid organic-inorganic CH3NH3BX3 (B = Sn, Pb; X =

Br, I) perovskites for solar cell absorbers," *APL Materials,* vol. 2, no. 8, 2014.

[16] J. Han *et al.*, "Nanoindentation cannot accurately predict the tensile strength of graphene or other 2D materials," *Nanoscale,* vol. 7, no. 38, pp. 15672-9, Oct 14 2015.

[17] J. H. Noh *et al.*, "Chemical management for colorful, efficient, and stable inorganic-organic hybrid nanostructured solar cells," *Nano Letters,* vol. 13, no. 4, pp. 1764-9, Apr 10 2013.

[18] B. Suarez *et al.*, "Recombination Study of Combined Halides (Cl, Br, I) Perovskite Solar Cells," *The Journal of Physical Chemistry Letters,* vol. 5, no. 10, pp. 1628-35, May 15 2014.

[19] D. Sabba *et al.*, "Impact of Anionic Br– Substitution on Open Circuit Voltage in Lead Free Perovskite (CsSnI3-xBrx) Solar Cells," *The Journal of Physical Chemistry C,* vol. 119, no. 4, pp. 1763-1767, 2015.

[20] J. C. Tan and A. K. Cheetham, "Mechanical properties of hybrid inorganic-organic framework materials: establishing fundamental structure-property relationships," *Chemical Society Reviews,* vol. 40, no. 2, pp. 1059-80, Feb 2011.

[21] Z. Xiao *et al.*, "Solvent annealing of perovskite-induced crystal growth for photovoltaic-device efficiency enhancement," *Advanced Materials,* vol. 26, no. 37, pp. 6503-9, Oct 8 2014.

[22] Y. Liu *et al.*, "Single-Crystal-like Perovskite for High-Performance Solar Cells Using the Effective Merged Annealing Method," *ACS Applied Materials & Interfaces,* vol. 9, no. 14, pp. 12382-12390, Apr 12 2017.

[23] J. Liu *et al.*, "Improved Crystallization of Perovskite Films by Optimized Solvent Annealing for High Efficiency Solar Cell," *ACS Applied Materials & Interfaces,* vol. 7, no. 43, pp. 24008-15, Nov 4 2015.

[24] G. Li *et al.*, "Atomistic explanation of brittle failure of thermoelectric skutterudite CoSb 3," *Acta Materialia,* vol. 103, pp. 775-780, 2016.

[25] Z. D. Sha *et al.*, "Inverse pseudo Hall-Petch relation in polycrystalline graphene," *Scientific Reports,* vol. 4, p. 5991, Aug 8 2014.

[26] Y. Shao *et al.*, "Grain boundary dominated ion migration in polycrystalline organic–inorganic halide perovskite films," *Energy & Environmental Science,* vol. 9, no. 5, pp. 1752-1759, 2016.

[27] W.-S. Lei, "A generalized weakest-link model for size effect on strength of quasi-brittle materials," *Journal of Materials Science,* vol. 53, no. 2, pp. 1227-1245, 2017.

[28] M. Park *et al.*, "Mechanically Recoverable and Highly Efficient Perovskite Solar Cells: Investigation of Intrinsic Flexibility of Organic-Inorganic Perovskite," *Advanced Energy Materials,* vol. 5, no. 22, 2015.

5. Summary

Owing to exhaustion of resources such as fossil fuels and increased energy consumption, exploring alternative energy sources is one of important assignment in the world. The sun is a sustainable, reliable and almost infinite source of energy that can make significant contributions to the global demand for energy. Therefore, photovoltaic energy is currently drawing attention as an upcoming alternative energy sources, and organic-inorganic metal halide perovskite solar cells have been studied as attractive candidates for next-generation photovoltaic devices. The photovoltaic efficiency of perovskite-based solar cells has recently soared rapidly from 3.8% to above 20% in less than 10 years. Such perovskite-based solar cells have many advantages: remarkable optical properties, longer charge, electron and hole, diffusion lengths, high light absorption coefficients and good cost-effectiveness, and show promise not only in photovoltaic applications but also in other applications After all these merits, however, these materials are still afflicted with long-term stability and mechanical reliability issues. To solve these long-term stability issues multiple studies have been developed such as doped halogen element and mixed cations and coated encapsulation or passivation layer and so on. Likewise, there has been rapid studied in long-term stability issues, but very few experimental or theoretical studies have been reported on mechanical properties.

The organic-inorganic metal halide perovskite solar cells (PSCs) hold promising candidate for flexible photovoltaic devices. All of its precursor materials are plentiful on earth and all fabrication process can be carry out at low temperature below 150℃. Strong light absorption is a main figure-of-merit required for high-performance absorber material. The hybrid perovskite materials have excellent absorption in this regard, only about 300 nm-thick is enough to light-absorption at all range of visible light. Furthermore, its absorption range can be tuned by substitution and composition change in perovskite structure. The bandgap of the perovskite materials can be modified by simple mixing process, resulting it possible to design matched charge transport layers for enhancing performance. On the other hand, many previous studies have exhibited that high-quality perovskite materials with uniform morphology, free of pin-holes, and great crystallinity can be successfully fabricated using low temperature process, indicating these materials and procedures are promising candidate for fabrication on flexible polymeric substrates. Recently many studies have focused on designing low-cost, light weight, high performance, and mechanically flexible PSCs. Research on mechanical properties of flexible perovskite solar cells generally divided into the method of measuring flexibility using hundreds or thousands of times of repeatable bending testing and measuring mechanical properties using direct mechanical testing methods. The latter mechanical testing method has limitations in measuring fracture mechanical properties. Indeed, direct measurement of mechanical properties, especially tensile properties, are challenging because of too hard to fabricate specimen and to progress testing.

To measure flexibility of flexible perovskite solar cells, I have fabricated flexible PSCs using special electrode and substrate. The polymer-metal composite electrode shows great recoverable properties during extremely severe bending deformation. It was confirmed by repeatable bending tests with different bending radius using specific bending apparatus. The composite electrodes shown similar sheet resistance with ITO electrode, and also shown no change of resistance after severe bending deformation, it indicated suitable candidates for ultra-flexible electronic devices. However, this electrode has lower transmittance than ITO electrode, resulting in lower PCE values than ITO based PSCs. Nevertheless, it needs to complement transmittance, it was enough to demonstrate flexibility of flexible PSCs. Furthermore, this work performed repeatable bending tests on flexible PSCs with different bending radius and cycles. First 100 cycles bending tests shown no degradation of flexible PSCs, but smallest bending radius of 0.5 mm shown crack initiating after repeatable bending tests on perovskite materials. And then photovoltaic performances were rapidly decreased after 300 cycles bending radius due to severe crack occurring. But photovoltaic properties were not decreased after 1,000 cycles bending of 1 mm bending radius with no significant cracking. Therefore, results of this work were expected that possible reason of performance degradation is most vulnerable materials, perovskite materials in this work, in severe bending deformation.

And then, I have performed hole-nanoindentation tests for suspended functional constituent materials on hole-patterned substrate. As results, I had obtained the fracture strength of each layers was estimated to be 0.87 (±0.09) GPa for AI 4083, 0.49 (±0.01) GPa for $MAPbI_3$, and 0.92 (±0.09) GPa for $PC_{61}BM$, respectively. The elastic modulus was measured as 5.06 (±0.61) GPa for AI 4083, 13.67 (±1.85) GPa, and 11.90 (1.63) GPa for $PC_{61}BM$, respectively. It was converted to elastic limit because these results was obtained from the range of linear elastic modulus, this indicated the measured in elastic deformation sections. Therefore, fracture (or yield) strain is 17.19% for AI 4083, 3.58% for $MAPbI_3$, and 7.73% for $PC_{61}BM$, and conveted critical bending radius of 0.05 mm, 0,10 mm, and 0.22 mm of each materials, respectively. It was different to critical bending radius measured by repeatable bending tests of 0.5 mm due to mechanical properties measured by hole-nanoindentation is overestimated. The possible reasons of this, hole-nanoindenation is mesurement on local defect-free area and low driving force for occuring catastriphic failure. However, hole-nanoindentation results sugest that cracks initiate in the perovskite materials rather than other constituent materials, indicating perovskite materials dominate mechanical flexibility of flexible PSCs.

Therefore, to measure direct tensile properties, I occurred uni-axial tensile tests for four samples of $MAPbI_3$ and three $MAPb(I_{0.87}Br_{0.13})_3$ with different grain size fabricated by solvent annealing. Because of challenging sampling and handing issues for measuring mechanical properties of perovskite materials, this uni-axial tensile testing and sampling were carried out in isolated high vacuum state. All of results of tensile tests revealed linear elasticity, followed by negligible plasticity and failure.

It is means that perovskite materials are brittle nature, which can be confirmed in fracture behavior of intergranular fracture. This means grain boundaries are weaker than grain interiors, which is possibly because (1) grain boundaries naturally contain excess volume, (2) stress concentrates more at cusps, and (3) amorphous structure in grain boundaries caused by lattice distortion of Pb-X bonding. Interestingly, failures for solvent-annealed samples are accomplished by transgranular fracture. this indicates load-bearing ability of grain boundaries is similar to that of grain interiors for solvent-annealed samples. strengthening of grain boundaries during solvent annealing process is accomplished possibly because (1) excess volume in grain boundaries shrank and (2) cusps became so blunt that stress concentrations at cusps are reduced. Furthermore, the critical bending radius calculated by elastic limit, which is measured by tensile tests, is well-agreement with critical bending radius measured by repeatable bending radius. This indicates that mechanical flexibility of flexible PSCs, which are used in this work, is dominated by perovskite materials, especially tensile properties.